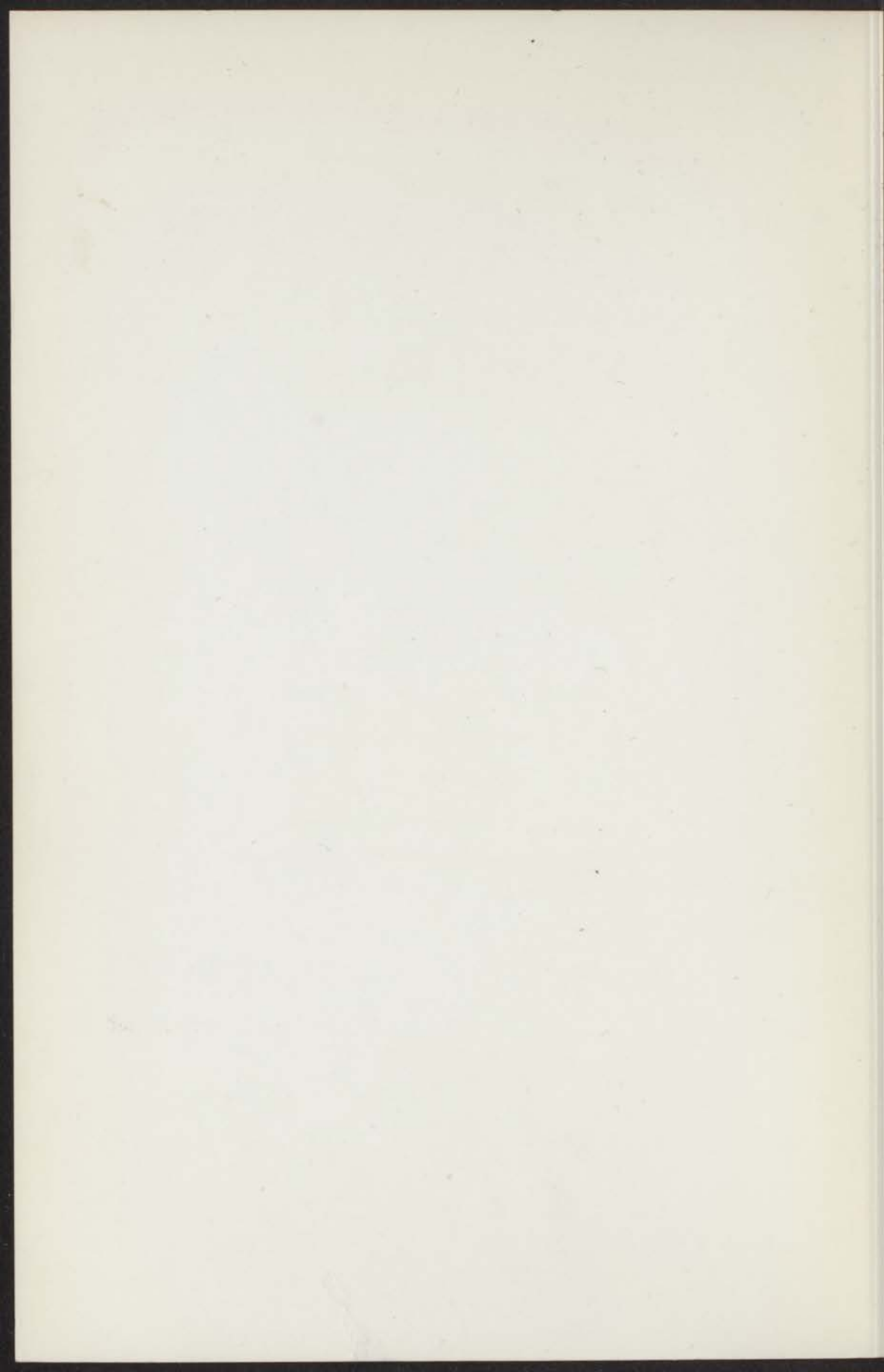


- 5 DEC. 1972

SUPERCONDUCTING POINT CONTACTS
WEAKLY CONNECTING TWO SUPERCONDUCTORS
AND
ELECTROSTATIC EFFECTS IN SUPERCONDUCTORS
DUE TO TEMPERATURE GRADIENTS

INSTITUUT-LORENTZ
voor theoretische natuurkunde
Nieuwstoeg 18-Leiden-Nederland

A. TH. A. M. DE WAELE



5 DEC. 1972

SUPERCONDUCTING POINT CONTACTS
WEAKLY CONNECTING TWO SUPERCONDUCTORS
AND
ELECTROSTATIC EFFECTS IN SUPERCONDUCTORS
DUE TO TEMPERATURE GRADIENTS

PROEFSCHRIFT

TER VERKRIJGING VAN DE GRAAD VAN DOCTOR
IN DE WISKUNDE EN NATUURWETENSCHAPPEN
AAN DE RIJKSUNIVERSITEIT VAN LEIDEN, OP GEZAG
VAN DE RECTOR MAGNIFICUS DR. A. E. COHEN,
HOOGLEERAAR IN DE FACULTEIT DER LETTEREN,
VOLGENS BESLUIT VAN HET COLLEGE VAN
DEKANEN TE VERDEDIGEN OP DONDERDAG
21 DECEMBER 1972, TE KLOKKE 14.15 UUR

DOOR

ALPHONS THEOPHILE AUGUSTA MARIA DE WAELE
GEBOREN TE KOEWACHT (THANS GEMEENTE AXEL)
IN 1944

INSTITUUT-LORENTZ
voor theoretische natuurkunde
Nieuwsteeg 18-Leiden-Nederland

kast dissertaties

1972
DRUKKERIJ J. H. PASMANS, 'S-GRAVENHAGE

1925

WEAKLY COUPLING TWO SUPERCONDUCTORS
AND
ELECTROSTATIC EFFECTS IN SUPERCONDUCTORS
DUE TO TEMPERATURE GRADIENTS

Promotor: Dr. R. de Bruyn Ouboter

INHOUDSTAFEL

DE VERHOUDING VAN DE GRAD VAN KOUDE
IN DE WILKING EN IN DE WILKING
VAN DE WILKING EN IN DE WILKING
VAN DE WILKING EN IN DE WILKING
VAN DE WILKING EN IN DE WILKING
VAN DE WILKING EN IN DE WILKING
VAN DE WILKING EN IN DE WILKING
VAN DE WILKING EN IN DE WILKING

DOOR

ALFRED H. ELLIOTT, ALBERTA AGRICULTURAL
COLLEGE, EDMONTON, ALBERTA, CANADA

HOOFDSTUK I

INLEIDING

1. Inleiding

2. De verhouding van de grad van koude

STELLINGEN

I

Vant-Hull, Simpkins en Harding hebben de magnetische ruis van een staaf normaal metaal gemeten door de staaf in de holte van een dubbelpuntcontact te schuiven. Bij de interpretatie van de uitkomsten van deze meting dient de invloed van dit normale metaal op de werking van het dubbelpuntcontact te worden betrokken.

L. Vant-Hull, R.A. Simpkins and J.T. Harding
Phys. Lett. 24, 736 (1967)
Dit proefschrift §4.6.

II

De alternatieve verklaring die Gubankov, Likharev en Margolin geven voor de gemeten i_c als functie van B_{\perp} , die wordt beschreven in figuur 16 van dit proefschrift, leidt niet tot bevredigende overeenstemming tussen de gemeten en de berekende waarden. De zelf-inductie van het omsloten oppervlak van het dubbelpuntcontact mag derhalve niet worden verwaarloosd.

V.N. Gubankov, K.K. Likharev and N.M. Margolin,
Sov. Phys.-Solid State 14, 819 (1972).

III

Het gebrek aan overeenstemming tussen de theorie, die Mercereau voor een dubbele Dayem-brug heeft ontwikkeld, en het experiment, is het gevolg van een foutieve beschrijving van het systeem en niet van het feit dat in de theorie thermische ruis buiten beschouwing werd gelaten.

J.E. Mercereau, Rev. de Phys. Appl. (Paris) 5, 13 (1970).

IV

De verklaring van het verdwijnen van het „patch-effect" bij vloeibaar-helium temperaturen wordt gezocht in de invloed die een geadsorbeerd laagje kan hebben op de uittreepotentiaal van verschillende kristaloppervlakken van een metaal. Deze verklaring kan worden getoetst door gebruik te maken van experimentele technieken die in deel II van dit proefschrift zijn beschreven.

F.C. Witteborn and W.M. Fairbank, *Nature* 220, 436 (1968).

V

In verband met de mogelijkheid om op eenvoudige wijze lage temperaturen te bereiken, is het van belang de thermische effecten te bestuderen die gepaard gaan met veldemissie van electronen.

VI

In verband met de theorie van Misner dat de gravitatiestraling die door Weber is waargenomen het gevolg is van gravitatie-synchrotron straling, verdient het aanbeveling ook de polarisatie van de gravitatiestraling te meten.

C.W. Misner, *Phys. Rev. Lett.* 28, 994 (1972).

VII

Het argument waarmee Einstein de algemene geldigheid van de door hem ontwikkelde theorie over gravitatiestraling in twijfel trekt is niet steekhoudend.

A. Einstein, *Sitzungsberichte der Preussischen Akademie der Wissenschaften*, Berlin, 154 (1918).

VIII

De druk in de damp juist buiten een heliumfilm, waarin de superfluïde component al dan niet beweegt, is in een stationaire toestand gelijk aan de verzadigde dampdruk.

V.M. Kontorovich, Sov. Phys. JETP 3, 770 (1956).

D.L. Goodstein and P.G. Saffman, Proc. R. Soc. A 325, 447 (1971).

IX

Voor het meten van de spontane magnetisatie en van de gemiddelde domeingrootte in de transmissierichting van een ferromagneet met behulp van neutronen-depolarisatie, zijn bij gegeven reactorflux en gelet op de beschikbare polarisertechnieken, koude neutronen (met een golflengte van ongeveer 4 \AA) te prefereren boven thermische (1 \AA).

X

Het besturen van een land als Nederland kan slechts door een multidisciplinair team van deskundigen worden overzien en uitgevoerd. Dit leidt voor de niet-gespecialiseerde buitenstaander (de overgrote meerderheid van de bevolking) tot een onduidelijkheid in de politiek die maar zeer ten dele door vereenvoudiging van de partijverhoudingen kan worden verbeterd.

A.Th.A.M. de Waele

21 december 1972

Van mijn Ouders en van Diering

...the ... of the ...
...the ... of the ...
...the ... of the ...
...the ... of the ...

...the ... of the ...
...the ... of the ...
...the ... of the ...
...the ... of the ...

...the ... of the ...
...the ... of the ...
...the ... of the ...
...the ... of the ...

...the ... of the ...
...the ... of the ...
...the ... of the ...
...the ... of the ...

...the ... of the ...
...the ... of the ...

INSTITUUT-LORENTZ
voor theoretische natuurkunde
Nieuwsteeg 18-Leiden-Nederland

Aan mijn Ouders en aan Ditty

E R R A T A, A.Th.A.M. de Waele, Thesis

P. 26 The captions to the figures 6 and 7 should be interchanged.

P. 32 In the last formula there has to be an equality sign between the two last fractions.

P. 77 The second line of eq. (6.1) should read

$$= -\vec{\nabla}\mu - m_4\vec{\nabla}H = -v_o\vec{\nabla}P + s\vec{\nabla}T + \frac{\rho_n}{\rho} \frac{m}{2} \vec{\nabla}(\vec{v}_n - \vec{v}_s)^2 - m_4\vec{\nabla}H \quad (6.1)$$

P. 78 On this page $m \equiv m_e$ = electron mass.

The second line of the first formula should read:

$$= -\vec{\nabla}2\mu + 2e(\vec{E} + \vec{v}_s \times \vec{B}) - 2m_e\vec{\nabla}H$$

CONTENTS

| | |
|----------------------|---|
| General Introduction | 7 |
|----------------------|---|

PART I

SUPERCONDUCTING POINT CONTACTS WEAKLY CONNECTING

TWO SUPERCONDUCTORS

| | |
|--|----|
| Contents of Part I | 11 |
| §1 Introduction | 12 |
| §2 Two superconductors weakly connected by a single superconducting point contact | 24 |
| §3 The critical current through a double point contact between two superconductors as a function of the applied magnetic field | 38 |
| §4 Two superconductors weakly connected by a double point contact in the resistive-superconductive region | 50 |
| §5 Description of the experimental set-up and the construction of double point contacts | 69 |

PART II

ELECTROSTATIC EFFECTS IN SUPERCONDUCTORS

DUE TO TEMPERATURE GRADIENTS

| | |
|---|-----|
| Contents of Part II | 75 |
| §6 Introduction | 76 |
| §7 Analysis of the measuring method; discussion of the effects contributing to the electrostatic signal | 85 |
| §8 Description of the apparatus. Noise sources and erroneous signals | 92 |
| §9 Experimental results | 99 |
| §10 Conclusions of Part II | 103 |
| References | 104 |
| Samenvatting | 108 |

CONTENTS OF PART I
CONTENTS OF PART II

CONTENTS OF PART I

1. Introduction

2. The experimental method; description of the apparatus and the results

3. The experimental results

4. Discussion of the experimental results and the results of the other workers

5. Conclusions

6. References

7. Appendix

8. Index

CONTENTS OF PART II
CONTENTS OF PART III

CONTENTS OF PART II

1. Introduction

2. The experimental method; description of the apparatus and the results

3. The experimental results

4. Discussion of the experimental results and the results of the other workers

5. Conclusions

6. References

7. Appendix

8. Index

GENERAL INTRODUCTION

The work described in this thesis deals with the macroscopic quantum effects in superconducting point contacts weakly connecting two superconductors and with the electrostatic effects in superconductors due to temperature gradients.

When two superconductors are completely isolated from each other it is possible to apply a voltage difference between both superconductors, while there is no current flowing between them ($V = \text{any value}$, $i = 0$). On the other hand, when two superconductors are tightly pressed against each other a supercurrent can flow through the contact region while the voltage is zero ($V = 0$, $i = \text{any value below the (bulk) critical current}$). From these considerations one can understand that there should be ways of connecting two superconductors that lead to current-voltage dependences that are in some way in between these two extreme (and trivial) cases. In order to find this intermediate region one must "weakly" connect the two superconductors. In 1962 and 1963 Josephson and Anderson predicted that weakly coupled superconductors should show a macroscopic quantum behaviour.

There are many ways to realize a weak coupling. One can separate the two superconductors by a thin insulation layer (tunnel junction), a layer of a normal metal (S-N-S junction) or by a narrow constriction of superconducting material (Dayem bridge) with a width of the order of one micrometer. The types of weak links that we deal with in part I of this thesis (§1 - §5) are the so-called superconducting point contacts. They consist of one or more points of one superconducting block that touch another superconducting block.

Although the detailed behaviour of the various types of weak links is different, they have many important features in common. One of them is that up to a certain critical value a current can flow through the weak link while the voltage across the link is zero, even in an oxide or an S-N-S junction. Another common feature is that weak links radiate electro-magnetic waves, obeying the relation $2e\bar{V} = h\nu$. These effects were predicted by Josephson in 1962.

Part I of this thesis deals with the dc and ac current-voltage-magnetic field dependences of several different point contact arrangements. It is shown (§2) that in a device with a single superconducting point contact, ac super and normal currents, and ac and dc voltages are generated when a dc current is supplied to the contact, larger than the maximum supercurrent ($\bar{V} \neq 0$). The ac impedances in the electrical circuit to the point contact have an influence on the dc current-voltage dependence. A direct way to show this feature (§4.5) is to put a point contact in the center of the bottom of a coaxial cavity.

The situation where the two superconducting blocks are connected by two point contacts gets much attention in this thesis. Such a device is called a double point contact. The maximum supercurrent through symmetrical double point contacts as a function of an applied dc magnetic field is calculated (§3). It will be shown that a circulating current around the hole, enclosed by the superconductors and the point contacts, gives rise to a self-induced flux in the hole that cannot be neglected. The self-inductance has to be taken into account. In this way quantitative agreement between the calculations and the experiment is obtained

(§3.3). The relationship with a strongly coupled double point contact where the total flux in the hole is quantized is treated in §3.2. The dynamic behaviour of symmetrical double point contacts in the resistive region ($\bar{V} \neq 0$) will be discussed (§4). There are ac magnetic fields in the hole between the contacts in addition to ac voltages and ac currents. A derivation is given of the fact that the dc voltage at constant applied dc current oscillates as a function of the applied dc magnetic field. The amplitude of these oscillations increases when one puts a normal metal (such as copper or platinum) in the hole, since the self-inductance of the hole is then frequency dependent. This fact can be used to improve the voltage sensitivity of a magnetometer where a double point contact is used as the magnetic-field-sensitive unit (§4.6).

The relation $2e\bar{V} = h\nu$ has been confirmed within 1 ppm by Parker, Taylor and Langenberg. Clarke proved that the quantity \bar{V}/ν is the same within 0.01 ppm for all the superconductors tested in his experiment. These high degrees of accuracy are possible because the ac Josephson relation gives a direct relationship between the frequency ν and the electrochemical potential difference $\Delta\bar{\mu}$ per electron across the junction: $2e\bar{V} = 2\Delta\bar{\mu} = h\nu$. In a superconducting circuit the only changes in the electrochemical potential occur at the junction, even when there are several different superconducting materials or temperature gradients. Hence, the measurement of \bar{V} is not affected by eventual thermal gradients in the superconducting parts of the circuit, since a voltmeter measures differences in the electrochemical potential (§1.3).

The influence of temperature gradients in superconductors is discussed in part II of this thesis (§6 - §10). It is a known fact that the Seebeck, Thompson and Peltier coefficients are zero in a superconductor. However a comparison between superconductors and superfluid helium II, leads to the suggestion that there is an electric field in the bulk of a superconductor when a temperature difference is applied on the superconductor. This electric field multiplied by the electron charge ($e\bar{E}$) is exactly equal to the gradient in the chemical potential per electron $\bar{\nabla}\bar{\mu}$. The essential difference between a superconductor and a normal metal being that the equality holds exactly for a superconductor, while in a normal conductor these two terms differ by a quantity related to the differential thermo-electric power of the normal metal. The difference in the electrostatic potential in the bulk of a superconductor due to a temperature difference can be regarded as the analogy of the fountain pressure in superfluid helium II.

The analogy between the properties of superconductors and helium II has always been of theoretical and experimental interest*. Essentially this similarity is due to the fact that in helium II and in superconductors a macroscopic number of (quasi) particles is condensed in the same single (quasi) particle wave function. Therefore they both show a macroscopic quantum behaviour. Because of this fundamental common feature such striking phenomena as superconduction (the absence of friction), the Meissner effect, flux quantization and the Josephson effect in a superconductor, all have their analogue in helium II. It is then natural to ask whether this analogy can be extended to the fountain effect in helium

* "Stromen zonder wrijving" by R. de Bruyn Ouboter, 19 december 1967, Universitaire Pers, Leiden.

II. In other words whether in a superconductor electrostatic voltage differences can exist, which can be considered as the analogue of the fountain pressure in helium II. Several theoretical papers showed that this effect should exist indeed. The so-called "fountain voltage" shows up in the temperature dependence of the work function of a superconductor. In part II of this thesis an experiment is described where the temperature dependences of the work functions of niobium and lead are measured. It turns out however that the fountain voltage shows up together with other terms due to the temperature dependence of the surface dipole layer of the superconducting metal. Furthermore it appears that the change in the chemical potential due to a change in temperature is a very complicated property of the material and cannot be interpreted only in terms of the entropy per conduction electron. This seems to be a fundamental difficulty in measuring the fountain voltage. Apart from this, the measurements described in part II give a fairly good insight in the magnitude of the electric fields in superconductors due to a temperature gradient.

The first part of the document discusses the importance of maintaining accurate records of all transactions. It emphasizes that every entry should be supported by a valid receipt or invoice, and that these documents should be stored in a secure and accessible location. The text also mentions the need for regular audits to ensure the integrity of the financial data.

The second part of the document outlines the procedures for handling discrepancies. It states that any differences between the recorded amounts and the actual amounts should be investigated immediately. The document provides a step-by-step guide for identifying the source of the error and for correcting it. It also discusses the importance of documenting the findings and the actions taken to resolve the issue.

The third part of the document discusses the role of management in ensuring the accuracy of the financial records. It states that management should establish a clear policy regarding the recording and reporting of transactions. It also emphasizes the need for management to provide adequate training and supervision to the staff responsible for maintaining the records.

The fourth part of the document discusses the importance of maintaining the confidentiality of the financial records. It states that all information contained in the records should be treated as confidential and should not be disclosed to unauthorized persons. The document also discusses the need for appropriate access controls and security measures to protect the records from theft or loss.

The fifth part of the document discusses the importance of maintaining the accuracy of the financial records over the long term. It states that the records should be maintained for a sufficient period of time to allow for the resolution of any disputes. It also discusses the need for regular backups and the use of secure storage methods to ensure the long-term preservation of the records.

PART I

SUPERCONDUCTING POINT CONTACTS WEAKLY CONNECTING
TWO SUPERCONDUCTORS

CONTENTS

- §1 INTRODUCTION, §1.2 the Meissner effect and flux quantization, §1.3 the ac and dc Josephson effect.
- §2 TWO SUPERCONDUCTORS WEAKLY CONNECTED BY A SINGLE SUPERCONDUCTING POINT CONTACT (THE AC JOSEPHSON EFFECT), §2.1 The resistive-superconductive region and the current-voltage characteristic for a single point contact. The influence of ac impedances on the dc current-voltage characteristic, §2.2 A single superconducting point contact shunted in parallel by a superconductor or a low-resistance normal conductor, §2.3 Microwave emission and absorption from superconducting point contacts and the constant voltage steps in the current-voltage characteristic, §2.4 Applications: radio-frequency, micro-wave and far-infrared spectroscopy, noise thermometry and voltage standards. The determination of the flux quant $h/2e$.
- §3 THE CRITICAL CURRENT THROUGH A DOUBLE POINT CONTACT BETWEEN TWO SUPERCONDUCTORS AS A FUNCTION OF THE APPLIED MAGNETIC FIELD, §3.1 Two superconductors weakly coupled by a double point contact when the self-induced flux in the enclosed area is ignored (symmetrical and asymmetrical), §3.2 Two superconductors strongly coupled by a double point contact (symmetrical and asymmetrical). §3.3 Two superconductors weakly coupled by a symmetrical double point contact when the self-induced flux in the enclosed area is taken into account, §3.4 The interference grating.
- §4 TWO SUPERCONDUCTORS WEAKLY CONNECTED BY A DOUBLE POINT CONTACT IN THE RESISTIVE-SUPERCONDUCTIVE REGION, §4.1 A general introduction and a survey of the experimental data, §4.2 When the self-induced flux in the enclosed area is ignored, §4.3 When the self-induced flux in the enclosed area is taken into account, §4.4 The rectification process for an asymmetrical double junction, §4.5 A double point contact placed in the center of the bottom of a coaxial cavity, §4.6 The influence of a normal metal in the hole between the superconductors on the $\bar{i}-\bar{V}-B_{\perp}$ dependence, §4.7 Applications: the magnetic-flux meter and the voltmeter; the London Moment.
- §5 DESCRIPTION OF THE EXPERIMENTAL SET-UP AND THE CONSTRUCTION OF DOUBLE POINT CONTACTS, §5.1 The experimental set-up, §5.2 The construction of double point contacts.

§1 INTRODUCTION

§1.1 Many aspects of the properties of weakly-coupled superconductors have been described previously by P.W.Anderson ¹⁾ in Progress in Low Temperature Physics (Vol 5, Chap. I: The Josephson effect and quantum coherence measurements in superconductors and superfluids (1967)). The microscopic and macroscopic theory of the Josephson effect ²⁾ were described and experiments measuring the transmission of *supercurrents* through thin insulating oxide barriers (a Josephson tunnel junction) were discussed mainly in terms of quantum-mechanical tunneling. An explanation was given of the interference of the tunnel current when the magnetic field is applied (the dc diffraction experiment of Rowell ³⁾⁴⁾ and the double-junction dc macroscopic interference experiments of Mercereau and co-workers ⁵⁾). Furthermore experiments were reviewed which are related to the ac Josephson effect ⁶⁻¹⁰⁾: when a constant voltage difference V is established across the junction the super-current oscillates at a frequency $(2e/h)V$ ¹⁰⁾.

Soon after the discovery of the Josephson effect ²⁾ in 1962 it was demonstrated that this effect was not only related to the transmission of supercurrents through very thin (10 \AA to 20 \AA) oxide barriers but could also be observed in narrow superconducting constrictions (a technique due to Anderson and Dayem ¹¹⁾ (1964)) and in superconducting point contacts ¹²⁾. In these experiments the ac Josephson effect appeared to be related to the motion of quantized vortices (Anderson's phase slippage concept).

In 1964-1965 Zimmerman and Silver ¹²⁾ constructed Mercereau ⁵⁾ double-junction interferometers in which the oxide tunnel junctions were replaced by superconducting point contacts. A point contact between two superconductors is formed when a point of one superconductor touches the other. The contact resistance at room temperature is in the order of 0.1 to 1000 Ω . The critical current of the contact (which is the maximum dc current that can flow through the contact while the voltage across the contact is zero) is several orders of magnitude less than the critical current of the bulk superconductor.

The behaviour of the evaporated tunnel junctions (oxide layers) was fully understood at the time of Anderson's review article (1967), contrary to the case of point contacts which are of a quite different nature. Since that time considerable progress has been made in understanding the behaviour of superconducting point contacts mainly by the work of Zimmerman and Silver ¹³⁻²³⁾, Dayem and Grimes ²⁴⁻²⁵⁾, Stewart ²⁶⁾, McCumber ²⁷⁾, Baratoff, Blackburn and Schwartz ²⁸⁾ and the Leiden group ²⁹⁻³⁷⁾.

This part of this thesis concerns dc and ac interference phenomena in superconducting point contacts weakly connecting two superconductors. They will be treated here in four sections (2-5) preceded by a short summary of the phenomenological theory of superconduction, containing some topics from the London ³⁸⁾⁴⁶⁾ and the Ginzburg-Landau theory ³⁹⁾, namely the Meissner effect ³⁸⁾⁴⁶⁾, flux quantization ⁴⁰⁻⁴⁵⁾ and the ac and dc Josephson effect ¹⁾²⁾⁴⁶⁾. This summary serves to facilitate the discussion of the presented material.

The properties of a single superconducting point contact will be discussed in §2. Special attention will be paid to the *resistive-superconductive region*, the current-voltage characteristic and the radiative properties. The point contact will be treated using a *two-fluid* model in which the *total current* is the sum of an ideal Josephson supercurrent $i_s(t) = i_J \sin \Delta\phi(t)$ and a *normal current* $i_n(t) = V/R_n = -(\hbar/2e)(\partial\Delta\phi(t)/\partial t)/R_n$. The influence of a shunt capacitance and a series inductance will be taken into account.

In §3, the magnetic field dependence of the critical current (the dc Josephson effect) through a double point contact, when the *self-induced flux* in the enclosed area is taken into account, is studied extensively. Its relation with flux quantization is discussed.

§4 deals with the properties of double point contacts in the resistive-superconductive region, in relation with both the ac and dc Josephson effects. Device applications such as in very sensitive magnetometers and voltmeters are discussed. An experiment is described where a double point contact is used to measure the magnetic flux due to a rotating superconductor (the London Moment).

Finally, the last section of part I (§5) gives a description of the experimental set-up and of the construction of the devices studied in this research.

§1.2 THE MEISSNER EFFECT AND FLUX QUANTIZATION

The essential feature of superfluidity (superconduction) is according to London³⁸⁾ a condensation of a macroscopic number of particles (bound-electron pairs, first described by Cooper⁴⁷⁾) in the same single quasi-particle quantum state. Such a condensation can be described, as usual, by an internal order parameter. According to the phenomenological theory of Ginzburg and Landau³⁹⁾ the order parameter Ψ_s is a complex quantity, with properties similar to those of the wave function of the macroscopically occupied single quasi-particle quantum state. This complex order parameter Ψ_s has an amplitude $\Psi_0(\vec{r}, t)$ and a phase $\phi(\vec{r}, t)$:

$$\Psi_s = \Psi_0(\vec{r}, t) e^{i\phi(\vec{r}, t)}. \quad (1.1)$$

In the Ginzburg-Landau theory³⁹⁾ $|\Psi_s|^2$ is interpreted as the internal order parameter of the original two-fluid model of Gorter and Casimir:⁴⁸⁾ the charge density $\rho_s(T)$ of the superfluid particles at a given temperature T is equal to the square of the amplitude: $\rho_s = |\Psi_s|^2$ and hence:

$$\Psi_s = \sqrt{\rho_s(\vec{r}, t)} e^{i\phi(\vec{r}, t)}. \quad (1.2)$$

The absolute phase is not observable, but we will show that phase differences are directly observable quantities.

In the Ginzburg-Landau theory, the current density \vec{I}_s is related to the probability current density of quantum mechanics in terms of the wave function Ψ_s of this single quasi-particle quantum state:

$$\begin{aligned} \vec{I}_s &= \frac{-i\hbar}{2(2m)} (\Psi_s^* \vec{\nabla} \Psi_s - \Psi_s \vec{\nabla} \Psi_s^*) - \frac{(2e)}{(2m)} |\Psi_s|^2 \vec{A} = \\ &= |\Psi_s|^2 \frac{\hbar}{(2m)} (\vec{\nabla} \phi - \frac{2e}{\hbar} \vec{A}) = |\Psi_s|^2 \vec{v}_s = \rho_s \vec{v}_s. \end{aligned} \quad (1.3)$$

The charge ($2e$) which enters in this expression is equal to twice the charge of a free electron, since according to the microscopic theory of Bardeen, Cooper and Schrieffer⁴⁷⁾ bound electron pairs are involved in the ordering process. The mass ($2m$) is very nearly equal to twice the mass of a free electron⁴⁹⁾. From eq. (1.3) one can define the fundamental relation for the generalised dynamical momentum \vec{p}_s of the superconducting pairs:

$$\vec{p}_s \equiv 2m \vec{v}_s + 2e\vec{A} = \hbar \vec{\nabla} \phi. \quad (1.4)$$

Taking the curl of the equation (1.4) the London³⁸⁾ relation is obtained:

$$\vec{\nabla} \times \vec{p}_s = 0 \quad (1.5)$$

or:

$$\vec{\nabla} \times \vec{v}_s = - \frac{(2e)}{(2m)} \vec{\nabla} \times \vec{A} = - \frac{e}{m} \vec{B}. \quad (1.6)$$

Combining eq. (1.6) with the Maxwell equation

$\epsilon_0 c^2 \vec{\nabla} \times \vec{B} = \vec{I}_s = \rho_s \vec{v}_s$ gives the following relations:

$\vec{\nabla}^2 \vec{B} = \vec{B}/\lambda^2$ and $\vec{\nabla}^2 \vec{I}_s = \vec{I}_s/\lambda^2$ (in which $\lambda^2 \equiv \epsilon_0 mc^2/\rho_s e$ is the London-Ginzburg-Landau penetration depth) explaining the Meissner effect: the magnetic field (the magnetic induction) \vec{B} vanishes completely in the bulk of a non-rotating superconductor ($\vec{B} = 0$). Even if the magnetic field was already inside the metal before cooling through the critical temperature, the magnetic field is expelled below the critical temperature. We should like to remark that the eqs. (1.3) and (1.4) are gauge invariant under the following transformations for the vector potential, the scalar potential, the phase and the generalized dynamical momentum:

$$\begin{aligned} \vec{A}' &= \vec{A} + \vec{\nabla} \chi, & v' &= v - \frac{\partial \chi}{\partial t}, \\ \phi' &= \phi + \frac{2e}{\hbar} \chi, & \vec{p}'_s &= \vec{p}_s + 2e \vec{\nabla} \chi \end{aligned} \quad (1.7)$$

If one deals with a multiply-connected superconductive region instead of a simply-connected region, for instance a superconducting cylinder whose thickness is large compared to the penetration depth, one finds that although everywhere in the superconductor $\vec{\nabla} \times \vec{p}_s = 0$, the circulation of the generalized dynamical momentum (and hence the generalized angular momentum) around the hole of the cylinder is quantized, $\oint \vec{p}_s ds = nh$. The circulation of \vec{p}_s is also related to the magnetic flux Φ enclosed by the hole. For each point in the superconductor there can be only one value of the wave function Ψ_s . Thus the phase ϕ cannot change arbitrarily in the superconductor. If one adds the phase changes in a closed loop around the cylinder, the wave function must stay single valued. Hence irrespectively of how the phase ϕ changes as one goes around the cylinder, when one comes back to the starting point the phase must give the same value for the wave function Ψ_s , hence $\oint \vec{p}_s d\phi = n2\pi$ ($n = \text{any integer}$). Inside the bulk of the superconductor $\vec{v}_s = 0$, hence eq. (1.4) gives

$$\vec{p}_s = 2e\vec{A} = \hbar\vec{\nabla}\phi \quad (1.8)$$

and the magnetic flux ϕ enclosed by the hole is equal to ^{38,42-46}):

$$\phi = \iint_a B_n da = \oint_s A_s ds = \frac{1}{2e} \oint_s p_s ds = \frac{\hbar}{2e} \oint_s d\phi = n \frac{\hbar}{2e}. \quad (1.9)$$

In 1948 F. London ³⁸) predicted that the magnetic flux trapped by a superconducting cylinder would be quantized. The amount of trapped flux has been experimentally found to be quantized in units $h/2e$ by Deaver and Fairbank ⁴⁰) and Doll and Näbauer ⁴¹) in 1961. For a closed path in a region of non-zero current ($\vec{v}_s \neq 0$) one has fluxoid quantization ³⁸):

$$\frac{1}{2e} \oint_s p_s ds = \frac{m}{e} \oint_s v_s ds + \oint_s A_s ds = \frac{m}{e} \oint_s v_s ds + \phi = n \frac{\hbar}{2e}. \quad (1.10)$$

When, starting with the material in the normal state, a magnetic flux is applied through the hole (area 0) of the cylinder equal to $B_\perp 0$ and the cylinder subsequently is cooled into the superconducting state, a persistent circulating current i_{circ} is induced in such a way that the total magnetic flux enclosed by the cylinder is quantized:

$$B_\perp 0 + L i_{\text{circ}} = n \frac{\hbar}{2e}, \quad (1.11)$$

in which L is the self-inductance of the cylinder. Hence we stress again this relation: the sum of the product of the external magnetic field strength B_\perp and the enclosed area 0 and the product of the circulating current i_{circ} and the self-inductance L is quantized. When the applied magnetic flux is equal to an integral number of magnetic-flux quanta, $B_\perp 0 = nh/2e$, the circulating current is equal to zero and when the applied magnetic flux is equal to a half-integral number of flux quanta, $B_\perp 0 = (n + \frac{1}{2})h/2e$, the circulating current has a maximum, at points where the quantum state jumps from the state with n quanta to the state with $n + 1$ quanta. A schematic plot of the total enclosed magnetic flux and the circulating current as a function of the magnetic field applied in the normal state is given in fig. 1b. If the cylinder is cooled in an applied magnetic field from the normal to the superconductive state it passes into that quantum state, quantum number n , with the lowest Gibbs free energy. This quantum state is conserved during the further cooling process even if the field is switched off. A mechanism which can be responsible for choosing one of these particular quantum states (described in fig. 1b) is explained in §2.2.

§1.3 THE AC AND DC JOSEPHSON EFFECT

The dc and ac macroscopic quantum interference effects are observed when two superconductors are "weakly" connected. The two superconductors are at least in two dimensions much larger than the coherence length or the London penetration depth, so that they can be considered as "bulk" superconductors. The (non-zero) critical current of the weak link has to be several orders of magnitude less than the critical current of the

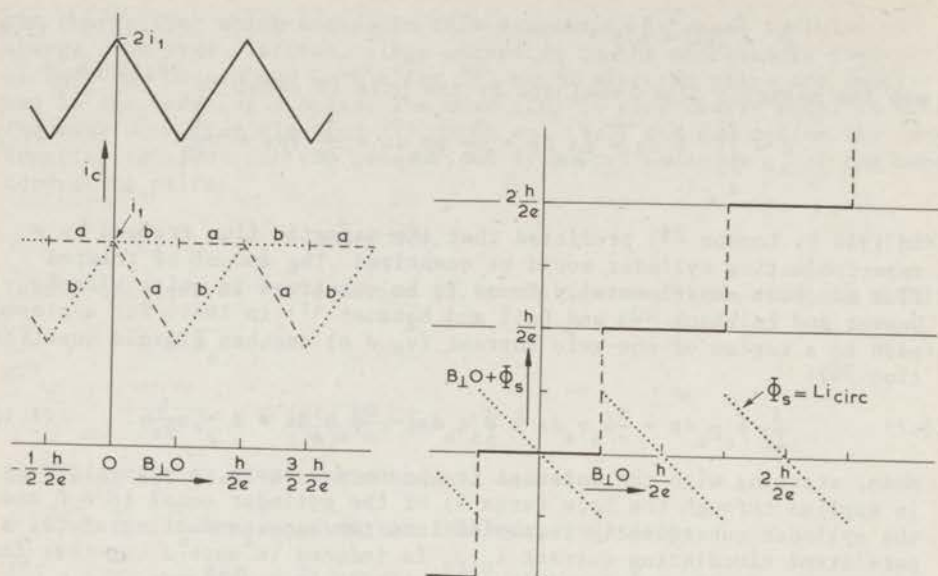


Fig. 1a The critical current i_c (—) and the current through the individual contacts "a" and "b" as a function of the applied magnetic flux for a "strongly" coupled double junction. The total magnetic flux is quantized. See fig. 6 for a schematic diagram of a double junction. When the applied flux is increased from zero, a circulating current is induced in such a way (see fig. b) that the total flux in 0 remains zero. In one of the contacts the circulating current *adds* to half the applied current and the critical current of the total junction is therefore smaller than when $B_{\perp 0} = 0$. Increasing $B_{\perp 0}$ increases the circulating current and i_c decreases. The current through "b" is constant and equal to the critical current i_1 of the individual contact "b". When $B_{\perp 0}$ surpasses $\frac{1}{2}(h/2e)$, the circulating current changes sign. It is now contact "a" which carries its critical current. The total flux in the hole is now equal to $h/2e$ (see fig. 1b). When $B_{\perp 0}$ is further increased, the circulating current decreases, the current through "b" increases, and the critical current increases. When $B_{\perp 0} = h/2e$ the circulating current is zero and the critical current is again equal to $2i_1$ (see §3.2).

Fig. 1b The total flux $B_{\perp 0} + \Phi_s$ in the area 0 as a function of the applied flux $B_{\perp 0}$, for the double junction discussed in fig. 1a. This figure is identical with the $B_{\perp 0} + \Phi_s$ versus $B_{\perp 0}$ dependence obtained by cooling the junction through its transition temperature in an applied field B_{\perp} . The dotted line represents the self-induced flux, $\Phi_s = Li_{circ}$, in the hole.

bulk superconductors. The observed interference effects can be summarized as follows:

- 1) When two superconductors are weakly coupled, either by a very thin oxide layer, or by a superconducting point contact, or by a narrow constriction or by a super-normal-super sandwich junction, a dc superconducting tunnel current of limited magnitude i_1 can flow through the junction in the absence of voltage difference ($V = 0$) between both superconductors (the dc Josephson effect).

- 2) When a constant voltage difference V is established across the weak link the supercurrent oscillates with a frequency $(2e/h)V$ and with an amplitude i_J (the ac Josephson effect). These oscillations are accompanied by electromagnetic radiation with the same frequency.
- 3) If one deals with a double contact or with a contact of finite extension the supercurrents give rise to interference phenomena in an applied magnetic field.

As an introduction, a simplified derivation of the Josephson relations in analogy with Feynman⁴⁶⁾ (but extended by including the influence of the vector potential \vec{A} on the weak link³⁴⁾, by a discussion of the gauge invariance of the equations and by introducing the electrochemical potential instead of the voltage) will be presented here.

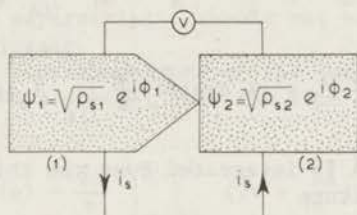


Fig. 2 A schematic diagram of a single point contact.

When two superconductors are separated by a weak link (see fig. 2) the two (base state) wave functions Ψ_1 and Ψ_2 of these two superconductors (fig. 2) are coupled by means of the Hamilton equations:

$$i\hbar \frac{\partial \Psi_i(t)}{\partial t} = \sum_{j=1}^2 H_{ij} \Psi_j(t) \quad , \quad H_{ij} = H_{ji}^*$$

which, in the absence of a magnetic field, can be written in the following way

$$i\hbar \frac{\partial \Psi_1}{\partial t} = - \frac{2\Delta\bar{\mu}}{2} \Psi_1 + K\Psi_2 \quad , \quad (1.12)$$

$$i\hbar \frac{\partial \Psi_2}{\partial t} = + \frac{2\Delta\bar{\mu}}{2} \Psi_2 + K\Psi_1 \quad . \quad (1.13)$$

In (1.12) and (1.13) $\Delta\bar{\mu} = \bar{\mu}_2 - \bar{\mu}_1$ is the electrochemical potential difference per electron across the point contact ($\bar{\mu} \equiv \mu + eV$, μ is the chemical potential per electron). The factor 2 arises from the fact that Cooper pairs are tunneling ($H_{22} - H_{11} = 2\Delta\bar{\mu}$) and $H_{12} = H_{21} = K$ is the coupling constant (see fig. 2). In the presence of a magnetic field the coupling constants K in eqs. (1.12) and (1.13) change by the factors

$$\exp\left(-i \frac{2e}{\hbar} \int_{1\delta}^2 A_s ds\right) \text{ and } \exp\left(+i \frac{2e}{\hbar} \int_{1\delta}^2 A_s ds\right)$$

respectively, where the integral is taken across the contact (δ); since ³⁴⁾⁴³⁾

$$\begin{aligned} H_{21} &= \langle 2|H|1 \rangle_{\vec{A} \neq 0} = \langle 2|H|1 \rangle_{\vec{A}=0} \exp\left(i \frac{2e}{\hbar} \int_{1\delta}^2 A_s ds\right) \\ &= K \exp\left(i \frac{2e}{\hbar} \int_{1\delta}^2 A_s ds\right) = H_{12}^* \end{aligned}$$

Eqs. (1.12) and (1.13) now change to

$$i\hbar \frac{\partial \Psi_1}{\partial t} = -\frac{2\Delta\bar{\mu}}{2} \Psi_1 + \{K \exp(-i \frac{2e}{\hbar} \int_{1\delta}^2 A_s ds)\} \Psi_2 \quad (1.14)$$

$$i\hbar \frac{\partial \Psi_2}{\partial t} = \frac{2\Delta\bar{\mu}}{2} \Psi_2 + \{K \exp(+i \frac{2e}{\hbar} \int_{1\delta}^2 A_s ds)\} \Psi_1 \quad (1.15)$$

The vector potential \vec{A} is integrated over the thickness δ of the contact layer. First we substitute

$$\Psi_j = \sqrt{\rho_j} e^{i\phi_j} \quad (\text{with } j = 1, 2)$$

in which now ρ_j is the total charge of the superfluid particles in j , then we equate the real and imaginary parts of eqs. (1.14) and (1.15) and take $\rho_1 = \rho_2$:

$$i_s = \dot{\rho}_1 = -\dot{\rho}_2,$$

$$2K\sqrt{(\rho_1\rho_2)}/\hbar \equiv i_1,$$

$\phi_2 - \phi_1 \equiv \Delta\phi(t) \equiv$ the phase difference across the weak link. In this way it is found that the super current is given by

$$i_s(t) = i_1 \sin(\Delta\phi(t) - \frac{2e}{\hbar} \int_{1\delta}^2 A_s ds) \equiv i_1 \sin\Delta\phi^*(t) \quad (1.16)$$

and the electrochemical potential difference by

$$\Delta\bar{\mu} = -\frac{\hbar}{2} \frac{\partial \Delta\phi}{\partial t} \quad (1.17)$$

Recently several theoretical papers (Baratoff, Blackburn and Schwartz ²⁸⁾, Bardeen and Johnson ¹⁰²⁾, and Gregers-Hansen, Levinsen and Fog Pedersen ¹⁰³⁾) have been published concerning the question which experimental conditions have to be satisfied in order eq. (1.16) to be valid. Unfortunately none of the models that are introduced in the calculations applies on point contacts. In §3.3 (fig. 16) a measurement of the criti-

cal current-magnetic field dependence of a double point contact will be compared with the values calculated from eq. (1.16). The close agreement between theory and experiments is strong evidence that eq. (1.16) is correct for point contacts.

The eqs. (1.16) and (1.17) are gauge invariant. This can be verified by using the definitions of $\Delta\mu$, $\bar{\mu}$ and $\Delta\phi$ and the transformations (1.7) for V and ϕ . In eq. (1.16) we introduced a quantity $\Delta\phi^*$ called the gauge-invariant phase difference of the weak link defined by

$$\Delta\phi^* \equiv \Delta\phi - \frac{2e}{h} \int_{1\delta}^2 A_s ds. \quad (1.18)$$

In this definition the superscript $*$ should not be confused with the symbol for complex conjugate.

For two identical superconductors at the same temperature $\mu_1 = \mu_2$ and hence $\Delta\mu = eV$. In this special case the time dependence of $\Delta\phi^*$ is given by

$$\begin{aligned} \Delta\phi^*(t) &= \Delta\phi^*(0) - \frac{2e}{h} \int_0^t \int_{1\delta}^2 (\vec{\nabla}V + \frac{\partial \vec{A}}{\partial t'}) ds dt' \\ &= \Delta\phi^*(0) + \frac{2e}{h} \int_0^t \int_{1\delta}^2 E_s ds dt', \end{aligned} \quad (1.19)$$

in which $\vec{E} = -\vec{\nabla}V - \frac{\partial \vec{A}}{\partial t}$.

In order to see how the eqs. (1.16) and (1.17) are related to the experiment we introduce the quantity $\bar{\mu}$ which is called the gauge-invariant electrochemical potential⁵⁰). It is defined by

$$\vec{\nabla} \bar{\mu}^* \equiv \vec{\nabla} \bar{\mu} + e \frac{\partial \vec{A}}{\partial t}.$$

Using the definition of $\bar{\mu}$ we obtain

$$\begin{aligned} \vec{\nabla} \bar{\mu}^* &= \vec{\nabla} \bar{\mu} + e \vec{\nabla}V + e \frac{\partial \vec{A}}{\partial t}, \\ \vec{\nabla} \bar{\mu}^* &= \vec{\nabla} \bar{\mu} - e \vec{E}. \end{aligned} \quad (1.20)$$

Since $\bar{\mu}$ and \vec{E} are gauge invariant $\bar{\mu}^*$ is gauge invariant. In a normal metal $\bar{\mu}^*$ is constant in parts of a circuit where the temperature is constant and where currents are absent. In a bulk superconductor $\bar{\mu}^*$ is also constant when there is a temperature gradient (see PART II). From eqs. (1.17) and (1.18)

$$\bar{\Delta\mu} = -\frac{h}{2} \frac{\partial \Delta\phi^*}{\partial t} - e \int_{1\delta}^2 \frac{\partial A_s}{\partial t} ds,$$

or

$$\int_{1\delta}^2 (\vec{V}_s \bar{\mu} + e \frac{\partial A_s}{\partial t}) ds = -\frac{\hbar}{2} \frac{\partial \Delta \phi^*}{\partial t} ,$$

$$\Delta \bar{\mu}^* = -\frac{\hbar}{2} \frac{\partial \Delta \phi^*}{\partial t} . \quad (1.21)$$

The gauge-invariant electrochemical potential difference across a voltmeter $\Delta \bar{\mu}_{VM}^*$ is equal to

$$\Delta \bar{\mu}_{VM}^* = (\mu_2 - \mu_1)_{VM} + e(V_2 - V_1)_{VM} + e \int_1^2 \frac{\partial A_s}{\partial t} ds .$$

In this case $\mu_1 = \mu_2$ and $\int_1^2 \frac{\partial A_s}{\partial t} ds = 0$. Hence the quantity measured by the voltmeter is equal to $(\Delta \bar{\mu}_{VM}^*)/e$. When a voltmeter is connected very close to the point contact, the inductance of the leads between the voltmeter and the point contact can be neglected ($\oint A_s ds = 0$) and consequently $\Delta \bar{\mu}_{VM}^* = \Delta \bar{\mu}_{\text{point contact}}^*$. Hence using eq. (1.20)

$$V_P = -\frac{\hbar}{2e} \frac{\partial \Delta \phi^*}{\partial t} , \quad (1.22)$$

where V_P would be the voltage if measured by a voltmeter very close to the contact.

Eqs. (1.16) and (1.22) are a quantitative formulation of the Josephson effect: a dc supercurrent $i_s = i_1 \sin \Delta \phi^*$ can flow through a weak link when no voltage difference is present and its maximum value i_1 is reached when $\Delta \phi^* = \pi/2$. When V_P is constant in time the supercurrent $i_s(t) = i_1 \sin \Delta \phi^*(t) = i_1 \sin \{\Delta \phi^*(0) - (2e/\hbar)V_P t\}$ oscillated with a frequency

$$\nu = \frac{2e}{\hbar} V_P . \quad (1.23)$$

Eq. (1.23) is the simplest form of the ac Josephson effect.

In general however the voltmeter is not connected very close to the contact. In that case the measured voltage $V_M \neq V_P = -\frac{\hbar}{2e} \frac{\partial \Delta \phi^*}{\partial t}$ but the relation $\nu = 2e\bar{V}_M/\hbar = 2e\bar{V}_P/\hbar$ still holds. A circuit for measuring \bar{V}_M is given in fig. 3. The only requirement for the circuit is that the voltmeter is connected to the contact with leads

* With the bar $\bar{\quad}$ above V or i we indicate the time average of a voltage or a current over times which are an order of magnitude larger than the time periods of V or i due to the Josephson effect. This means that \bar{V} and \bar{i} can be varying with time but in general slower than with the Josephson frequency.
On the other hand, a bar above " μ " indicates that we deal with the electrochemical potential $\bar{\mu}$ instead of with the chemical potential μ .

that have a purely inductive impedance (no resistance, no capacitance). Connected in parallel to those leads may be any impedance (dotted region), such as a combination of resistances (§2), capacitances (§2.1), self-inductances (§2.2) or even a cavity (§4.5) or another point contact (§4).

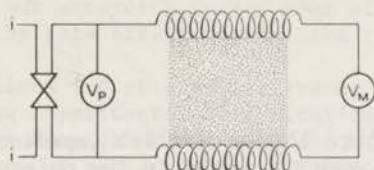


Fig. 3 Diagram representing the voltmeter circuit. V_P is a voltmeter very close to the point contact. V_M is the actual voltmeter at room temperature. The leads to V_M are represented by pure inductances. The dotted area between the leads indicates that any impedance may be connected to those leads in parallel with the voltmeter and the point contact. i are the current leads to the contact.

For the loop through V_P , V_M and the inductances

$$V_M = V_P - \frac{\partial}{\partial t} \oint_{\text{circuit}} A_S(x,t) dx . \quad (1.24)$$

From eqs. (1.16) and (1.22) we obtain

$$i_s(t) = i_1 \sin\{\Delta\phi^*(0) - \int_0^t 2\pi(2e/h)V_P(t')dt'\} .$$

If $V_P > 0$ at all times the integral will be increasing in time and after a certain time τ the current $i_s(\tau) = i_s(0)$. The value of τ will be such that

$$2\pi \frac{2e}{h} \int_0^\tau V_P(t) dt = 2\pi .$$

Hence

$$v = \frac{1}{\tau} = \frac{2e}{h} \frac{1}{\tau} \int_0^\tau V_P(t) dt = \frac{2e}{h} \bar{V}_P .$$

From eq. (1.24)

$$\begin{aligned} v &= \frac{2e}{h} \frac{1}{\tau} \int_0^\tau \{V_M(t) - \frac{\partial}{\partial t} \oint A_S(x,t) dx\} dt \\ &= \frac{2e}{h} \frac{1}{\tau} \int_0^\tau V_M(t) dt - \frac{2e}{h} \oint \{A_S(x,\tau) - A_S(x,0)\} dx . \end{aligned}$$

When no ac external fields or currents are applied, the flux in the leads and the voltage V_M are periodic in time with period τ . Hence

$$\frac{1}{\tau} \int_0^{\tau} V_M(t) dt = \overline{V_M(t)} \quad \text{and} \quad A_s(x, \tau) = A_s(x, 0)$$

and we obtain

$$v = \frac{2e}{h} \overline{V_M} \quad (1.25)$$

In the simple case of fig. 32 the parallel impedances will contain the capacitive coupling between the wires to the point contact (of order 100 pF). Together with the self-inductance of the wires ($\sim 1 \mu\text{H}$) it forms a low-pass filter with a cut-off frequency of the order 10^8 Hz which is equivalent with a voltage of 0.2 μV according to eq. (1.25). Hence for values higher than 0.2 μV , the measured voltage V_M will in good approximation be constant in time. The important difference with the $\frac{\partial}{\partial t} \oint A_s ds = 0$ case is that now the ac current through the point contact is not sinusoidal as a function of time (§2.1 and §2.2). The radiated frequencies will contain harmonics of the fundamental frequency given by (1.25). The occurrence of the ac Josephson effect was first demonstrated by Shapiro⁶) (1963) and then experimentally investigated by Fiske⁷) (1964); Yanson, Svistuno and Dmitrenko⁸) (1965) and, very intensely, by Eck, Scalapino, Parker, Taylor and Langenberg^{9,10}) (1964-1967). Finnegan, Denenstein and Langenberg¹⁰) confirmed the relation $\overline{V_M} = (h/2e)v$ within 0.12 ppm and found experimentally that $v = 483.59372(6)$ MHz/ μV NBS 69 or $h/2e = 2.0678515(2) \cdot 10^{-15}$ Weber.

Further discussions of the ac and dc Josephson effect will be postponed to the following sections in Part I. Especially their relation with the relevant phenomena, observed in superconducting point contacts, will be emphasized. For simplicity we will assume that the two superconductors are of the same material and at the same temperature. In this case $\Delta\mu = eV$. The more general case will be treated in Part II of this thesis, where the influence of temperature gradients in the superconducting material will be discussed.

There is considerable interest in the intrinsic accuracy of the Josephson frequency-voltage relation (eq. 1.25). The ac Josephson effect establishes a relationship between frequency and electrochemical potential difference ($\Delta\mu^*$) across a Josephson junction by means of the basic relations: $\partial\Delta\phi^*/\partial t = -2\Delta\mu^*/h$ (eq. 1.21). This relation does not involve e . The charge of the free electron e enters in the equations when $\Delta\mu^*$ across the junction is compared with $\Delta\mu^*$ across the voltage standard cell. When these two are equal, no current is flowing through the standard cell and in this case $\Delta\mu^*$ across the cell is defined as eV . A discussion of the general validity of the relation $2eV = h\nu$ and its significance for the measurements of the fundamental constant h/e is given in the introduction of the paper by Finnegan, Denenstein and Langenberg¹⁰). The conclusion is that the value of h/e determined by the Josephson effect is correct within the present measuring accuracy of 0.12 ppm.

There has been a theoretical prediction by Nordtvedt¹⁰⁸) that the value of e in the Josephson equation should be different from the

free-electron charge with an amount of the order of $10^{-10} e$, but Langenberg and Schrieffer ¹⁰⁹⁾ and Hartle, Scalapino and Sugar ¹¹⁰⁾ showed that this conclusion is wrong. According to Stephen ¹¹¹⁾ and Scully and Lee ¹¹²⁾ the coupling of the radiation field with the junction would cause the relation $\nu = 2eV/h$ to be wrong with an amount of the order of $10^{-8} \nu$, but according to McCumber also the electrochemical potential is shifted by this effect so that the relation $h\nu = 2\Delta\mu$ remains correct.

These considerations are of great relevance with respect to the reliability of the new experimental determination of the atomic constants h and e and the fine structure constant $\alpha (\alpha^{-1} = 2\epsilon_0 hc/e^2 = 137.036,1 (2))$ by means of the Josephson effect.

§2 TWO SUPERCONDUCTORS WEAKLY CONNECTED BY A SINGLE SUPERCONDUCTING POINT CONTACT (THE AC JOSEPHSON EFFECT).

Superconducting point contacts have several advantages over the usual evaporated thin film tunnel junctions (superconductor, oxide-layer, superconductor) which are very delicate and extremely sensitive to damage. The point-contact areas are at least four or five orders of magnitude smaller than the areas of the evaporated oxide junctions and hence no single-point contact "diffraction-like" effects^{3,4)} are expected to occur due to the small size of the contacts. Zimmerman and Silver¹²⁾ observed that the interference phenomena persist undiminished up to fields as large as 3000 gauss and even at these fields no diffraction-like attenuation was observed. Furthermore the point contacts have more favourable coupling, capacitive, radiative, mechanical and fabrication properties than evaporated tunnel junctions. Evaporated tunnel junctions have a relatively large shunt capacitance while superconducting point contacts have a relatively large series inductance²⁷⁾. In practice, different types of weak contacts have been used by various physicists⁵¹⁾. Originally Zimmerman and Silver¹²⁾ made weak contacts by pressing two mutually perpendicular niobium wires together in such a way that the contact resistance was between 0.1 and 10 ohm at room temperature. At liquid-helium temperatures the critical current of these contacts varied between zero and 1 mA. However these weak contacts were not reliable and reproducible and later on they constructed weak contacts by means of niobium screws. The contact pressure could then be adjusted from outside the cryostat. Nowadays these authors make weak contacts by mounting a *single* niobium screw in a solid block of niobium²¹⁻²³⁾ (§2.2). These rf biased point contacts (SQUID's) seem to be satisfactorily reliable and reproducible for the application as a magnetometer. The abbreviation SQUID stands for Superconducting Quantum Interference Device, a magnetometer which will be discussed in §2.2.

The construction of reliable and reproducible *double* point contacts is more complicated and forms a part of this research. It will be discussed in §5.2.

Clarke⁵²⁾ and others^{29,30)} employed another technique of dipping a thin niobium wire in molten tinlead solder, whereby a droplet of solder is caused to encircle the niobium wire. After Clarke⁵²⁾, such a device is called a SLUG, which is an abbreviation for Superconducting Low-inductance Undulating Galvanometer, a galvanometer based on the Josephson phenomenon. This will be discussed in §4.7. Depicted in the figs. 4-7 are different types of single and double point contacts as they were used in our laboratory; see also the references^{31,51-59)} and §5.2.

§2.1 THE RESISTIVE-SUPERCONDUCTIVE REGION AND THE CURRENT-VOLTAGE CHARACTERISTIC FOR A SINGLE POINT CONTACT. THE INFLUENCE OF THE AC IMPEDANCE ON THE CURRENT-VOLTAGE CHARACTERISTIC.

The system of two superconductors connected by one point contact is the most simple of all possible weak connections between two superconductors. Nevertheless, it is a complicated system because very small induc-

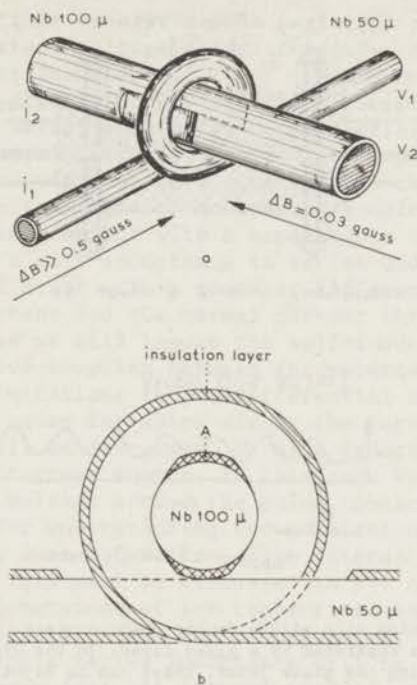


Fig. 4 Top: A double junction made by winding an uninsulated 50μ Nb wire around a 100μ Nb wire, from which the insulation on opposite sides has been partially removed ³¹). The weak contacts are anchored by means of a sealing wax droplet. i_1 and i_2 are the current leads. V_1 and V_2 are the voltage leads.

Bottom: A cross section showing the weak contacts.

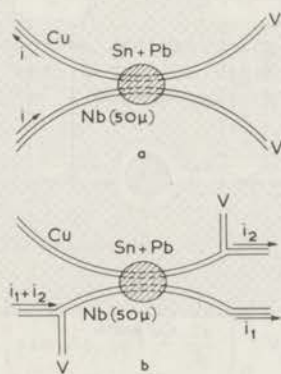


Fig. 5 The Sn-Pb solder droplet junction ^{29,30,52}). i_1 and i_2 are current leads and V voltage leads; i_1 are the additional current leads which can generate a magnetic field in the double junction.

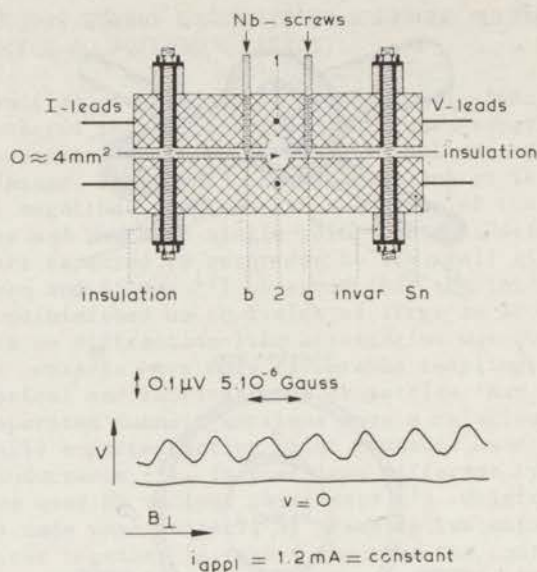


Fig. 7 Cross section of a stable double point contact. The cross-hatched areas represent niobium blocks separated by a glass layer. In the upper block there are two niobium screws penetrating the glass layer. These can be adjusted at room temperature to give a contact resistance of 1 to 10Ω . In order to study the influence of a normal metal in the hole on the $i - \bar{V} - B_{\perp}$ dependence, a copper bar can be pushed into the hole and pulled back out again while the device remains at liquid helium temperatures. For a permanent set-up a thin-walled cylinder of Cu or Pt, fitting tightly in the hole, is baked together with the glass and the niobium to form a solid unit.

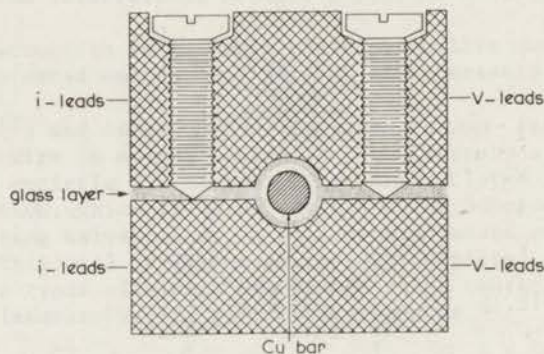


Fig. 6 The cross section of a double point contact with a large area $34(12)15)$ (4 mm^2) used to measure the $\bar{V} - B_{\perp}$ dependence at constant applied current (see §4). The cross-hatched areas represent tin blocks separated by an insulating layer ($10 - 30 \mu$). In the upper tin block there are two niobium screws penetrating the insulation layer. These can be adjusted at room temperature to give a contact resistance of about 1Ω . At the bottom of the figure is shown the measured $\bar{V} - B_{\perp}$ dependence.

tances and capacitances that usually can be neglected play an important role, even in its dc current-voltage characteristics. Also joule heating in the contact can affect the shape of the $\bar{I} - \bar{V}$ characteristic, but we will not deal with this effect in this thesis.

It is necessary to select some models characterising essential theoretical and experimental features ²⁶⁾²⁷⁾³⁴⁾ of a point contact. Stewart ²⁶⁾ performed calculations on a single point contact with a capacitance in parallel with the contact. McCumber ²⁷⁾ calculated the $\bar{I} - \bar{V}$ characteristics of a point contact with a capacitance in parallel and also of a point contact with a self-inductance in series under different circuit conditions. Here we will start with a somewhat different approach ³⁴⁾. At first both the super current and the normal current through the contact will be taken into account and we will ignore the self-inductance of the point contact and the capacitive coupling between the superconductors. Furthermore we will apply certain limitations to the differential equations of the contact. Primarily the two cases for which either the current or the voltage are constants of time will be discussed. We also ignore the impedance of the leads of the voltage or current source. In this case $V_p = V_M$ and we will simply denote V for the voltage across the point contact. This approach appears to be convenient for understanding the modulation in the voltage \bar{V} at constant applied current i as a function of an external magnetic field B_x for a *double* point contact. This will be discussed in §4. As usual, ²⁶⁾²⁷⁾³⁴⁾ we assume that the linear dimensions of the contact are so small that the influence of an applied magnetic field can be neglected. Later on the influence of a shunt capacitance and a series inductance will be discussed ²⁶⁾²⁷⁾.

According to Josephson (eqs. (1.16) and (1.22)), the supercurrent through a single point contact is equal to:

$$i_s(t) = i_1 \sin \Delta\phi^*(t) = i_1 \sin \left\{ \Delta\phi^*(0) - \frac{2e}{\hbar} \int_0^t V(t') dt' \right\}. \quad (2.1)$$

If the junction is brought into the resistive-superconductive region ($V(t) \neq 0$), a normal current also has to be taken into account. As mentioned in the introduction we will assume that this normal current $i_n(t)$ is equal to

$$i_n(t) = \frac{V(t)}{R_n}, \quad (2.2)$$

in which R_n is the ideal ohmic resistance of the junction. The total current is equal to

$$i(t) = i_s + i_n = i_1 \sin \left\{ \Delta\phi^*(0) - \frac{2e}{\hbar} \int_0^t V(t') dt' \right\} + \frac{V(t)}{R_n}. \quad (2.3)$$

We first take V as a constant in time. The integral can then easily be evaluated and gives:

$$i(t) = i_1 \sin \left\{ \Delta\phi^*(0) - \frac{2e}{\hbar} Vt \right\} + V/R_n. \quad (2.4)$$

If $V = 0$, this expression reduces to $i = i_s = i_1 \sin \Delta \phi^*(0)$, thus any dc current between $-i_1$ and $+i_1$ can flow through the junction. If $V \neq 0$, then $i_s(t)$ is the sinusoidal ac Josephson current at a frequency $\nu = (2e/h)V$ (eq. (1.23)) and an amplitude i_1 . The time average of $i_s(t)$ is equal to zero and only the normal component contributes to the dc current. The $\bar{i} - \bar{V}$ characteristic which is measured with dc or low-frequency methods can be described with:

$$V = 0, \quad 0 \leq \bar{i}(t) \leq i_1 \quad (2.5a)$$

$$V \neq 0, \quad \bar{i}(t) = V/R_n \quad (2.5b)$$

and is given in fig. 8a.

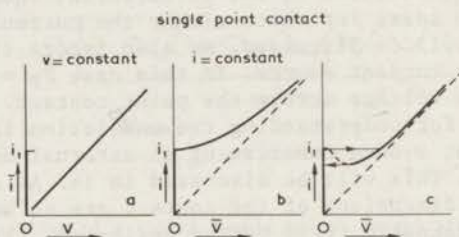


Fig. 8 The current-voltage characteristic of a single point contact

- a) When the voltage is constant in time (eq. (2.5))
 b) When the current is constant in time (eq. (2.9))
 c) When there is a capacitance in parallel with the junction, and a self-inductance and resistance in series with the point contact. Due to a combination of ac impedances, connected to the point contact, the $\bar{i} - \bar{V}$ characteristic can be very non-linear.

Now we take $i(t)$ constant in time in eq. (2.3) and calculate $\bar{V}(t)$. With eq. (1.22) we obtain

$$\begin{aligned} i &= i_1 \sin \Delta \phi^*(t) + \frac{V(t)}{R_n} = \\ &= i_1 \sin \Delta \phi^*(t) - \frac{1}{R_n} \frac{\hbar}{2e} \frac{\partial \Delta \phi^*(t)}{\partial t} = \text{constant}. \end{aligned} \quad (2.6)$$

The analytical solution of this equation is given by Aslamazov and Larkin (60). When $i > i_1$, then $V(t)$ is a periodic function of $\Delta \phi^*(t)$ with period 2π . The voltage derived from this equation is a sharply peaked function of time, especially when i is only slightly larger than i_1 (see fig. 9). The peak height is equal to $2i_1 R_n$ and the width is of the order $(\hbar/2e)/(i_1 R_n)$. With a typical value $i_1 R_n \approx 200 \mu\text{V}$ this gives 10^{-2} ns. Furthermore we derive from eq. (2.6)

$$t = \frac{1}{R_n} \frac{\hbar}{2e} \int_{\Delta \phi^*(0)}^{\Delta \phi^*(t)} \frac{-d\Delta \phi^*}{i - i_1 \sin \Delta \phi^*};$$

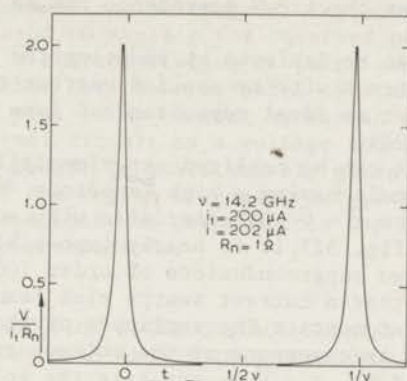


Fig. 9 Time dependence of the voltage across a point contact when the current i through the junction is constant in time. From this figure the time dependence of the normal current $i_n(t) = V(t)/R_n$ can easily be obtained. The supercurrent $i_s(t)$ can be obtained from $i_s(t) = i - i_n(t)$. The signal is sharply pulsed and therefore there are strong harmonics. The time average of this voltage as a function of i is given in fig. 8b.

hence

$$\frac{1}{v} = \tau = \frac{1}{R_n} \frac{\hbar}{2e} \int_0^{-2\pi} \frac{-d\Delta\phi^*}{i - i_1 \sin\Delta\phi^*}, \quad (2.7)$$

in which v is the fundamental frequency of the complete signal belonging to the mean voltage $\overline{V(t)}$. The time average of the voltage is equal to the time average in one period, hence

$$\overline{V(t)} = \frac{1}{\tau} \int_0^{\tau} V(t) dt = v \frac{\hbar}{2e} \int_0^{\tau} \frac{-\partial\Delta\phi^*}{\partial t} dt = \frac{\hbar}{2e} v. \quad (2.8)$$

Which is again eq. (1.25).

Substituting eq. (2.7) in eq. (2.8) gives:

$$i > i_1, \quad \overline{V(t)} = \frac{2\pi R_n}{\int_0^{-2\pi} \frac{-d\Delta\phi^*}{i - i_1 \sin\Delta\phi^*}} = R_n \sqrt{i^2 - i_1^2}. \quad (2.9a)$$

For the values of i between 0 and i_1 we obtain:

$$0 \leq i \leq i_1, \quad \overline{V(t)} = 0. \quad (2.9b)$$

From these two equations the $\bar{i} - \bar{V}$ dependence can be calculated and is given in fig. 8b.

Voltage biasing can be achieved by shunting the junction with a parallel ideal resistance R with an applied current through R much larger than i_1 (see ref. 13) or an ideal capacitance C (see below, eq. (2.10) and also refs. 26 and 27).

A constant current can be realized experimentally if one applies the current with a circuit having a high impedance^{34,27}). However if one tries to measure the $\bar{i} - \bar{V}$ characteristic with such a constant-current circuit (e.g. fig. 32) it is nearly impossible to avoid capacitive coupling between the two superconductors of order 100 pF.

We will now show that a current source plus leads may act as a voltage source on the point contact. The amplitude of the ac current is of the order of i_1 . Hence the ac component of the voltage across the capacitance $V_{ac} \approx i_1/(2\pi\nu C)$. Now if $V_{ac} \ll \bar{V}$ we can take the voltage as constant in time, hence

$$V \equiv \bar{V} + V_{ac} \approx \bar{V} > > \frac{i_1}{2\pi C} \frac{1}{\nu} = \frac{i_1}{2\pi C} \frac{h}{2eV}$$

or

$$(iR_n)^2 = \bar{V}^2 > > \frac{h}{2e} \frac{i_1}{2\pi C} \quad (2.10)$$

Situations can occur where $i < i_1$ and (2.10) is still satisfied, if

$$(i_1 R_n)^2 > (iR_n)^2 > > \frac{h}{2e} \frac{i_1}{2\pi C}$$

hence $i_1 R_n^2 > > \frac{h/2e}{2\pi C}$ or $\beta_c > > 1$, with $\beta_c = \frac{2\pi i_1 R_n^2}{h/2e} C$.

In this case there are at least two solutions for eq. (2.11), namely one with $\bar{V} > 0$ satisfying (2.10), and one with $V = 0$. This shows the physical significance of the parameter β_c introduced by McCumber. When β_c is large (with the typical values of $i_1 = 100 \mu A$, $R_n = 1 \Omega$, and $C = 100$ pF, the value of $\beta_c = 30$), a current source shunted by a capacitance acts like a voltage source on the point contact. Stewart and McCumber^{26,27}) have performed more detailed computer calculations on the system of a point contact with a capacitance C in parallel driven by a constant-current circuit. They both solve the equation

$$i = C \frac{dV(t)}{dt} + \frac{V(t)}{R_n} + i_1 \sin \Delta\phi(t) = \text{constant} . \quad (2.11)$$

McCumber²⁷) also performed calculations on a point contact in series with a self-inductance while the system is voltage biased. Again for values of \bar{i} between i_1 and a certain value $\alpha_c i_1$, (where $0 < \alpha_c < 1$), two solutions for V are possible: $V = 0$ and $V > 0$. The value of α_c depends on a characteristic value $\beta_L \equiv (h/2e)/(2\pi Li_1) \equiv 1/(2\mathcal{L})$. Decreasing \bar{i} from values $\bar{i} > i_1$ the transition to $V = 0$ at $\bar{i} = i_1 \alpha_c$ is continuous with $dV/d\bar{i}$ finite at $V \neq 0$ (except when $\beta_L = 0$). Both parameters β_L and β_c are temperature dependent because i_1 is temperature dependent. The fact that the $\bar{i} - \bar{V}$

characteristic depends on the temperature-dependent values of β_L and β_C probably can be used to explain the observed temperature dependence of the observed $\bar{i} - \bar{V}$ characteristics of point contacts. The calculations of Stewart and McCumber have been extended to a more realistic model of an external circuit plus point contact by Warman and Blackburn⁶¹). They represent the external circuit by a voltage source in a series with a resistance. A typical result is qualitatively given in fig. 8c. The hysteresis (a consequence of the region of negative resistance) is often observed in point contacts especially at temperatures far below the critical temperature of the superconductors.

§2.2 A SINGLE SUPERCONDUCTING POINT CONTACT SHUNTED IN PARALLEL WITH A SUPERCONDUCTOR OR A LOW-RESISTANCE NORMAL CONDUCTOR.

Zimmerman and Silver²¹⁻²³) have performed experiments on a superconducting point contact shunted in parallel with a superconductor (pure self-inductance L) or with a low-resistance copper shunt from which the resistance R can be neglected compared with its self-inductance L when high-frequency techniques are used ($\omega L \gg R$)²¹⁾²³).

Especially a device (SQUID) where the self-inductance and the point contact form a closed loop has got great attention because of its simple reliable way of construction. The self-inductance is a solid "C"-shaped block of superconducting material (niobium), supporting a screw that closes the "C" and forms the weak contact (see fig. 10b). These devices are mechanically rigid while the adjustment of the point contact does not change due to thermal cycling because the screw and the block are made out of the same material. Hence there is no stress in the sample due to differences in the thermal expansion in the device. Both the mechanical and thermal properties make it sufficiently reliable and reproducible to use it as a magnetometer. In order to understand the behaviour of these devices we apply Kirchoff's law to the circuit of fig. 10a.

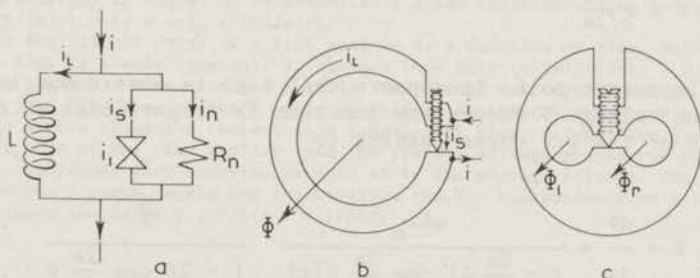


Fig. 10a) A circuit representing a point contact (carrying a supercurrent i_s and a normal current i_n) in parallel with a pure self-inductance L (carrying a current i_L).

b) Schematic drawing of a single-loop SQUID. A solid superconducting ring supports the niobium screw.

c) Schematic drawing of a double-loop SQUID.

$$L \frac{di_L}{dt} = \frac{d\phi(t)}{dt} = + V = \frac{-\hbar}{2e} \frac{\partial \Delta\phi^*(t)}{\partial t} \quad (2.12)$$

in which ϕ is the magnetic flux in the self-inductance. When $\Delta\phi^*$ changes by some reason from 0 to 2π during a time τ then the change in magnetic flux is equal to

$$\int_0^\tau \frac{d\phi}{dt} dt = \Delta\phi = \frac{\hbar}{2e} \int_0^{2\pi} \frac{\partial \Delta\phi^*}{\partial t} dt = \frac{\hbar}{2e}.$$

This means that the change of the flux in L is equal to one flux quantum, independent of whether L is a superconductor or not and also independent of whether a normal current (resistance R_n) flows through the point contact or not. In order to understand how the system under discussion behaves, we neglect the normal current in the point contact (R_n infinitely large) and take a current i linearly increasing in time: $i = i_0 \omega t$. This total current is equal to

$$i = i_0 \omega t = i_s + i_L = \frac{\phi(t)}{L} - i_1 \sin \frac{2e}{\hbar} \phi(t), \quad (2.13)$$

where we have used $\Delta\phi^* = -\frac{2e}{\hbar} \phi(t)$.

From eq. (2.13), $\phi(t)$ can be obtained as a function of time by graphical methods. In the solution of eq. (2.13), the value of the parameter \mathcal{L} defined by

$$\mathcal{L} \equiv \frac{\pi Li_1}{h/2e} \quad (2.14)$$

plays an important role. It appears that $\phi(t)$ is continuous in time when $2\mathcal{L} < 1$. The voltage V across the junction is proportional to the first derivative of the ϕ - t curve leading to

$$V = \frac{d\phi}{dt} = \frac{\omega Li_0}{1 - \frac{2e}{h} Li_1 \cos \frac{2e}{h} \phi(t)} \frac{\bar{V}}{1 - 2\mathcal{L} \cos \frac{2e}{h} \phi}$$

where $\bar{V} = i_0 \omega L$ is the time average of the voltage across the point contact. When $2\mathcal{L} > 1$, then ϕ is not a continuous function of time (fig. 11a). At values of ϕ_1 with $2\mathcal{L} \cos\{(2e/h)\phi_1\} = 1$ a discontinuous transition takes place and ϕ_1 jumps to a certain value ϕ_2 (fig. 11b). This jump corresponds to a δ peak in the voltage (see fig. 11c) equal to: $(\phi_2 - \phi_1)\delta(t)$.

In the limit $2\ell \gg 1$ the jump occurs when i_s is equal to the critical current i_1 (because $\cos \Delta\phi_1^* \approx 0$) of the junction while $\phi_2 - \phi_1$ is almost equal to $h/2e$. This means that a flux quantum is trapped in L every time the critical current is reached in the point contact. The jumps are somewhat less than a flux quantum. Between two jumps the flux in the hole is almost constant (much smaller than a flux quantum), while the voltage across the system is almost zero (much smaller than the average voltage $\bar{V} = i_0 \omega L$). The current through the point contact is essentially a sawtooth. An example of the time dependences of ϕ , V and i_s is given in fig. 11. The observed ac phenomena can also be explained in good approximation by assuming flux quantization in the hole.

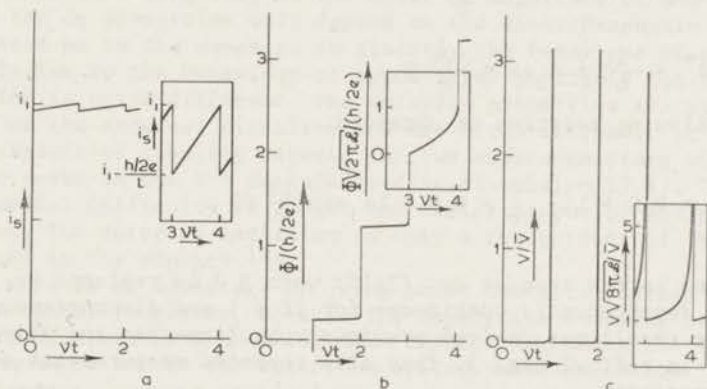


Fig. 11 Time dependences of i_s , ϕ and V of a single-loop SQUID (fig. 10a, b) with $\ell = 100$. The preamble phenomena are not shown. The jumps occur with a frequency $\nu = \bar{V}/(h/2e)$ where $\bar{V} = i_0 \omega L$. An external current $i = \omega t i_0$ is applied.

a) Supercurrent i_s as a function of time. The changes in i_s are very small. The peak to peak amplitude is approximately $(h/2e)/L = (\pi/\ell)i_1 \approx 0.03 i_1$. The insert gives $i_s - t$ on a larger i_s scale. It is essentially a saw tooth according to $i_s = i_1 - (1 - \nu t)(h/2e)/L = i_1 + \omega t i_0 - (h/2e)/L$.

b) Flux in the hole in units of a flux quantum as a function of time. Between two jumps the flux is almost constant. It changes then only $(h/2e)/\sqrt{(2\pi\ell)} \approx 0.04 h/2e$. The insert gives $\phi - t$ on a larger ϕ scale. The change is proportional to $(h/2e) \times \sqrt{1 - \nu t} / \sqrt{2\pi\ell}$. The zero of the ϕ scale is shifted an integral number of times $h/2e$.

c) Voltage across the point contact as a function of time. Between two jumps the voltage is most of the time smaller than the average voltage across the point contact. The continuous part contributes only 4% to the average voltage. The rest comes from the δ peaks. Again the insert gives the $V - t$ dependence on a larger scale. Between two peaks $V \approx V/\{(1 - \nu t)\sqrt{8\pi\ell}\}$.

As large voltages are involved in this system, the normal current in the point contact also can play an important role in determining the behaviour of the system. Taking the normal current into account, eq. (2.13) becomes a second order differential equation and we cannot describe the behaviour of the system in simple physical terms. However we believe that the general features remain unchanged, namely that periodically a flux quantum is trapped in L , that this occurs at values of $i_s \approx i_1$ and that the trapping of flux is accompanied with voltage peaks.

Instead of applying a current linearly increasing in time, Zimmerman and Silver ²¹⁾²³⁾ studied the system of a point contact shunted in parallel with a self-inductance (SQUID) by putting the coil of a tank circuit in the hole. A radio-frequency current equal to $i_0 \sin \omega t$ is then applied on the tank circuit. The rectified voltage across the tank circuit depends on the amount of energy dissipated in the SQUID per cycle. For a constant value of i_0 this rectified voltage is observed to be periodic in the externally applied magnetic field with a period $(h/2e)/\phi$.

In order to get meaningful results about the static behaviour of the system, L has to be a superconductor. The flux ϕ in L is then equal to the sum of an applied flux $B_1 0$ and the self-induced flux $\phi_s = Li_{\text{circ}} = -Li_1 \sin \Delta\phi^*$, (see later on §3). From the single valued nature of the wave function one obtains

$$\Delta\phi^* = \frac{-2e}{h} \oint A_s ds = \frac{-2e}{h} \phi .$$

Thus the following relation is obtained:

$$\phi = B_1 0 + Li_{\text{circ}} = B_1 0 + Li_1 \sin\left(\frac{2e}{h} \phi\right) . \quad (2.15)$$

This equation is the same as eq. (2.13) when $B_1 0$ is replaced by $i_0 \omega t L$. The $\phi - B_1 0$ dependence is continuous for $2f \leq 1$ and discontinuous when $2f > 1$. This result was derived previously by Zimmerman and Silver ²²⁾²³⁾ and resumed in ref. 23 fig. 3. They also reported measurements of the $\phi - B_1 0$ dependence.

The mechanism responsible for the choice of the quantum state when a cylinder is cooled through its transition temperature with a magnetic field B_1 applied on the enclosed area 0 can probably be understood from the f dependence of the solutions of eq. (2.15). When $T \leq T_c$, then $f \ll 1$ and the field will penetrate almost completely. When the temperature is decreased, i_1 will increase and $2f$ will become of the order one. Solving eq. (2.15) now gives that a circulating current flows in the sample. The flux quantization is still incomplete and there is only one solution of the $B_1 0 + \phi_s$ versus $B_1 0$ dependence. The final number of flux quanta trapped in 0 can be found by continuously increasing f with a fixed $B_1 0$ value. It appears that the solutions for the total $B_1 0 + Li_{\text{circ}}$ tend to $nh/2e$ in which n has such a value that $|i_{\text{circ}}|$ is the smallest possible value which satisfies eq. (1.1) (fig. 1b).

Devices where the point contact is shunted by more than one superconducting loop are also of experimental interest ²³⁾⁵¹⁾. An example is given in fig. 10c. The formula corresponding to eq. (2.15) gives the flux ϕ_r in the right-hand-side hole:

$$2\phi_r = (L + M) i_1 \sin \frac{2e}{h} (\phi_r + B_1 0) .$$

Here $B_1 0$ is the flux applied to the right-hand-side hole, L is the self-

inductance of the hole and M is the mutual inductance between the two holes. The flux Φ_2 in the other hole is given by the condition that the sum of fluxes in both holes is constant.

§2.3 MICROWAVE EMISSION AND ABSORPTION FROM SUPERCONDUCTING POINT CONTACTS AND THE CONSTANT-VOLTAGE STEPS IN THE DC CURRENT-VOLTAGE CHARACTERISTIC.

In the previous sections it has been shown that the current or voltage of a point contact are strongly time dependent. From eq. (1.25) one obtains that a dc voltage of $1\mu\text{V}$ across the contact corresponds to a frequency of 483.6 MHz. Consequently a point contact will emit radiation with a frequency of the order of magnitude of 500 MHz. Furthermore the dc properties will depend on the electromagnetic radiation radiated on to the contact. In general, the behaviour of point contacts is similar to the behaviour of oxide layer junctions but the antenna problem is quite different. The emission properties are strongly dependent on the external circuitry and are often difficult to calculate. The capacitive coupling between the two superconductors will flatten sharp peaks in the V - t dependence (see discussion §2.1). The main experimental difficulty is to get the radiation out of the point-contact region. The detected radiation is only a few percent of the power generated in the contact¹³).

Here is an advantage in using point contacts instead of oxide-layer tunnel junctions, because the capacitive coupling between the two superconductors is smaller for point contacts and hence the radiation can be coupled better to the detection system. When radiation is supplied to the contact, current steps of constant voltage can be observed in the dc current-voltage characteristic at values $V = (n/m)(h/2e)$ (n and m are here integers). These steps can be understood theoretically by considering a voltage-biased case in which a small ac voltage with amplitude v is superimposed on the dc voltage V_0 (and $v \ll V_0$) in the following elementary way: $V(t) = V_0 + v \cos \omega t$.

The time dependence of phase difference $\Delta\phi^*(t)$ is given by

$$\begin{aligned} \Delta\phi^*(t) &= \Delta\phi^*(0) - \frac{2e}{h} \int_0^t V(t') dt' = \\ &= \Delta\phi^*(0) - \frac{2e}{h} \int_0^t (V_0 + v \cos \omega t') dt' = \\ &= \Delta\phi^*(0) - \frac{2e}{h} V_0 t - \frac{2e}{h} \frac{v}{\omega} \sin \omega t \end{aligned}$$

and the supercurrent by

$$i_s(t) = i_1 \sin \left[\Delta\phi^*(0) - \frac{2e}{h} V_0 t - \frac{2e}{h} \frac{v}{\omega} \sin \omega t \right] .$$

When $v \ll V_0$ one gets:

$$i_s(t) = i_1 \sin(\Delta\phi^*(0) - \frac{2e}{h} V_0 t) - i_1 \frac{2e}{h} \frac{v}{\omega} \sin \omega t \cdot \cos(\Delta\phi^*(0) - \frac{2e}{h} V_0 t).$$

The time average of the first term is equal to zero, hence the time average of $i_s(t)$ is equal to the time average of the second term, which is unequal to zero only when $(2e/h)V_0 = v$, (with $\omega = 2\pi\nu$). The magnitude of

$$\overline{i_s(t)} = -\frac{1}{2}(v/V_0) i_1 \sin \Delta\phi^*(0)$$

can be varied by varying $\Delta\phi^*(0)$. In this way the current steps at constant voltage are explained. For a general calculation see ref. 113. Current steps at constant voltage have been observed many times in single point contacts, for example by Parker et al. 10) and by Grimes et al. 25, 24) (see also §4.5). Shapiro 52) has observed them in droplet junctions which behave very similarly to point contacts. Detailed analog computer studies of the Josephson radiation effects have been reported by Werthamer and Shapiro 62), and Sullivan and Zimmerman 113).

Fig. 24 shows a contact placed in the center of the bottom of a coaxial cavity. In §4.5 the influence of its resonant electromagnetic radiation field is discussed. Fig. 25 shows the observed current steps at constant voltage.

§2.4 APPLICATIONS: RADIO-FREQUENCY, MICROWAVE AND FAR-INFRARED SPECTROSCOPY, NOISE THERMOMETRY AND VOLTAGE STANDARDS. THE DETERMINATION OF THE FLUX QUANT.

Both the ac properties and the non linearity of the dc current-voltage characteristic can be employed to construct a detection or measuring instrument from a point contact. The possible applicability has been proposed by several authors 1, 24, 25).

The most direct application is the use of point contacts to measure the quantity $h/2e$ by measuring the voltage across the junction and the frequency of the radiation absorbed (or emitted) by the contact. In the experiment of Parker, Taylor, Finnegan, Denestein and Langenberg 10) it appeared that $2e/h = 483.59372(6)$ MHz/ μ V. Clarke shunted two droplet junctions 52) in parallel and observed that no current flowed in the circuit when both junctions were exposed to the same radiation and biased in the corresponding constant-voltage steps. From his observation he concluded that the values of $h/2e$ are the same for two different superconductors within 0.01 ppm. This high degree of accuracy is possible because the Josephson relation $h\nu = 2\Delta\bar{\pi}^*$ is a direct relationship between the frequency and time averaged electrochemical potential difference $\Delta\bar{\pi}^*$ across the junction. In a superconducting circuit the only change in $\bar{\pi}^*$ occurs at the junction. The value of $\bar{\pi}^*$ is con-

stant everywhere else even when different materials are used or when there are temperature gradients (see also Part II).

Voltage-biased point contacts can probably be used as voltage standards, by defining the value $h/2e$ and using eq. (1.25). The unknown voltage is measured by determining the frequency ν of the emitted radiation. By this technique several orders of magnitude can be gained in accuracy because frequencies can be measured within 1 part in 10^{10} while voltages are only known within 1 ppm ¹⁰). According to eq. (1.25), a voltage of $2 \cdot 10^{-15}$ volt across the contact gives rise to a frequency of the order of 1 Hz, so that voltages of this order of magnitude can be measured. This result can be compared with the accuracy of the other voltage measurement devices discussed in §4.7.

Zimmerman and Silver showed a possible application of point contacts in radio-frequency spectroscopy by coupling a voltage biased point contact to Co 59 ¹⁸). Used as a spectrometer, the point contact is shown to be a continuously tunable ultra-low power oscillator-detector from 1 to $3 \cdot 10^8$ Hz. It appeared that the frequency limit could be extended to the superconducting gap frequency.

Zimmerman, Silver and Kamper ¹⁹) showed still another possibility to use point contacts namely by shunting a point contact with a small resistance R and applying a dc current on this circuit. In this case the voltage across the contact is approximately constant apart from an additional random voltage due to thermal noise in the resistance. The mean square of this voltage $\bar{V}_n^2 = 4kTR\Delta\nu$ (Nyquist theorem) where k is the constant of Boltzman, T the absolute temperature, R the resistance and $\Delta\nu$ a cutoff frequency, which is in general a geometric constant. The line width of the emitted radiation is now temperature dependent and this property enables one to measure the temperature.

As the $\bar{i} - \bar{V}$ characteristic is non-linear, the shape of the dc characteristic is changed when ac currents flow through the contact. This property can be used to detect electromagnetic radiation. By properly biasing the contact, the change in the dc voltage can be made roughly proportional to the amplitude of the applied radiation, hence it is possible to get the amplitude of the unknown applied radiation in arbitrary units. Grimes et al. ²⁵) showed that such a point-contact device can be used to detect radiation in the far-infrared region even when the frequency is beyond the superconducting energy gap. The measurement of the frequency of an unknown ac signal can be performed by measuring the current steps at constant voltage in the dc $\bar{i} - \bar{V}$ characteristic ^{10),11),25}).

§3 THE CRITICAL CURRENT THROUGH A DOUBLE POINT CONTACT BETWEEN TWO SUPERCONDUCTORS AS A FUNCTION OF THE APPLIED MAGNETIC FIELD.

The critical current i_c is defined as the maximum current that can flow through a double point contact without any voltage appearing across the junction. Therefore neither the calculations nor the measurements are complicated by shunt capacitances or inductances in the current supply. This makes the comparison between theory and experiment rather easy. Furthermore, the $i_c - B_1$ dependence corresponds roughly with the $\bar{V} - B_1$ dependence at constant applied current $i > i_c$. This property can be used to check theoretical results on the $i_c - B_1$ dependence by measuring the $\bar{V} - B_1$ dependence (see the discussion in §4).

The critical current i_c of a double point contact between two superconductors is a function of the magnetic field B_1 , applied perpendicularly to the enclosed area O between the contacts. This is a consequence of the fact that the phase differences across the two weak contacts are related to the enclosed magnetic flux in the following way (see fig. 6):

$$\oint d\phi = n2\pi = 0 = \Delta\phi_a - \Delta\phi_b + \frac{2e}{h} \oint_s^* A_s ds$$

(\oint_s^* = junctions excluded) in which

$$\Delta\phi_a \equiv (\phi_2 - \phi_1)_a \text{ and } \Delta\phi_b \equiv (\phi_2 - \phi_1)_b$$

are the phase differences across the weak contacts a and b respectively. The phase differences inside the bulk superconductors (1) and (2) are found by integrating eq. (1.8) around the hole (junctions excluded). The wave function is single valued, hence the line integral of $\vec{\nabla}\phi$ along the closed loop is equal to $n2\pi$. Without loss in generality we take $n = 0$. The gauge-invariant phase differences $\Delta\phi^*$, as defined by eq. (1.18), thus differ by $2e/h$ times the total enclosed magnetic flux³⁴):

$$\Delta\phi_b^* - \Delta\phi_a^* = \frac{2e}{h} \oint_s A_s ds \quad (\oint_s = \text{junctions included}). \quad (3.1)$$

§3.1 TWO SUPERCONDUCTORS WEAKLY COUPLED BY A DOUBLE POINT CONTACT WHEN THE SELF-INDUCED FLUX IN THE ENCLOSED AREA IS IGNORED ($\oint_s A_s ds = B_1 O \neq nh/2e$).

In order to show some of the essential features of a double junction we shall first ignore the self-induced flux in the area O . The total flux in O is then equal to the applied flux $\oint_s A_s ds = B_1 O$ and in general is not equal to an integral number of flux quanta. Hence from eq. (3.1) it follows that:

$$\Delta\phi_b^* = \Delta\phi_a^* + \frac{2e}{h} B_1 O. \quad (3.2)$$

The total current through the double junction is equal to the sum of the currents through the individual contacts.

$$i(B_{\perp}, \Delta\phi_a^*) = i_1 \sin\Delta\phi_a^* + i_2 \sin\Delta\phi_b^* = \\ = i_1 \sin\Delta\phi_a^* + i_2 \sin(\Delta\phi_a^* + \frac{2e}{h} B_{\perp} 0).$$

The maximum of $i(B_{\perp}, \Delta\phi_a^*)$ with respect to $\Delta\phi_a^*$ is equal to the critical current of the junction, hence:

$$i_c(B_{\perp}) = \sqrt{(i_1 - i_2)^2 + 4i_1 i_2 \cos^2 \frac{e}{h} B_{\perp} 0}. \quad (3.3)$$

When $i_1 = i_2$ this equation reduces to $1)5)46)63)$:

$$i_c(B_{\perp}) = 2i_1 \left| \cos \frac{e}{h} B_{\perp} 0 \right|. \quad (3.4)$$

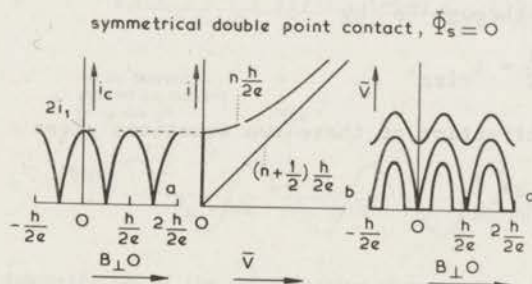


Fig. 12a) The critical-current oscillations as a function of the applied magnetic flux $B_{\perp} 0$ in an area 0 for a symmetrical double point contact when the self-induced flux is ignored ($\Phi_s = 0$).

b) Two $\bar{I} - \bar{V}$ characteristics ($i(t) = i = \text{constant}$). One at an applied flux $n \frac{h}{2e}$ and one at $(n + \frac{1}{2}) \frac{h}{2e}$. When the applied flux is not equal to one of these values the $\bar{I} - \bar{V}$ characteristic lies between these two curves.

c) Voltage oscillations at several applied currents which are constant both with respect to time and magnetic field. The current values are $2/3$, 1 and $4/3$ times $2i_1$ respectively.

This relationship is represented in fig. 12a. One of the significant features of this $i_c - B_{\perp} 0$ dependence is that $i_c = 0$ when $B_{\perp} 0 = (n + \frac{1}{2}) \frac{h}{2e}$ ($n = \text{integer}$). However this result has never been observed. This might be due to an asymmetry (eq. (3.3)), but the main reason is most likely the self-induced flux in 0 which we ignored. This will be discussed in §3.3.

§3.2 TWO SUPERCONDUCTORS STRONGLY COUPLED BY A DOUBLE POINT CONTACT

$$\oint_{\mathcal{S}} \mathbf{A}_s \cdot d\mathbf{s} = B_1 0 + Li_{\text{circ}} = nh/2e.$$

When the two superconductors are so closely connected that they can be considered as one superconductor (having a hole), fluxoid quantization holds (eq. (1.10)). When $\mathbf{v}_s = 0$ everywhere in the integration loop, one obtains from eq. (1.11)

$$\begin{aligned} \oint_{\mathcal{S}} \mathbf{A}_s \cdot d\mathbf{s} &= B_1 0 + Li_{\text{circ}} = nh/2e, \\ i_{\text{circ}} &= \frac{1}{L} \left(n \frac{h}{2e} - B_1 0 \right). \end{aligned} \quad (3.5)$$

Due to flux conservation the applied current i divides equally between both contacts of the symmetrical double junction. The circulating current adds to the applied current in one of the contacts (a) and subtracts from the other (b). The total current through point contact "a" is given by

$$i_a = \frac{i}{2} + i_{\text{circ}} \quad (3.6)$$

and the current through "b" by

$$i_b = \frac{i}{2} - i_{\text{circ}}. \quad (3.7)$$

Addition and subtraction of these two equations gives

$$i = i_a + i_b \quad (3.8)$$

and

$$2i_{\text{circ}} = i_a - i_b. \quad (3.9)$$

Suppose that through each contact a certain maximum supercurrent can flow and that for instance its critical value i_1 is determined by the Silsbee⁶⁴⁾ or Ginzburg-Landau³⁹⁾ value. When the applied current i is increased from zero the critical current is reached when the total current through one of the contacts (a), in which the applied current and the circulating current have the same direction, reaches its critical current value i_1 , hence $\frac{1}{2}i_c + |i_{\text{circ}}| = i_1$. Here it is assumed that the junction is symmetrical, that L is independent of the currents and that $2i_1 > (h/2e)/L$. The critical current is equal to³⁴⁾:

$$i_c = 2i_1 - 2|i_{\text{circ}}| = 2i_1 - \frac{2}{L} \left| n \frac{h}{2e} - B_1 0 \right|, \quad (3.10)$$

in which n is an integer determined by the condition that i_c is a maximum with respect to n but smaller than or equal to $2i_1$. The $i_c - B_1$ dependence described by eq. (3.10) is symmetric with respect to $B_1 = 0$

and is given in fig. 1 together with the total flux in Φ and $L i_{\text{circ}}$ as a function of B_1 . These results apply to a symmetrical double junction. However when $i_1 \neq i_2$ the curve representing the $i_c - B_1$ dependence is shifted along the B_1 axes by an amount $L|i_1 - i_2|/0$ with respect to the curve $|-i_c| - B_1$ ³³, which is obtained by reversing the direction of the applied current (the magnetic field being in the same direction). When an ac current is applied on such an asymmetrical double junction a dc voltage can appear across it, even though the applied dc current is equal to zero ³³ (see fig. 13).

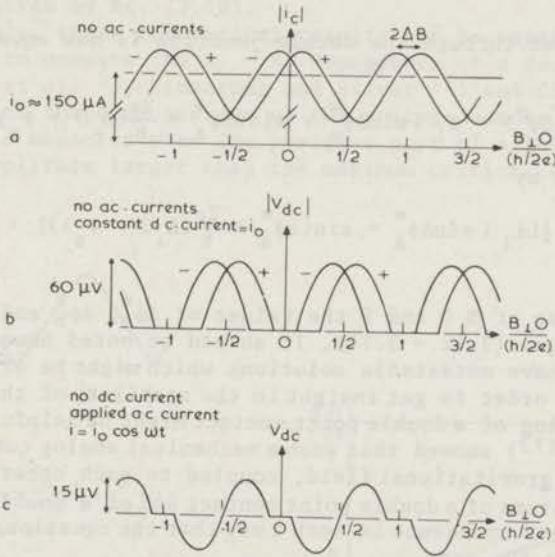


Fig. 13 A demonstration of the rectification process of an asymmetrical double junction.

a) Schematic drawing of the critical current as a function of the applied flux in the absence of ac currents (no rf signals).

+ = critical current in the positive direction

- = critical current in the negative direction

The total shift of the two curves is equal to $L|i_1 - i_2|(2e/h)/0$. The points of intersection are situated at $B_1 O / (h/2e) = \frac{1}{2}m$ (m integer).

b) The measured dc voltage at constant dc current = i_0 , applied in the positive (+) and negative (-) directions, in the absence of ac currents.

c) The observed rectified dc voltage when an ac current with amplitude i_0 is applied in the absence of a dc current.

§3.3 TWO SUPERCONDUCTORS WEAKLY COUPLED BY A SYMMETRICAL DOUBLE POINT CONTACT WHEN THE SELF-INDUCED FLUX IN THE ENCLOSED AREA IS TAKEN INTO ACCOUNT ($\oint_{S_s} A_s ds = B_1 O + L i_{\text{circ}} \neq nh/2e$).

When the currents through the individual contacts in a symmetrical double junction are unequal due to an applied magnetic flux $B_1 O$ it follows from eq. (3.9) that a *self-induced flux*

$$\phi_s \equiv Li_{\text{circ}} = \frac{1}{2}L(i_a - i_b) = \frac{1}{2}Li_1(\sin\Delta\phi_a^* - \sin\Delta\phi_b^*) \quad (3.11)$$

has to be added to the applied flux $B_1 0$. The total enclosed magnetic flux is equal to $\oint_s A_s ds = B_1 0 + Li_{\text{circ}}$. This is in general *not* equal to an integral number of flux quanta. It follows from eq. (3.1) that

$$\Delta\phi_b^* = \Delta\phi_a^* + \frac{2e}{h} (B_1 0 + \phi_s). \quad (3.12)$$

The total current through the double junction is now equal to

$$i(B_1, \Delta\phi_a^*) = i_1 [\sin\Delta\phi_a^* + \sin\{\Delta\phi_a^* + \frac{2e}{h}(B_1 0 + \phi_s)\}] \quad (3.13)$$

and ϕ_s is given by

$$\phi_s = \frac{1}{2}Li_1 [\sin\Delta\phi_a^* - \sin\{\Delta\phi_a^* + \frac{2e}{h}(B_1 0 + \phi_s)\}] \quad (3.14)$$

For given values of $B_1 0$ and i the values of $\Delta\phi_a^*$, $\Delta\phi_b^*$ and ϕ_s can be calculated from eqs. (3.12 - 3.14). It should be noted however that eqs. (3.12 - 3.14) have metastable solutions which might be of no practical importance. In order to get insight in the stability of the solutions a mechanical analog of a double point contact might be helpful. Sullivan and Zimmerman¹¹³⁾ showed that such a mechanical analog consists of two pendulums in a gravitational field, coupled to each other by a torsion bar. The parameters of a double point contact and of a double pendulum have a one-to-one correspondence in such a way that the equations governing the two systems are the same.

In general there are several stable solutions $\phi_{s,\alpha}$ for a certain value of $\Delta\phi_a^*$ and $B_1 0$. The index α in $\phi_{s,\alpha}$ is used to distinguish between these different solutions. From eq. (3.14) $\phi_{s,\alpha}$ can be calculated as a function of $\Delta\phi_a^*$ and B_1 . Each of these $\phi_{s,\alpha}$ functions have to be substituted in eq. (3.13). Then $i_\alpha(B_1)$ is determined as the maximum of $i(\Delta\phi_a^*, B_1, \phi_{s,\alpha})$ with respect to $\Delta\phi_a^*$ and fixed values of B_1 and α . Finally the critical current is the largest current of all currents $i_\alpha(B_1)$ for different values of α . At B_1 values where an $i_\alpha - B_1$ curve intersects an other $i_\alpha - B_1$ curve, a discontinuity occurs in the slope of the $i_c - B_1$ dependence. For the double point contacts treated in this chapter this is the case when $B_1 0 = (n + \frac{1}{2})h/2e$. The result of this calculation is shown in fig. 14. Also $B_1 0 + \phi_s$ (the total flux in 0) and $\phi_s = Li_{\text{circ}}$ (the induced flux in 0) are derived for the situation where the critical current is flowing through the double point contact and are represented in the figure. The critical current when half a flux quantum is applied ($i_c \text{ min}$) is a function of ℓ (see fig. 17)³⁴⁾³⁶⁾. The reduced self-inductance ℓ is defined in eq. (2.14). When $\ell < 1$ this critical current is equal to ℓi_1 . Hence, when $\ell = 0$, the critical current is zero ($i_a + i_b = 0$) and the circulating current equal to $\frac{1}{2}(i_a - i_b) = i_1/\sqrt{2}$. When $\ell \gg 1$ one obtains from eq. (3.14) that

$$\sin \Delta \phi_a^* - \sin \left\{ \Delta \phi_a^* + \frac{2e}{\hbar} (B_{\perp} 0 + \phi_s) \right\} = \frac{2\phi_s}{Li_1} \lesssim \frac{2\hbar/2e}{Li_1} = \frac{2\pi}{f} \ll 1,$$

from which we derive

$$B_{\perp} 0 + \phi_s \approx nh/2e.$$

This relation shows that in this limit the total flux in the hole is nearly quantized in units $\hbar/2e$. The critical current derived from eq. (3.13) is now given by eq. (3.10).

In principle, these theoretical results can be verified in several ways. In order to measure the $i_c - B_{\perp}$ dependence of a double point contact, Jaklevic et al.⁵⁾, Zimmerman and Silver¹²⁾ and Clarke⁵²⁾ used a method in which the time average of the voltage across the double point contact is measured when the positive part of a low-frequency ac current with amplitude larger than the maximum critical current, is

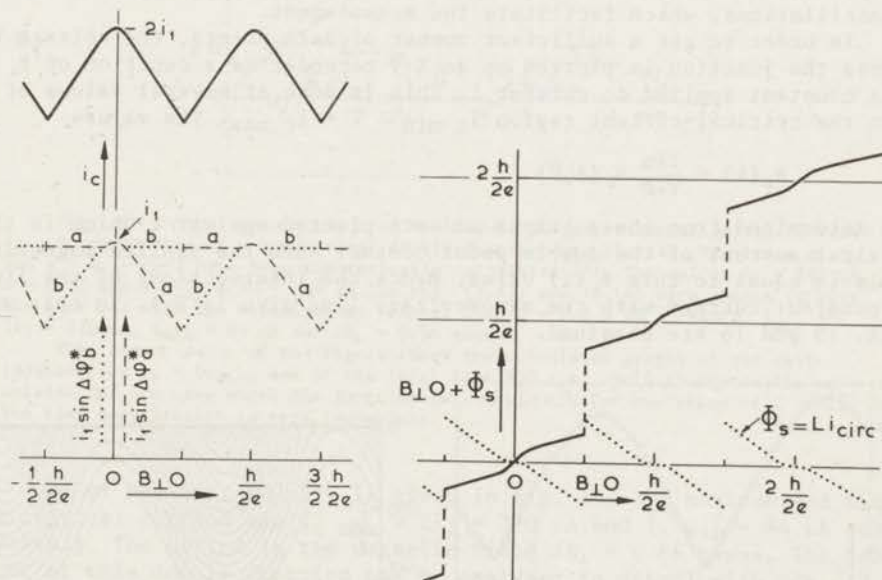


Fig. 14a) Curves representing the critical current of a weakly coupled double junction (—), the current in point contact a (----) and in b (.....) as functions of the applied flux through the hole. This may be compared with fig. 1 which shows the case for strong coupling. The self-induced flux ϕ_s is taken into account. In this figure $f = 5$. The difference between the currents through a and b can be interpreted as twice the circulating current.

b) The flux induced in the hole by the currents through the contacts a and b, and the total flux in the hole as a function of the applied flux $B_{\perp} 0$. Because f is small, the flux quantization is not complete.

applied on the junction. This complicated time average as a function of B_{\perp} is more closely related to the complete $\bar{i} - \bar{V} - B_{\perp}$ dependence^{31),34)} (see §4) than to the real $i_c - B_{\perp}$ curve. Hence this method cannot be used to study the details of the $i_c - B_{\perp}$ dependence. Only a method determining $\lim_{\bar{V} \rightarrow 0} \bar{i}(\bar{V}, B_{\perp})$ gives the critical current of the junction. There can still be some discussion as to whether the critical current determined in this way is equal to the calculated critical current (due to an apparent reduction as a consequence of the external circuitry of the double point contact^{27,61)}, but we will disregard complications of this kind. In order to measure the $i_c - B_{\perp}$ dependence we employed double point contacts with a small enclosed area 0 obtained by pressing a single superconducting needle on a superconducting sheet (§5.2). An interesting feature of junctions with $2i_1 L < h/2e$ (where $2i_1 = i_{c \text{ max}}$ is the maximum critical current of the double contact) is that a theory assuming complete flux quantization in 0 is unable to explain why the critical current is larger than zero when a half integral number of flux quanta is applied. Hence with junctions having a small enclosed area it is possible to decide whether there is complete flux quantization or not. Furthermore, these small areas give rise to a long period and a large amplitude in the i_c -oscillations, which facilitate the measurement.

In order to get a sufficient number of data points, the voltage \bar{V} across the junction is plotted on an X-Y recorder as a function of B_{\perp} at a constant applied dc current i . This is done at several values of i in the critical-current region $i_{c \text{ min}} < i < i_{c \text{ max}}$. The values

$$B_{\perp}(i) \equiv \lim_{\bar{V} \rightarrow 0} B_{\perp}(i, \bar{V})$$

are determined from these graphs and are plotted against i which is the critical current of the double point contact when the applied magnetic field is equal to this $B_{\perp}(i)$ value. Hence the intersections of the lines of constant current with the zero-voltage line give $i_c(B_{\perp})$. In this way figs. 15 and 16 are obtained.

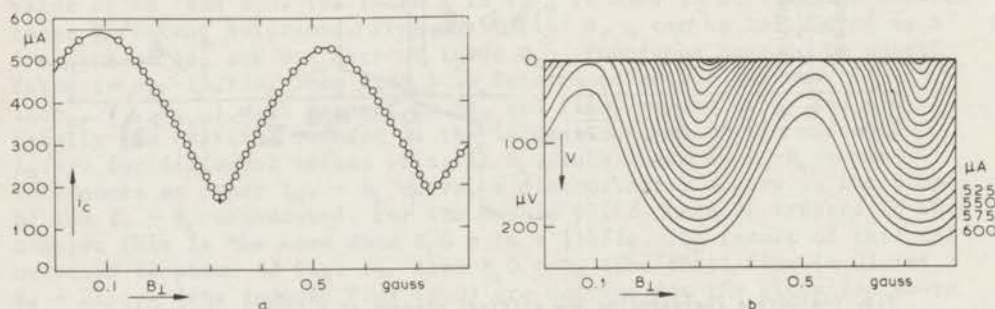


Fig. 15a) Critical current i_c of an asymmetrical multiple point contact as a function of the applied magnetic field B_{\perp} (constructed from fig. 15b).

b) $V - B_{\perp}$ dependence at several different applied dc currents i in the critical-current region. In this example the applied current is varied with steps of 25 μA . At every value of i the limits $B_{\perp}(i) = \lim_{\bar{V} \rightarrow 0} B_{\perp}(i, \bar{V})$ are determined and plotted as a function of i (which is the critical current i_c at that particular B_{\perp} value) in fig. 15a.

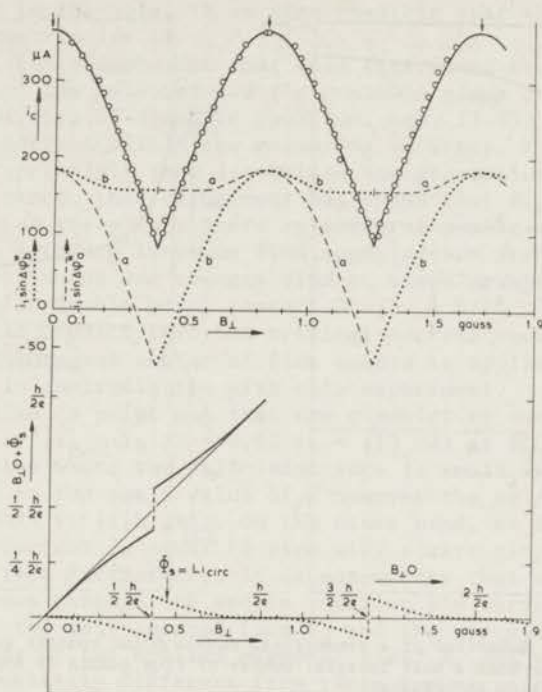


Fig. 16 In the upper part of the figure the experimental points for the $i_c - B_L$ dependence of a symmetrical double junction are plotted. The lines a, b and a + b (—) have been theoretically calculated³⁶. The values $i_1 = 185 \mu\text{A}$, $\lambda = 0.5$, and $O = 24 \times 10^{-8} \text{ cm}^2$ in the eqs. (3.13) and (3.14) were chosen to give the best fit with the experimental points. Thus $L = 1.8 \times 10^{-12}$ henry, $i_{\text{max}} = 2i_1 = 370 \mu\text{A}$, $i_{\text{min}} = 84 \mu\text{A}$ and $\Delta B_L = 0.86$ gauss.

The lower part of the figure shows the calculated graphs of the self-induced flux $\phi_s = Li_{\text{circ}}$ and of the total flux $B_L O + \phi_s$, both theoretically calculated for the case where the junction is critical. For the value of $\lambda = 0.5$ the flux quantization is very incomplete.

One of our best results is given in fig. 16. The maximum and minimum critical current are $i_{c \text{ max}} = 2i_1 = 370 \mu\text{A}$ and $i_{c \text{ min}} = 84 \mu\text{A}$ respectively. The period in the magnetic field $\Delta B_L = 0.86$ gauss. The behaviour of this double junction can be analysed in detail with eqs. (3.13) and (3.14). In order to find the characteristic value λ of this particular double junction the general relationship between the minimum critical current $i_{c \text{ min}}$ for an applied magnetic field $B_L = (n + \frac{1}{2}) (h/2e)/O$ ($n = \text{integer}$), is calculated and plotted as a function of λ (fig. 17).

From this figure and from the observed $i_{c \text{ max}} (= 2i_1)$ and $i_{c \text{ min}}$ the value of λ can be determined. The experimental results given in fig. 16 are consistent with $\lambda = 0.5$ (where $2i_1 = 370 \mu\text{A}$ and hence $L = 1.8 \times 10^{-12} \text{ H}$). As $\Delta B_L = 0.86$ gauss the area O can be calculated with $\Delta B_L O = h/2e$ giving $O = 24 \times 10^{-8} \text{ cm}^2$. The values of O and L are not

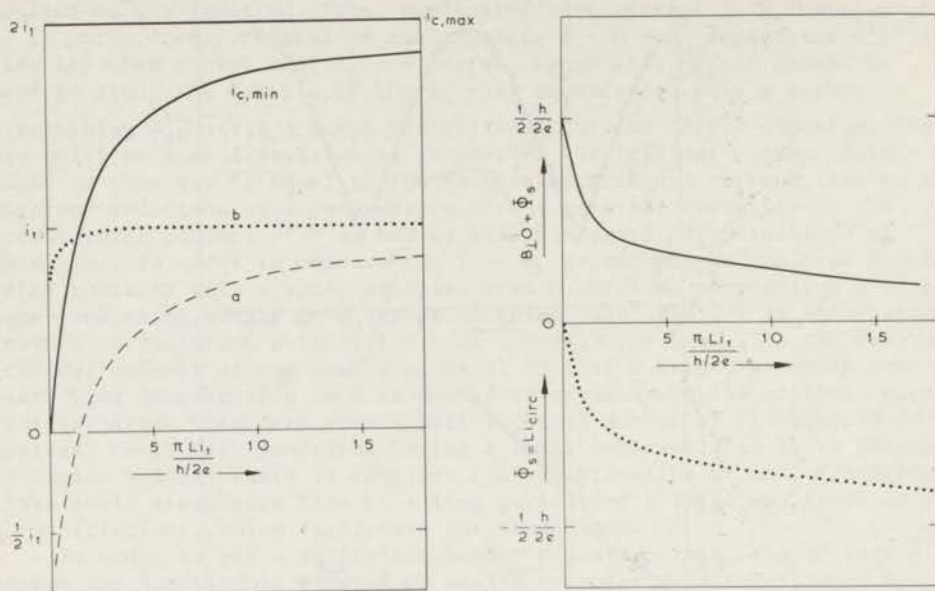


Fig. 17 Behaviour of a symmetrical double point contact as a function of $l = \pi Li_1 / (h/2e)$ when a half integral number of flux quanta is applied on 0 and when the junction is critical.

a) critical current of the double contact, $i_c = i_{c \text{ min}}$ (—) and the currents in contact a (— · —) and in b (·····).
 b) self-induced flux $\phi_s = Li_{\text{circ}}$ in 0 (·····) and the total flux $B_1 0 + \phi_s$ in 0 (—).

When 0 is of the order 4 mm^2 , then $L \approx 10^{-9} \text{ H}$. With $i_1 = 500 \mu\text{A}$ the value of l is of the order 1000. For this value the amplitude of the i_c oscillations is $(h/2e)/L$ and the flux quantization is almost complete.

completely independent because the self-inductance depends on the dimensions of the hole. Suppose for example that the area 0 is the area inside a closed superconducting ring with inner radius $R \approx 3 \mu\text{m}$ and thickness $2a$. From the values of L and 0 and with the formula $L = \mu_0 R (\ln(R/a) + 0.08)$ we obtain $R/a = 1.5$ and $a \approx 2 \mu\text{m}$. This seems reasonable and shows that the values chosen for L and 0 are consistent with each other.

For the case where the double contact is critical (using the known values of i_1 , l and 0) we can calculate the total critical current i_c , the current through each of the individual contacts, and the self-induced flux ϕ_s in 0, as functions of B_1 . The results are given in fig. 16. The experimental points are also plotted in fig. 16, showing that the agreement between theory and experiment is within the experimental accuracy. The three parameters i_1 , l and 0 were chosen to fit the experimental results. The fact that the maximum of i_c is somewhat shifted from $B_1 = 0$ (see arrow in fig. 16) may be due to a constant external magnetic field superimposed on the applied magnetic field, for instance currents in the leads to the double point contact can generate

a magnetic field in the hole. It is also possible that the junction may be slightly asymmetric (§4.4).

We should like to emphasize that this experiment shows that the *self-inductance of the hole between the contacts plays an important role in the properties of a double junction*. Eqs. (3.13) and (3.14) are found to be correct within the measuring accuracy. Flux quantization is not the basic principle that determines the properties of a double contact. For instance, this experiment has shown that di_c/dB_1 is continuous and zero at the points where an integral number of flux quanta is applied on 0. A theory assuming flux quantization predicts that di_c/dB_1 is discontinuous and changes sign at these points. Furthermore for this particular double point contact $2Li_1 \approx \frac{1}{3} h/2e < h/2e$. Flux quantization would predict that the critical current should then be zero when a half-integral number of flux quanta is applied on the junction, again in contradiction with this experiment.

We should like to point out that the *circulating current* is considerable ($i_{\text{circ}} = |i_a - i_b|/2 = 0.62 i_1 = 115 \mu\text{A}$) at $B_1 0 = (n + \frac{1}{2}) \times h/2e$ in a situation where the self-inductance is small (as presented in fig. 16). Due to the small value of l however the *self-induced flux* $\phi_s = Li_{\text{circ}}$ is small ($\approx \frac{1}{4}(\frac{1}{2}h/2e)$). On the other hand, at $B_1 0 = nh/2e$, the circulating current is equal to zero with a zero slope as a function of B_1 (fig. 16). Furthermore, it is noteworthy that when the *critical* current flows through the double junction the curves of the total enclosed flux ϕ , the self-induced flux ϕ_s and the circulating current i_{circ} as functions of the applied magnetic field B_1 (as presented in fig. 16), are completely different from these curves in the situation in which the applied current is zero. Eq. (3.13) with $i = 0$ is satisfied by

$$\Delta\phi_a^* + \Delta\phi_b^* = 2\pi n$$

and also by

$$\Delta\phi_a^* - \Delta\phi_b^* = 2\pi n + \pi.$$

An analysis of the dynamical equations of a double point contact leads to the requirement that in a stable equilibrium position $\cos \Delta\phi_a^*$ and $\cos \Delta\phi_b^*$ both must be larger than zero. Therefore the second solution is not acceptable because in this case $\cos \Delta\phi_a^* = -\cos \Delta\phi_b^*$ so one of the two must be negative. Substituting the solution $\Delta\phi_a^* + \Delta\phi_b^* = 2\pi n$ in eqs. (3.12 - 3.14) one obtains

$$\phi_s = -Li_1 \sin \left\{ \pi n + \frac{e}{h} (B_1 0 + \phi_s) \right\}$$

where n has to be chosen in such a way that

$$\cos \left\{ \pi n + \frac{e}{h} (B_1 0 + \phi_s) \right\} > 0.$$

The close agreement between the calculated and the measured $i_c - B_1$ dependence (fig. 16) is strong evidence that the relation $i = i_1 \sin \Delta\phi^*$ is correct for point contacts. Later on Fulton³⁷⁾ extended eqs. (3.11) and (3.13) in order to include several types of asymmetry in the double point contact. His calculations and measurements also support this conclusion.

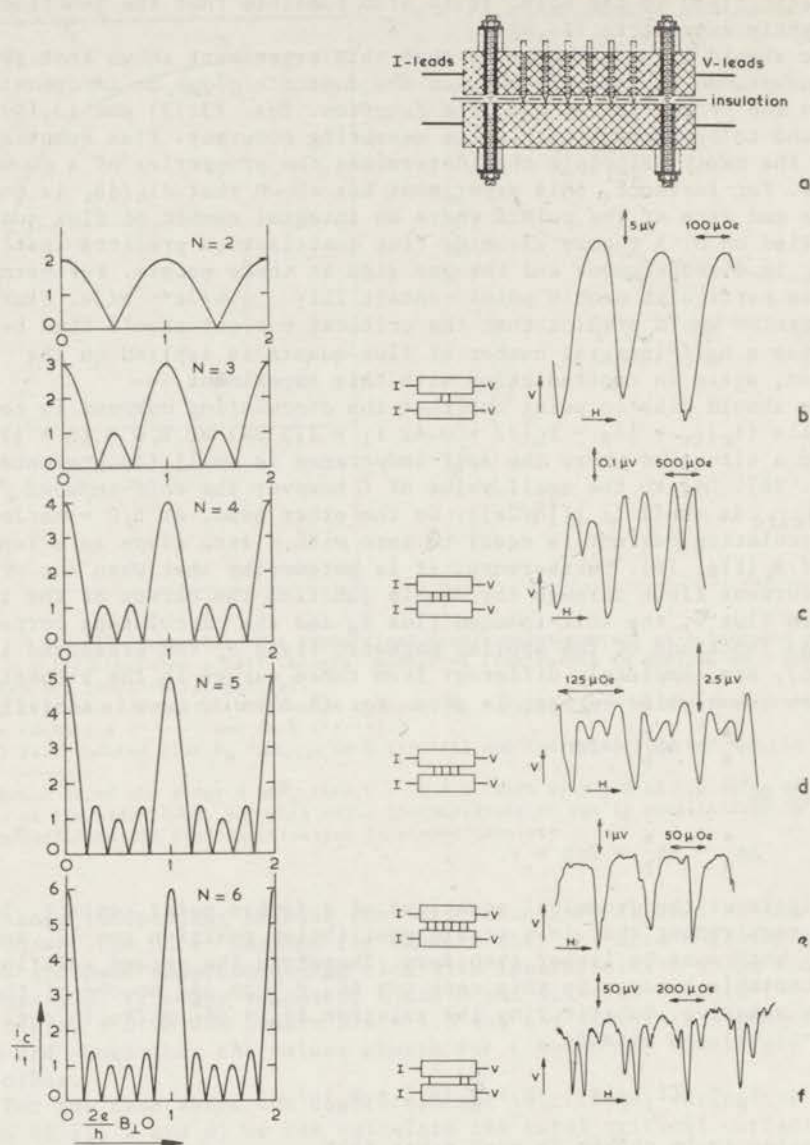


Fig. 18 The interference grating-multiple point contacts. The left series of graphs give the calculated i_c/i_1 as a function of $(2e/h)B_{\perp 0}$ for gratings of 2 to 6 weak contacts ignoring self-inductances and mutual inductances and assuming that all of the contacts are identical.

The right-hand side of this figure gives the observed voltage oscillations as functions of the applied magnetic field for various assemblies. The type of assembly is indicated at the left of each experimental curve.

§3.4 THE INTERFERENCE GRATING.

A logic extension of the discussions given above can be made by connecting two superconductors by *more than two* point contacts, which are adjusted on a straight line in such a way that an interference grating is formed. The possible importance of such an interference grating has been mentioned by Feynman ⁴⁶⁾ in his lectures. When we take a large number of point contacts the slope of the $\bar{V} - B_{\perp}$ characteristic (see later on §4) becomes large and hence a sensitive magnetometer can be constructed in principle. Experiments of this kind were first performed by Zimmerman and Silver ¹²⁾. However it was uncertain whether all the point contacts in their grating were operating in the same way.

By neglecting the self-inductances and the mutual inductances of the holes between the contacts and using eq. (3.2) we obtain by straightforward calculations ³⁴⁾³⁵⁾

$$i_c(B_{\perp}) = i_1 \left| \frac{\sin N(\pi \frac{2e}{h} B_{\perp} 0)}{\sin (\pi \frac{2e}{h} B_{\perp} 0)} \right| \quad (3.15)$$

(see fig. 18a). Within the experimental limitations (e.g. the self-inductance and the mutual inductances can in fact not be neglected) this relation has been confirmed by an experiment ³⁵⁾ the results of which are given in fig. 18b. Here we assume that the shape of the curves representing the voltage oscillations as a function of the applied magnetic field at constant applied current is in qualitative agreement with the calculated shape of the critical current oscillations of eq. (3.15) (see §4).

From the experiments described above we have the impression that it is difficult to construct a grating of more than six contacts with an acceptable chance on being successful. Increasing the number of point contacts decreases the probability that all contacts are in such a condition, that the optimal $\partial\bar{V}/\partial B_{\perp}$ value is obtained.

§4 TWO SUPERCONDUCTORS WEAKLY CONNECTED BY A DOUBLE POINT CONTACT IN THE RESISTIVE-SUPERCONDUCTIVE REGION.

§4.1 A GENERAL INTRODUCTION AND A SURVEY OF THE EXPERIMENTAL DATA.

In §3 we demonstrated that the critical current of a double point contact is an oscillating function of the applied magnetic field. It is also observed^{29-31,34)} that the dc voltage across a double point contact *oscillates as a function of the applied magnetic field* when a *constant current is applied* on the junction. The complete $\bar{i} - \bar{V} - B_{\perp}$ dependence can be represented by a corrugated surface³¹⁾. The critical current i_c and the dc voltage \bar{V} (at constant applied current) are both periodic functions of the applied magnetic field with a period $\Delta B_{\perp} = (h/2e)/0$. A maximum in the critical current corresponds to a minimum in the voltage. The amplitudes of both the i_c and \bar{V} oscillations decrease when the enclosed area 0 between the contacts is increased. Double point contacts with a small enclosed area ($0 \approx 60 \mu\text{m}^2$, $L \approx 10^{-12}-10^{-11}$ henry) can be obtained by simply pressing a superconducting point on a superconducting sheet or by using a solder-droplet junction (fig. 4) (see §5.2). Some typical results are represented in figs. 19 and 20. When two superconductors are pressed together the irregularities of the contact area sometimes result in a double point contact between the two superconductors. When there are more than two contacts it is still possible that the system behaves as a *double* contact because a small enclosed area gives rise to larger amplitudes in the i_c and \bar{V} oscillations than when a large area is enclosed. Hence the influences of the large areas can often be neglected¹²⁾ (see §5.2). The largest area with an

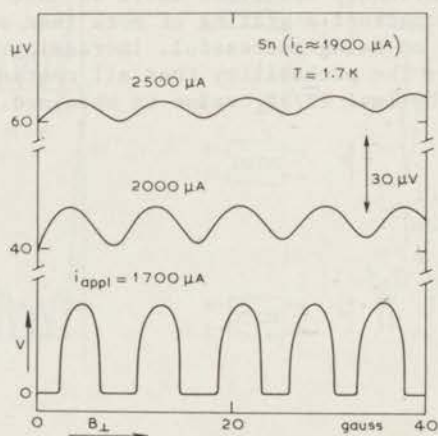


Fig. 19 Voltage oscillations of a double point contact in the resistive-superconductive state as functions of the applied magnetic field at various constant applied currents. These were measured using droplet junctions²⁹⁻³¹⁾.

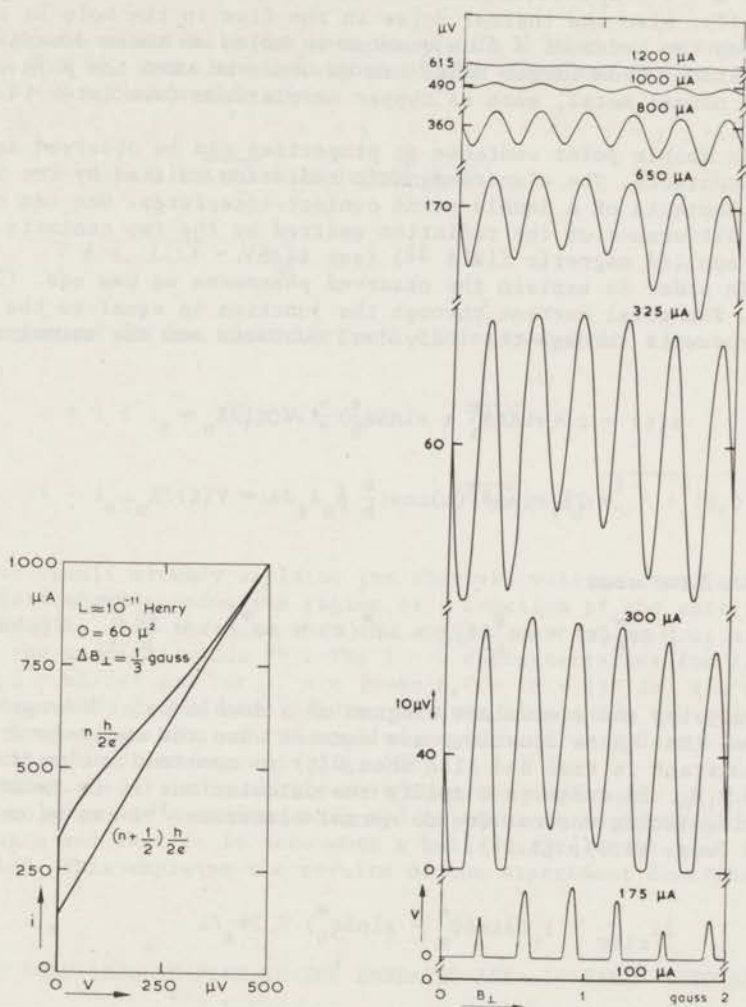


Fig. 20a) X-Y recorder plots of two $\bar{I} - \bar{V}$ characteristics of a double junction. One at $B_{\perp 0} = nh/2e$ and one at $B_{\perp 0} = (n + \frac{1}{2})h/2e$ (31). These apply to the type of junction shown in fig. 4.

b) Voltage oscillations at constant applied current for the junction of fig. 20a. The amplitude of the oscillations can be deduced from the voltage differences (at the given applied constant currents) of the two lines shown in fig. 20a.

empty hole in which oscillations were measured was 0.75 cm^2 , $L \approx 10^{-8}$ henry ¹²⁾. This limit is determined by the fact that the amplitudes in the $\bar{i} - \bar{V} - B_1$ oscillations diminishes when the area 0 becomes large (fig. 17). Also the thermal noise in the flux in the hole is estimated to be on the order of a flux quantum in holes of these dimensions. Oscillations from larger holes can be observed when the hole is filled with a normal metal, such as copper or platinum (see later §4.6, and table I).

In double point contacts ac properties can be observed as in single point contacts. The electromagnetic radiation emitted by the individual point contacts of a double point contact interferes. One can control the phase difference of the radiation emitted by the two contacts by means of an applied magnetic field ³²⁾ (see §4.5).

In order to explain the observed phenomena we use eqs. (2.1) and (3.1). The total current through the junction is equal to the sum of the supercurrents through the individual contacts and the normal current

$$\begin{aligned} i(t) &= i_1 (\sin \Delta \phi_a^* + \sin \Delta \phi_b^*) + V(t)/R_n = \\ &= 2i_1 \sin \Delta \phi^*(t) \cos\left(\frac{e}{h} \oint_S A_s ds\right) + V(t)/R_n. \end{aligned} \quad (4.1)$$

Here we have used

$$\frac{1}{2} \{ \Delta \phi_b^*(t) + \Delta \phi_a^*(t) \} \equiv \Delta \phi^*(t) = \Delta \phi^*(0) - \frac{2e}{h} \int_0^t V(t') dt'. \quad (4.2)$$

By analysing the equivalent diagram of a double point contact it can be derived that these equations are correct when the applied current $i(t) = i = \text{constant}$ in time and also when $V(t)$ is constant in time if $f \approx 0$ or if $V \gg i_1 R_n$. In order to simplify the calculations it is assumed that the circulating current due to normal electrons ³⁴⁾ can be neglected, hence (eqs. (3.9), (3.11)):

$$2i_{\text{circ}} \equiv i_1 (\sin \Delta \phi_a^* - \sin \Delta \phi_b^*) \equiv 2\phi_s/L$$

or

$$\phi_s/Li_1 = -\sin\left(\frac{e}{h} \oint_S A_s ds\right) \cos \Delta \phi^*(t). \quad (4.3)$$

The eqs. (4.1), (4.2) and (4.3) are the basic relations ³⁴⁾ of the $\bar{i} - \bar{V} - B_1$ dependence.

§4.2 WHEN THE SELF-INDUCED FLUX IN THE ENCLOSED AREA IS IGNORED

The advantage of ignoring the self-induced flux in the hole ($\phi_s = 0$) is that eq. (4.1) has a simple analytical solution

$$i(t) = 2i_1 \sin \Delta\phi^*(t) \cos \frac{e}{h} B_1 0 + V(t)/R_n. \quad (4.4)$$

Eq. (4.4) is essentially the same as eq. (2.3) when i_1 is replaced by $2i_1 |\cos \frac{e}{h} B_1 0|$. Hence the solutions of the equations are the same. If $V(t) = V = \text{constant}$ in time,

$$V = 0, \quad 0 \leq \overline{i(t)} \leq 2i_1 |\cos(\frac{e}{h} B_1 0)| \quad (4.5a)$$

$$V \neq 0, \quad \overline{i(t)} = V/R_n. \quad (4.5b)$$

More important is the limit $i(t) = i = \text{constant}$ in time:

$$0 \leq i \leq i_c = 2i_1 |\cos(\frac{e}{h} B_1 0)|, \quad \overline{V(t)} = 0 \quad (4.6a)$$

$$i > i_c, \quad \overline{V(t)} = R_n \sqrt{i^2 - i_c^2(B_1)}. \quad (4.7a)$$

This result already explains the observed voltage oscillations in the resistive-superconductive region as a function of the external magnetic field B_1 , for the case that the applied current is constant and exceeds the critical value i_c . The $i - \overline{V}$ characteristics for $i_c = 2i_1$ (when $B_1 0 = nh/2e$) and for $i_c = 0$ (when $B_1 0 = (n + \frac{1}{2})h/2e$) are represented in fig. 12b. In the same figure, we have also shown the voltage oscillations \overline{V} as a function of the applied magnetic flux $B_1 0$ at several values of a constant applied current (fig. 12c).

From eq. (4.4) it is easily seen that the amplitudes of the ac current or voltage are a maximum when $B_1 0$ is equal to an integral number of flux quanta and that it is zero when a half integral number of flux quanta is applied. This explains the results of the experiment described in §4.5.

§4.3 WHEN THE SELF-INDUCED FLUX IN THE EMBRACED AREA IS TAKEN INTO ACCOUNT.

If we drop the condition that the self-induced flux in the hole is equal to zero ($\phi_s \neq 0$) it is no longer possible to give a simple analytical solution of eqs. (4.1) - (4.3). We first consider eqs. (4.1) - (4.3) for the case that V is constant in time:

$$i(t) = 2i_1 \sin(\Delta\phi^*(o) - \frac{2e}{h} Vt) \cos \frac{e}{h} (B_1 0 + \phi_s) + \frac{V}{R_n}, \quad (4.7)$$

$$\frac{\phi_s}{Li_1} = -\sin \frac{e}{h} (B_1 0 + \phi_s) \cos(\Delta\phi^*(o) - \frac{2e}{h} Vt). \quad (4.8)$$

When $V = 0$ these expressions reduce to

$$i = 2i_1 \sin \Delta\phi^*(0) \cos \frac{e}{h}(B_1 0 + \phi_s), \quad (4.9)$$

$$\frac{\phi_s}{Li_1} = -\sin \frac{e}{h}(B_1 0 + \phi_s) \cos \Delta\phi^*(0). \quad (4.10)$$

The $i_c - B_1$ dependence calculated from these two equations is the same as the $i_c - B_1$ dependence derived in §3.3. When $V \neq 0$, we may take $\Delta\phi^*(0) = \pi$ in eqs. (4.7) and (4.8) without losing generality. From eq. (4.8) we can derive that ϕ_s is a function of $\cos\{(2e/h)Vt\}$ and therefore that $\cos\{(e/h)(B_1 0 + \phi_s)\}$ is also a function of $\cos\{(2e/h)Vt\}$. According to eq. (4.7) the supercurrent $i_s(t) = i(t) - V/R_n$ is equal to $2i_1 \sin\{(2e/h)Vt\}$ times a function of $\cos\{(2e/h)Vt\}$, and therefore $i_s(t) = -i_s(-t)$. Furthermore, $i_s(t)$ is a periodic function of time with a frequency $(2e/h)V$. Hence the time average of $i_s(t)$ is zero. The $\bar{i} - V$ dependence is described with the equations:

$$V = 0, \quad 0 \leq \bar{i}(t) \leq i_c; \quad (i_c \text{ calculated in §3.3}) \quad (4.11a)$$

$$V \neq 0, \quad \bar{i}(t) = V/R_n. \quad (4.11b)$$

In order to calculate the time dependence of i_s eq. (4.8) is solved with graphical methods. We plot both the right-hand side and the left-hand side of eq. (4.8) as functions of ϕ_s at a certain voltage, magnetic field and time in the same diagram (fig. 21). The ϕ_s values of the points of intersection are the solutions of eq. (4.8). The amplitude of the sin function representing the right-hand side of (4.8) is equal to $|\cos(2e/h)Vt|$.

By solving eq. (4.8) for different values of t we obtain ϕ_s as a function of time. In general there is more than one solution but there is only one solution that is of physical importance: it is the solution that has a continuous development in time. From fig. 21 it can be derived that this solution is such that $(nh/2e) - B_1 0 < \phi_s < ((n+1)h/2e) - B_1 0$, where n is an integer chosen in such a way that $nh/2e \leq B_1 0 \leq (n+1)h/2e$. In principle it is possible that ϕ_s is not in this interval, but this is not a stationary solution because every time $(2e/h)Vt = \frac{1}{2}(k + \frac{1}{2})$ (k integer) the only solution of (4.8) is $\phi_s = 0$ and the junction has to jump back into this state. Knowing $\phi_s(t)$ we can derive the time dependence of the total amount of flux in the hole between the contacts. It has the remarkable property that it oscillates between $nh/2e$ and $(n+1)h/2e$ (fig. 21). When $B_1 0$ is exactly equal to an integral number of flux quanta there are several solutions that are continuous in time, but in a practical situation this very special case will never occur. It is a prediction of the theory that the time average of the total flux in the hole is roughly equal to $(n + \frac{1}{2})h/2e$ if the junction is in the resistive region. From $B_1 0 + \phi_s(t)$ we derive $\cos(2e/h)(B_1 0 + \phi_s)$ as a function of time. Substituting this function in eq. (4.9) finally gives the total current as a function of time.

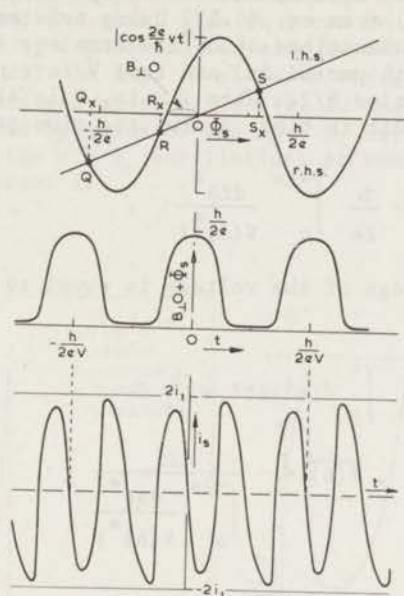


Fig. 21 Calculation of the time dependence of the total flux in the hole and of the total supercurrent of a double point contact in the case that the voltage is constant in time ($V \gg i_1 R_N$). In the upper part of the figure both the left-hand side and the right-hand side of eq. (4.8a) are given as functions of ϕ_s at a certain $B_{\perp 0}$ and time t . The ϕ_s values Q_x, R_x, S_x etc. from the points of intersection Q, R, S etc. of these two curves are the solutions of eq. (4.8a) and correspond to the flux that can be induced in the hole by currents through the contacts a and b . In order to find the solutions of eq. (4.8a) at another time the amplitude of the sin function must be changed (amplitude is equal to $|\cos(2e/h)Vt|$) and again the ϕ_s values of the points of intersection must be determined. In this way the time dependence of the solutions of eq. (4.8a) can be derived. There is only one solution that is continuous in time (when $t = (h/2eV)(\pi/2)$, then $\cos(2e/h)Vt = 0$ and $S_x = 0$ is the only solution). It is the solution in the interval $-B_{\perp 0} + nh/2e, -B_{\perp 0} + (n+1)h/2e$ where n is chosen in such a way that $nh/2e \leq B_{\perp 0} \leq (n+1)h/2e$. The solution S_x is the only solution that is of physical interest. From the time dependence of S_x , the time dependence of $\phi_s + B_{\perp 0}$ and of i_s can be calculated. The results are given in the middle and lower part of this figure, respectively.

A picture of the supercurrent $i_s(t)$ is given in fig. 21. The fundamental frequency is $2eV/h$ and there are strong harmonics. Especially the second harmonic seems to have a large amplitude. In the limit $l \rightarrow \infty$ the behaviour of the solution of eq. (4.10) is rather simple. The time dependence of the function $B_{\perp 0} + \phi_s(t)$ is a block-shaped function between the values $nh/2e$ and $(n+1)h/2e$. Now $i_s(t)$ is essentially a saw tooth at a frequency $2(2eV/h)$.

As in the previous sections, we will also consider the solutions of the eqs. (4.1) - (4.3) when i is constant in time³⁴). Again, $V(t) = 0$ when $i \leq i_c$ (with i_c derived in §3.3). When $i > i_c$, the values of $\phi_s =$

Li_{circ} and therefore also of $\cos\{(2e/h)(B_{10} + \Phi_s)\}$ can be obtained as functions of $\Delta\phi^*(t)$ from eq. (4.3). Using this result, $i_s(t)$ and $V(t)$ can be obtained as functions of $\Delta\phi^*(t)$ from eq. (4.1). V is a periodic function of $\Delta\phi^*$ with period 2π , and thus V is a periodic function of $\int_0^t V(t')dt'$ with period $h/2e$. When $i > i_c$, V is always positive and therefore $V(t)$ is periodic in time. Again, the time period is equal to

$$\frac{1}{v} = \tau = -\frac{h}{2e} \int_0^{-2\pi} \frac{d\Delta\phi^*}{V(\Delta\phi^*)} \quad (4.12)$$

The time average of the voltage is equal to the time average in one period:

$$\overline{V(t)} = \frac{1}{\tau} \int_0^{\tau} V(t')dt' = \frac{h}{2e} v$$

$$i > i_c, \quad \overline{V(t)} = -\frac{2\pi}{\int_0^{-2\pi} \frac{d\Delta\phi^*}{V(\Delta\phi^*)}} \quad (4.13a)$$

When $i \leq i_c$ then $V(t) = 0$:

$$0 \leq i \leq i_c, \quad V(t) = 0. \quad (4.13b)$$

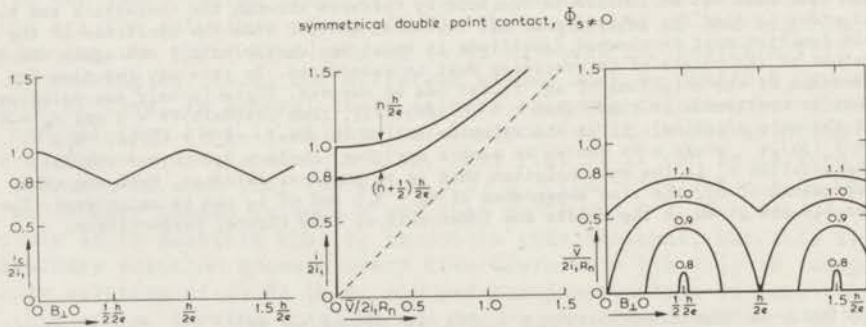


Fig. 22 Description of the $\bar{i} - \bar{V} - B_{10}$ dependence of a symmetrical double point contact when the self-induced flux is not ignored. This figure is obtained from computer calculations solving eq. (4.13).

- Critical current as a function of the applied flux on 0.
- Two $\bar{i} - \bar{V}$ characteristics ($i(t) = i = \text{constant}$). One at an applied flux $B_{10} = nh/2e$ and one at $B_{10} = (n + \frac{1}{2})h/2e$. The curves are not perfect hyperbolas. The voltages are slightly larger than that of a hyperbola $\bar{V} = R_n \sqrt{i^2 - i_c^2}$.
- Voltage oscillations at applied currents which are constant both with respect to time and magnetic field. The current values are 0.8, 0.9, 1.0 and 1.1 times $2i_1$ respectively.

Eqs. (4.1) - (4.3), with $i(t) = i = \text{constant}$ in time, can be solved numerically. The voltage and the total flux in 0 can be obtained as functions of time. The $i - \bar{V} - B_{\perp 0}$ dependence can also be calculated from these equations (see fig. 22). In fig. 23 pictures are given of V and of $B_{\perp 0} + \phi_s$ in units $h/2e$ as functions of time. In fig. 22 the calculated $i - \bar{V} - B_{\perp 0}$ dependence is depicted by means of the $i_c - B_{\perp 0}$ oscillations, two $i - \bar{V}$ characteristics and the $\bar{V} - B_{\perp 0}$ oscillations at several values of the applied constant current i .

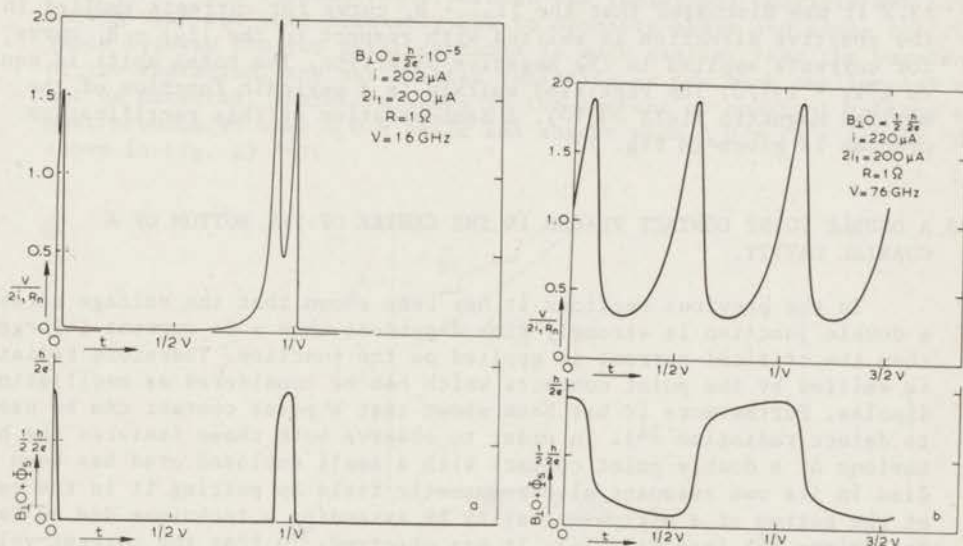


Fig. 23a) The top picture shows the time dependence of the voltage across a double point contact when a constant current is applied on the junction. In this example we have chosen $i = 202 \mu\text{A}$, $2i_1 = 200 \mu\text{A}$, $R_n = 1 \Omega$, $B_{\perp 0} = 10^{-5} h/2e$ and $\ell = 5$. The value of $B_{\perp 0}$ was chosen slightly different from zero because the $B_{\perp 0}$ dependence of the solutions of eqs. (4.1) and (4.3) is discontinuous at $B_{\perp 0} = 0$. As in fig. 9 the time dependence of the normal current can be obtained from the equation $i_n(t) = V(t)/R_n$ and the supercurrent from $i_s(t) = i - i_n(t)$. The significant differences from fig. 9 are that in the case of a double junction there are two peaks per cycle instead of one and that the $V - t$ dependence depends on the applied magnetic field.

In the lower part of the figure a picture is given of the total flux in 0 as a function of time. The sharp peaks in the upper part of the figure are associated with flux jumping in and out the enclosed area 0. With the value $\ell = 5$ the flux quantization is incomplete and thus the maximum flux in 0 is $0.82 h/2e$ and not $h/2e$. The minimum of $B_{\perp 0} + \phi_s = 1.7 \times 10^{-6} h/2e$.

b) The top picture shows the $V - t$ dependence of the same double junction as in fig. 23a (hence $\ell = 5$ and $2i_1 = 200 \mu\text{A}$) but now with an applied current equal to $220 \mu\text{A}$ and an applied flux $\frac{1}{2} h/2e$. For this particular $B_{\perp 0}$ value the time period is half the value calculated from eq. (4.12). The maximum i_s value is equal to $157 \mu\text{A}$. This is the critical current of the junction for $B_{\perp 0} = B_{\perp 0} = \frac{1}{2} h/2e$.

The lower picture gives the total flux $B_{\perp 0} + \phi_s$ in 0 as a function of time.

§4.4 THE RECTIFICATION PROCESS FOR AN ASYMMETRICAL DOUBLE JUNCTION.

When an ac current with an amplitude larger than the critical current is applied on a double junction, an ac voltage will be generated across the junction. When the critical current is smaller in the positive direction than in the negative direction, the amplitude of the voltage in the positive direction will be larger than the amplitude in the negative direction. Therefore the time average of the voltage will be positive and unequal to zero, even when the applied dc current is equal to zero. A situation in which the critical currents in the positive and negative directions are unequal occurs in an asymmetrical junction. In §3.2 it was discussed that the $|i_c| - B_1$ curve for currents applied in the positive direction is shifted with respect to the $|i_c| - B_1$ curve for currents applied in the negative direction. The total shift is equal to $L|i_1 - i_2|/0$. The rectified voltage is a periodic function of the applied magnetic field ³³⁾⁶⁵⁾. A demonstration of this rectification process is given in fig. 13.

§4.5 A DOUBLE POINT CONTACT PLACED IN THE CENTER OF THE BOTTOM OF A COAXIAL CAVITY.

In the previous sections it has been shown that the voltage across a double junction is strongly time dependent when a dc current i larger than the critical current is applied on the junction. Therefore radiation is emitted by the point contacts which can be considered as oscillating dipoles. Furthermore it has been shown that a point contact can be used to detect radiation ²⁴⁾. In order to observe both these features the behaviour of a double point contact with a small enclosed area has been studied in its own resonant electromagnetic field by putting it in the center of the bottom of a microwave cavity by extending a technique due to Dayem and Grimes ²⁴⁾ (see fig. 24). It was observed ³¹⁾ that the current-voltage curve shows steps at constant voltages which correspond to a resonant frequency of the cavity according to eq. (1.23). The steps at constant

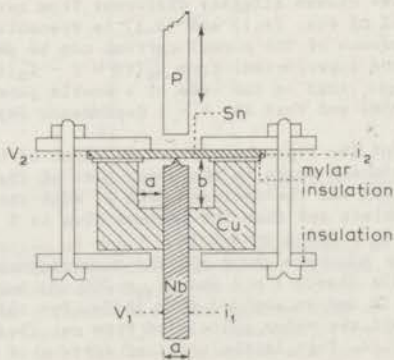


Fig. 24 The coaxial cavity ³²⁾. Cu = copper coaxial cavity, Nb = niobium center conductor, Sn = tin foil, P = load adjuster.

voltage were most pronounced when the applied flux on 0 was equal to an integral number of flux quanta ($B_{\perp 0} = nh/2e$) (critical current maximum, dc voltage minimum). The steps disappeared when the applied flux was equal to a half integral number of flux quanta ($B_{\perp 0} = (n + \frac{1}{2})h/2e$). Although the self-induced flux of a double point contact can never be ignored in principle, one can understand this behaviour from the results of §4.2, where it was concluded that the amplitude of the ac voltage is larger when an integral number of flux quanta is applied on 0. When $B_{\perp 0} = nh/2e$, the supercurrents through the individual contacts are oscillating with the same frequency and in phase, radiation is emitted. When $B_{\perp 0} = (n + \frac{1}{2})h/2e$ the supercurrents through the individual contacts are oscillating with the same frequency but in opposite phase and since the distance between the two point contacts is much smaller than the wavelength of the radiation, the net emitted radiation is now much smaller and can not be detected. Therefore steps in the current at constant voltage are most pronounced when $B_{\perp 0} = nh/2e$ and absent when $B_{\perp 0} = (n + \frac{1}{2})h/2e$, as is shown in fig. 25 32).

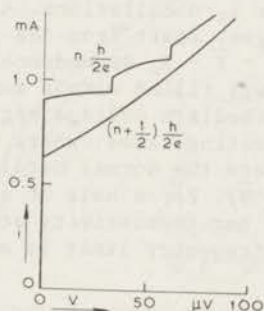


Fig. 25 The current-voltage curves for the cavity of fig. 24 for the cases $B_{\perp 0} = nh/2e$ and $B_{\perp 0} = (n + \frac{1}{2})h/2e$. The values of the constant-voltage steps are independent of the temperature. They depend only on the cavity dimensions a and b shown in the following table:

| cavity | a (cm) | b (cm) | Voltage steps occur at |
|--------|----------|----------|------------------------|
| 1 | 0.30 | 0.75 | 34 (μ V) 64 |
| 2 | 0.23 | 0.65 | 41 78 |
| 3 | 0.19 | 0.55 | 49 93 |

§4.6 THE INFLUENCE OF A NORMAL METAL IN THE HOLE BETWEEN THE SUPERCONDUCTORS ON THE $\bar{i} - \bar{V} - B_{\perp}$ DEPENDENCE.

Up to now we considered the L in eq. (4.3) frequency independent. If however the value of L depends on the frequency of the ac magnetic field in the hole, then an extra $V(t)$ dependence is introduced in eqs. (4.1-3) of §4.1.

When there is helium or vacuum in the hole between the two contacts then L is not a function of the frequency, but just a geometric constant of the sample. The value of L is an increasing function of the area 0

enclosed by the superconducting blocks and the point contacts. This means that a relatively small magnetic field period ΔB_{\perp} necessarily implies a small amplitude of the oscillations (fig. 17). What one would like to have, however, is a double point contact with at the same time a small ΔB_{\perp} and a large amplitude in the dc voltage (\bar{V}) oscillations. This can be achieved by putting a normal conductor (copper or platinum for example) in the hole, insulated from the blocks. In this case L is frequency dependent due to the skin effect of the normal metal. We denote the low-frequency limit of L by L_{lf} and the high-frequency limit by L_{hf} .

Low-frequency magnetic fields penetrate the normal metal completely, consequently the period ΔB_{\perp} is unchanged. Also the value of the critical current should be unchanged because this is the largest current flowing through the double point contact with $V = 0$ (and hence with $v = 0$). If, however, \bar{V} is so large that the penetration depth for an ac magnetic field with frequency $\nu = 2e\bar{V}/h$ is much smaller than the dimensions of the normal conductor, the ac magnetic field is completely excluded from the normal conductor. In this case L is equal to L_{hf} which is smaller than L_{lf} . From fig. 17 it can be seen that a smaller self-inductance leads to a larger amplitude in the i_c -oscillations. Also the amplitude of the voltage oscillations is larger. Apart from the period ΔB_{\perp} (which remains unchanged) the corrugated $\bar{I} - \bar{V} - B_{\perp}$ dependence for these values of \bar{V} is the same as if the hole was filled with a superconductor instead of a normal metal. In the intermediate voltage region there must be a transition between these two limiting cases: where the normal metal is absent (fig. 26a) (small \bar{V}) and where the normal metal is replaced by a superconductor (fig. 26b) (large \bar{V}). For a hole of a diameter of 1.8 mm partially filled with a copper bar (resistivity at 4.2 K equal to $0.1 \mu\Omega \text{ cm}$) the transition to the high-frequency limit is almost completed at 0.07 nV.

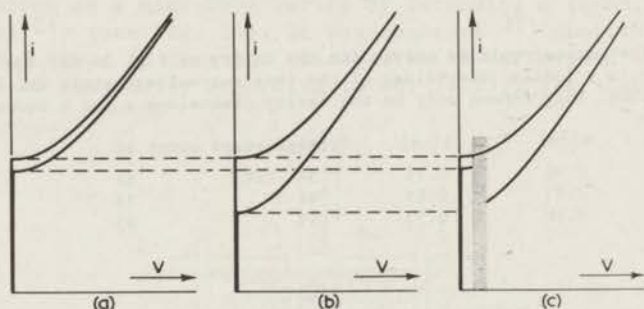


Fig. 26 These figures each give two $\bar{I} - \bar{V}$ characteristics of a double point contact: one at an applied magnetic field value where the critical current i_c is a maximum and one where the i_c is a minimum. Three different experimental situations are considered:

- Where the hole is empty.
- With a superconducting bar in the hole,
- With a normal metal bar in the hole. The bar has the same dimensions as the superconducting bar of fig. 26b. The curve with an applied field where the i_c is a maximum is unchanged compared with figs. 26a and b. All other curves are changed due to the presence of the normal metal. At low \bar{V} values the curves are the same as in fig. 26a. At high \bar{V} values the curves coincide with the curves of fig. 26b.

From the considerations given above the $\bar{I} - \bar{V} - B_{\perp}$ dependence of an ideal double point contact with a copper bar in the hole can be constructed (fig. 26c). In the case that $\ell \gg l$ the peak to peak amplitude of the i_c oscillations is equal to $(h/2e)/L$. If the $\bar{I} - \bar{V}$ characteristic of this double point contact can be represented in first approximation by a hyperbola $\bar{V} = R\sqrt{i^2 - i_c^2}$, then the amplitude of the \bar{V} oscillations is $R\sqrt{2}(h/2e)/L$ when $i \approx i_c$ max, and $(R^2/V)(h/2e)/L$ when $i \gg i_c$. When L_{lf} and L_{hf} are both large enough the amplification factor for the voltage oscillations is $\sqrt{L_{lf}/L_{hf}}$ when $i \approx i_c$ max and L_{lf}/L_{hf} when $i \gg i_c$.

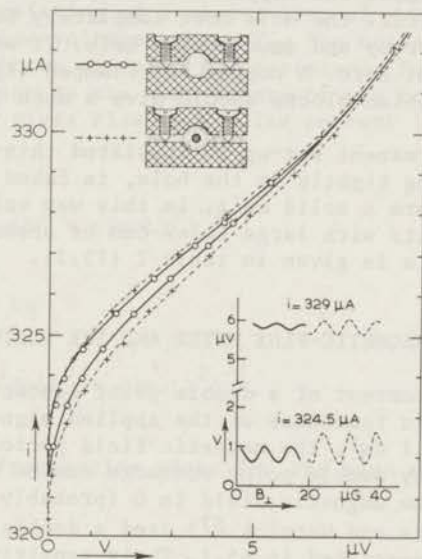


Fig. 27 The full lines are two $\bar{I} - \bar{V}$ characteristics of a double point contact with an empty hole: one is with an applied magnetic field where the i_c is a maximum, the other is at an applied magnetic field value where the i_c is a minimum.

The dotted lines give the two corresponding curves with a copper bar in the hole (see fig. 7). The maximum i_c is unchanged due to the presence of the copper. At the higher voltage values the $\bar{I} - \bar{V}$ curves are in the middle of the $\bar{I} - \bar{V}$ curves with copper.

In the insert are given the $\bar{V} - B_{\perp}$ dependence at two applied current values. Left: the empty hole, Right: with a copper bar in the hole.

An experimental result is given in fig. 27. The value of L_{lf}/L_{hf} was in this case equal to 4. The shape of the experimental $\bar{I} - \bar{V}$ curves deviates from the shape of the $\bar{I} - \bar{V}$ curves given in fig. 26 because the curves in fig. 26 are derived from a theory in which are neglected many properties of the double contact such as the capacitive coupling between the niobium blocks, and self-inductances and resistances in series with the double point contact (§2.2). Hence, also the calculation of the amplification factors of the amplitude of the V-oscillations is just an estimation. It is observed in fig. 27 that the maximum critical current is the same if

the copper bar is in or outside the hole. The transition region discussed above cannot be observed in this case because it is very small ($\bar{V} < 0.07$ nV). In the region of the $\bar{I} - \bar{V}$ curves with $\bar{V} > 4$ μ V the average values of the $\bar{I} - \bar{V}$ curves (in fig. 27) with and without the copper bar tend to coincide (see insert in fig. 27). In agreement with the order of magnitude calculation given above, the amplitude of the voltage oscillations is enhanced by a factor of 4 in this region. For currents just above the critical current ($V \sim 1$ μ V) this factor is about 2. Again in agreement with the estimation given above.

In this experiment the copper bar occupied only 75% of the area of the hole. We could not fill the hole more completely because we wanted to be able to move the bar up and down in the hole. It seems that there is much room for improvement here. A copper bar clamped tightly between (but insulated from) the niobium blocks should give a much larger amplification factor (table I).

For a more permanent set-up an insulated thin-walled tube of copper or platinum, fitting tightly in the hole, is baked together with the niobium and the glass to form a solid unit. In this way voltage oscillations from double point contacts with large holes can be observed. A summary of the experimental results is given in table I (§5.2).

§4.7 APPLICATIONS: THE MAGNETIC-FLUX METER AND THE VOLTMETER; THE LONDON MOMENT.

The critical current of a double point contact and the dc voltage across it are both periodic functions of the applied magnetic field with a period $(h/2e)/0$. When $0 = 1$ cm^2 , the magnetic field period is equal to 0.2 μ gauss. Due to this property double point contacts can be used to measure very small *changes* in the magnetic field in 0 (probably even on a level up to 100 kgauss). Forgacs and Warnick⁵⁷) used a double point contact in the feed-back mode as described in §5.1. Their sensitivity is of the order of 1 to 10 nanogauss. As an example of an application of this magnetometer they measured the fluctuations in the vertical component of the earth magnetic field. The response time of the meter was of the order of 0.1 s. This method can be compared with the SQUID's developed by Silver and Zimmerman²³⁾⁵¹⁾ who use a point contact shunted by a self-inductance as a sensor (§2.2). The sensitivity is of the order of 0.1 nanogauss and the response time 1 s. In principle the sensitivity of double point contact magnetometers can be increased by increasing the enclosed area 0 , which includes that the period in the magnetic field will be decreased. However, the amplitude of the voltage oscillations also decreases (§3.3) and this can pose a limit on the sensitivity or complicate the measurements. However, one can obtain a small ΔB_x and still have a large amplitude in the voltage oscillations, if one fills the hole as completely as possible with a normal conducting material such as copper or platinum (§4.6). Also a superconducting flux concentrator eventually in combination with this technique can be used. In a so-called flux concentrator the Meissner effect³⁵⁾ and the principle of flux conservation⁶⁶⁾ are used to concentrate a relatively large amount of flux, originating from a small magnetic field applied on a large area, into the small area between the contacts. Consequently also in this way it is possible to decrease the period in the oscillations without changing the amplitude. However, this fluxmeter has to be calibrated.

It is not possible to measure magnetic fluxes absolutely in units of the flux quantum $h/2e$.

Magnetic fields large compared to $(h/2e)/\phi_0$ can be measured by counting the number of oscillations corresponding to the unknown field (fig. 31c).

The ultimate sensitivity of a double point contact as a magnetometer is determined by the thermal magnetic-flux noise in the hole. In order to calculate the order of magnitude of the thermal noise of the magnetic flux in a normal metal cylinder or in the hole of a double point contact in the resistive region we assume that the system can be represented by an equivalent circuit consisting of a closed loop of self-inductance L , a resistance R and a noise-voltage source V_v . The noise voltage is supposed to be equal to the Johnson noise of the resistance R . Within a frequency band $\delta\nu$ the contribution to the mean square of the noise voltage is equal to $\delta V^2 = 4kTR\delta\nu$. This gives rise to a noise current i_v in the circuit determined by

$$\delta i_v^2 = 4kTR\delta\nu\{R^2 + (2\pi\nu L)^2\}^{-1}$$

and a noise flux in L by

$$\delta\phi_v^2 = 4kTRL^2\delta\nu\{R^2 + (2\pi\nu L)^2\}^{-1}.$$

Integration over all frequencies gives for the mean square of the flux noise

$$\overline{\phi^2} = kTL.$$

For a cylinder with a diameter of 2 mm and a length of 1 cm, the self-inductance is of the order of 4×10^{-10} henry. At 4 K the value of kT is 5.6×10^{-23} joule. Hence $\sqrt{\overline{\phi^2}} = 1.5 \times 10^{-16}$ weber. This is about 10% of a flux quantum.

The influence of the noise in the magnetic flux on the measured dc $\bar{V} - B_{\perp}$ dependence can be separated in two parts: The high-frequency components (faster than the voltmeter response) give rise to a decrease in the amplitude of the measured voltage oscillations. The amplitude of the time average of the voltage oscillations in the presence of noise can be calculated assuming a gaussian distribution for the flux noise. The width $\Delta\phi$ of the distribution can be obtained from the relation

$$\overline{\phi^2} \equiv \frac{\int_{-\infty}^{+\infty} \phi^2 \exp\left\{-\frac{\phi^2}{(\Delta\phi)^2}\right\} d\phi}{\int_{-\infty}^{+\infty} \exp\left\{-\frac{\phi^2}{(\Delta\phi)^2}\right\} d\phi} = kTL$$

This gives $(\Delta\phi)^2 = 2kTL$ and $\int_{-\infty}^{+\infty} \exp\left\{-\frac{\phi^2}{(\Delta\phi)^2}\right\} d\phi = \sqrt{2\pi kTL}$.

If the $\bar{V} - \phi$ dependence is given by

$$\bar{V} = -V_0 \cos\left(2\pi\frac{\phi}{h/2e}\right) + \text{constant},$$

where V_0 is the amplitude of the \bar{V} oscillations (in the absence of noise), we obtain for the amplitude $V_{0,n}$ of the average \bar{V} oscillation in the presence of noise

$$V_{0,n} = \frac{V_0}{\sqrt{2\pi kTL}} \int_{-\infty}^{+\infty} \cos\left(2\pi\frac{\phi}{h/2e}\right) \exp\left\{-\frac{\phi^2}{2kTL}\right\} d\phi$$

$$V_{0,n} = V_0 \exp\left\{-2\pi^2 \frac{kTL}{(h/2e)^2}\right\} . \quad (4.15)$$

When the total noise \sqrt{kTL} is larger than 1/5 of a flux quantum, the amplitude of the $\bar{V} - B_{\perp}$ oscillations may be reduced considerably.

The low-frequency components of the noise are directly observable as random fluctuations in the voltmeter output. The mean square value of the low-frequency noise in ϕ is equal to

$$\overline{\phi_{1f}^2} = kTL \frac{L/R}{\tau_M} , \quad (4.16)$$

where τ_M is the meter time constant. The value of τ_M is supposed to be large compared to L/R . From this equation we see that the flux noise, observed with a slow voltmeter decreases when R increases, while the total flux noise is independent of R . For a constant τ_M , the total noise flux and the low-frequency noise flux increase with L . When a normal metal cylinder is put in the hole (§4.6) the total flux noise in the double point contact is in good approximation unchanged. A detailed calculation (including the noise contribution of the normal metal cylinder, and the mutual inductance between the double point contact and the cylinder) shows that the cylinder only changes the frequency spectrum of the noise and not the total root-mean-square value. The presence of noise poses a limit (of several square centimeters) on the largest area O with which voltage oscillations can be observed, even when there is a normal metal cylinder in the hole (table I, §5.2). A rather special application of the applied flux dependence of the dc voltage across a double point contact has been performed by Zimmerman and Mercereau¹⁵⁾. They drew a niobium wire, with flux pinned in it (after the wire was brought into the mixed state due to an applied magnetic field), through the hole between the contacts and they showed that the flux was pinned in units $h/2e$.

When the magnetic field applied on O is due to a certain current, double point contacts can be used to measure this current⁶⁷⁾. By using

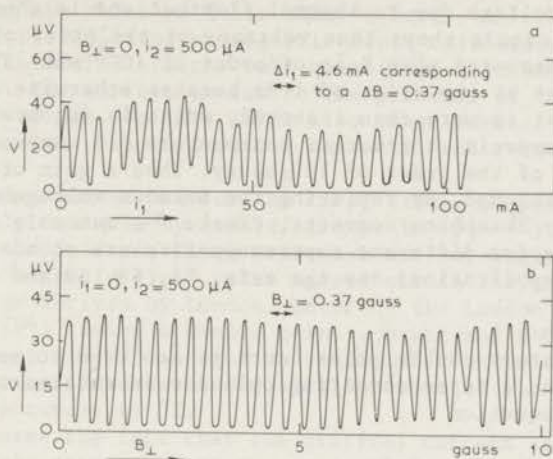


Fig. 28a) The voltage across a solder droplet junction (29) as a function of the additional current i_1 , when the current i_2 is held constant (see fig. 5). The oscillations in the voltage can be used to detect changes in i_1 (fig. 29). The maximum $dV/di_1 \approx 0.02 \Omega$.

b) Voltage oscillations as a function of applied magnetic field of this droplet junction with $i_1 = 0$. This figure can be compared with figs. 19 and 21b. By applying Ampère's law it is verified that the period in i_1 of fig. 28a is in agreement with the period in the applied magnetic field.

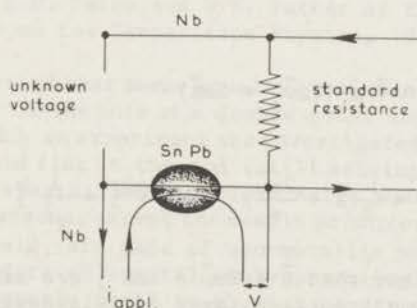


Fig. 29 The voltage-measuring device proposed by Clarke (52). The standard resistance is of the order of $10^{-8} \Omega$. A current i is applied to compensate the unknown voltage. The unbalance of the bridge is detected with a solder droplet junction. Current changes of the order of $1 \mu\text{A}$ can be detected. Since the standard resistance is $10^{-8} \Omega$, this corresponds with 10^{-14}V .

the device as a null detector also voltages can be measured. Clarke (52) used an analogous method to measure small voltages. The principle of this method is given in fig. 29. A solder droplet junction is used to detect the currents when the bridge is out of balance (see figs. 28 and 29). The estimated sensitivity is of order 10^{-15} volt. The response time L/R is less than one second because L can be as small as 10^{-8} henry. The

mean square of a voltage due to thermal fluctuations is equal to $4kTR\Delta\nu$ (see §2.4). This formula shows that voltages of the order of 10^{-15} volt can only be measured when R is of order of 10^{-8} ohm. The value of $\Delta\nu$ must be at least of the order of 1 Hz because otherwise the response time of the circuit is more than 1 second, which is inconvenient. The most sensitive commercial voltmeters can measure 0.1 nanovolt across 10 ohms with an L of the order of 10 μ henry. Thus a gain of 10^5 in sensitivity can be achieved. By replacing the unknown voltage and the standard resistance by Josephson contacts, Clarke ⁵² was able to prove that the values of $h/2e$ for different superconductors are equal within 0.01 ppm. For further applications see the refs. 51, 68, 69 and 107.

The London Moment

In our laboratory double point contacts are used to measure the London moment. When a superconducting cylinder is rotated around its axis the Maxwell equation

$$\epsilon_0 c^2 \vec{\nabla} \times \vec{B} = \vec{j} + \epsilon_0 \partial \vec{E} / \partial t$$

becomes in the stationary state

$$\epsilon_0 c^2 \vec{\nabla} \times \vec{B} = n_s e (\vec{v}_s - \vec{v}_0),$$

in which the current density $\vec{j} = n_s e (\vec{v}_s - \vec{v}_0)$, and $\vec{v}_0 = \vec{\omega} \times \vec{r}$ is the velocity of the lattice (solid-body rotation). Following London ³⁸ this equation with

$$0 = \vec{\nabla} \times \vec{p}_s = \vec{\nabla} \times (2m\vec{v}_s + 2e\vec{A})$$

gives

$$\vec{\nabla}^2 (\vec{B} + \frac{2m\vec{\omega}}{e}) = \frac{1}{\lambda^2} (\vec{B} + \frac{2m\vec{\omega}}{e}) \quad \text{and} \quad \vec{\nabla}^2 \vec{j} = \frac{1}{\lambda^2} \vec{j}.$$

These two equations show that $\vec{B} + 2m\vec{\omega}/e$ and \vec{j} are zero in the superconductor apart from a small surface layer of thickness λ . They imply that a magnetic field $\vec{B} = -2m\vec{\omega}/e$ is generated in the superconductor by the currents in the surface layer. Since $\vec{j} = 0$ in the bulk of the superconductor, the superconducting electrons are in the bulk of the superconductor in solid-body rotation with the lattice. Only near the surface the electrons lag a little behind, giving rise to a surface current. If one puts a rotating cylinder with radius R in the hole of a double point contact there will be a flux $\Phi = \pi(R - \lambda)^2 B = -\pi(R - \lambda)^2 2m\omega/e = -\pi(R - \lambda)^2 4\pi m\nu/e$ in the hole. The critical current and the dc voltage across the double point contact will oscillate as a function of the number of rotations per second $\nu = \omega/2\pi$ with a period $\Delta\nu$ given by

$$\Delta\nu = \frac{h/2e}{\pi(R - \lambda)^2 4\pi \frac{m}{e}} = \frac{h/m}{8\pi^2 (R - \lambda)^2}. \quad (4.17)$$

When $R \approx 3$ mm the value of Δv is about 1 hertz. In order to check the validity of this equation no magnetic field calibrations are necessary. In order to determine h/m the only quantities that have to be measured are R and Δv . The correction due to the presence of the λ layer is of the order of 20 ppm. On this level also other corrections are expected due to the surface dipole layer of the metal and relativistic effects (Anderson¹)).

The London moment was for the first time, independently and almost simultaneously measured by several groups in 1964⁷³) (Hildebrandt; Hildebrandt and Saffren; King, Hendricks and Rorschach; Bol and Fairbank). The measured magnetic field value agreed within the accuracy of 5 - 8% with the value derived by London. Later on the London moment was measured by Brickman¹⁰⁴) (using a double point contact and a flux transformer) and by Hendricks et al¹⁰⁵) using a conventional Flux-Gate Magnetometer. All these experiments however needed a calibration of the magnetometer which limited the accuracy to 3%.

If one uses the fact that the critical current and the dc voltage across a double point contact are periodic functions of the flux in the hole, with a period that is exactly equal to one flux quantum, no such calibration is necessary. Zimmerman and Mercereau¹⁰⁶) performed an experiment where they rotated the double point contact itself. Here it is difficult to define the value of R that has to be used in eq. (4.17).

In order to obtain the accuracy of 1 to 10 ppm that is necessary to see relativistic effects and surface dipole layer effects it is preferable to rotate a cylinder of insulating material on which a single-loop SQUID is evaporated. The present accuracy obtained in this experiment is 220 ppm as reported by C.M. Falco and W.H. Parker at the Thirteenth International Conference on Low Temperature Physics, 1972, Boulder, Colorado, USA.

A different method that seems equally promising is to rotate a superconducting cylinder in the hole of a double point contact (fig. 30). The possibilities of such an experiment are investigated in our laboratory. It turns out that trapped flux in the rod (still arising from small stray magnetic fields in the cryostat) are a serious noise source in this experiment. All parts of the apparatus, except the double point contact, the rod and a superconducting shield, are made of non-metallic materials (delrin, celoron). Two cylinders of μ -metal (moly permalloy) around the cryostat shield the earth magnetic field to about 1 μ gauss from the interior of the cryostat (see §5.1). The double point contact is used in the feedback mode (fig. 33c). When the cylinder in the hole is rotated the output oscillates around a certain main value that is determined by the London field. The amplitude of the oscillations is determined by the frozen-in field; the frequency is equal to the rotation frequency. A very preliminary result is given by the plot of the magnetometer output *versus* time in fig. 31. The London moment is visualized by the change in the level of the oscillations when the rotation speed is changed. In fig. 31 it can be seen that the frozen-in field is large (amplitude of the oscillations) compared to the signal (the change in level when the rotation frequency is changed). The value of h/m measured in this experiment (using eq. (4.17)) is 8 cm^2/s . The theoretical value is 7.3 cm^2/s . This result shows that, although the frozen-in field is large, a reasona-

ble accuracy (10%) can be obtained. The experiment is continued. The shielding will be improved and a better Meissner effect of the rod will be obtained by using a tin single crystal.

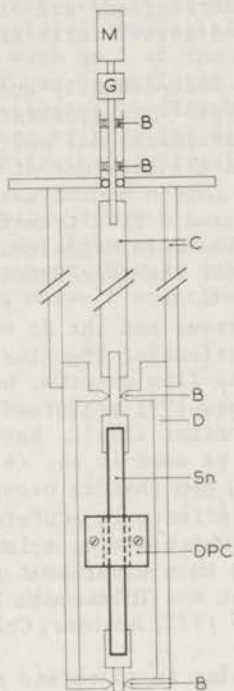


Fig. 30

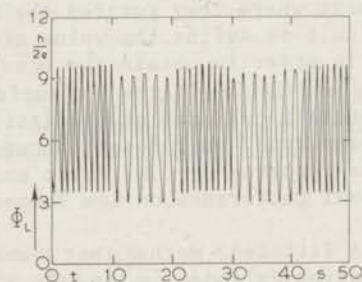


Fig. 31

Fig. 30 Cross section of the London moment apparatus. The suspension system and the rotation axes are made out of Celoron (C). The support system for the double point contact (DPC) is made out of Delrin (D). The Delrin part is shielded with lead foil. B are bearings; G is a 20:1 gear box (ESCAP G27); M is the motor (ESCAP 26 PL 11-210 dc motor; rotation speed variable up to 7100 rotations per minute); Sn is the tin rod generating the London moment. The double point contact has a hole diameter of 1.0 cm and is provided with a Pt cylinder.

Fig. 31 Output of a double-point-contact magnetometer (in units of a flux quantum) versus time. A tin rod of radius 3.2 mm is rotated in the hole. The large oscillations are due to a magnetic field in the rod. The London moment is proportional to the change in the level of the oscillations when the rotation frequency is changed (in this experiment between 1.0 and 0.5 Hz).

§5 DESCRIPTION OF THE EXPERIMENTAL SET-UP AND THE CONSTRUCTION OF DOUBLE POINT CONTACTS.

§5.1 THE EXPERIMENTAL SET-UP.

Electronics

A diagram of the electronics that we used to measure the $\bar{i} - \bar{V} - B_{\perp}$ dependence is given in fig. 32. It merely consists of a dc current supply to the magnetic field coils, a dc current supply for the current through the point contact and a dc voltmeter connected to it. All leads have low-pass filters to reduce the influence of pick-up noise from the building. With this circuit the $\bar{i} - \bar{V} - B_{\perp}$ dependences described in figs. 6, 16, 18, 19, 21 and 27 were measured. For the application of

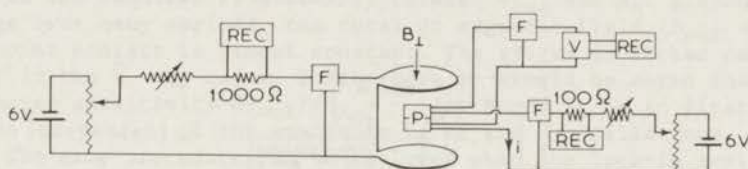


Fig. 32 Circuit to measure the $\bar{i} - \bar{V} - B_{\perp}$ dependence of a double point contact. The current supplies to the double point contact (denoted P in the figure) and the magnetic field coils are simply a battery, a potentiometer and a series resistance with a low-pass filter (F). The voltage is measured by connecting the voltmeter through a low-pass filter (F) with the point contact.

the double point contact as a magnetometer more advanced techniques are necessary. Following Forgacs and Warnick⁵⁴), we used a lock-in amplifier to improve the signal-to-noise ratio and to make the output of the magnetometer linear as a function of the unknown field B_x . The procedure is as follows (fig. 33). With the current supply to the point contact we apply a current larger than the critical current. The $\bar{V} - B_{\perp}$ dependence at this current is sketched in fig. 33a. For simplicity it is supposed to be sinusoidal. With the reference output of the lock-in amplifier we superimpose an ac magnetic field B_{ac} in the kilohertz region on the dc field B_{\perp} . The peak-to-peak amplitude of B_{ac} is smaller than $\frac{1}{2}\Delta B_{\perp}$. The ac field then gives rise to an ac voltage across the point contact of the reference frequency. In a maximum or minimum the frequency of the ac voltage is twice the frequency of the applied ac magnetic field. The amplitude and phase of the ac voltage are dependent on B_{\perp} . They are measured by a lock-in amplifier (Princeton Applied Research, type HR-8). In the inserts of fig. 33a the $\bar{V} - t$ dependence is given at several different B_{\perp} values. In fig. 33b the output V_{out} of the lock-in is given as a function of B_{\perp} . For small B_{ac} values it is proportional to the derivative $d\bar{V}/dB_{\perp}$ of the $\bar{V} - B_{\perp}$ curve. The signal-to-noise ratio in the $V_{out} - B_{\perp}$ curve is now improved considerably, compared to the dc measurement. For the application as a meter for magnetic fields smaller than or of the order of ΔB_{\perp} , we want the output V_{out} of the lock-in to be linear with B_x . This can be accomplished by applying a dc magnetic field B_{out} to the

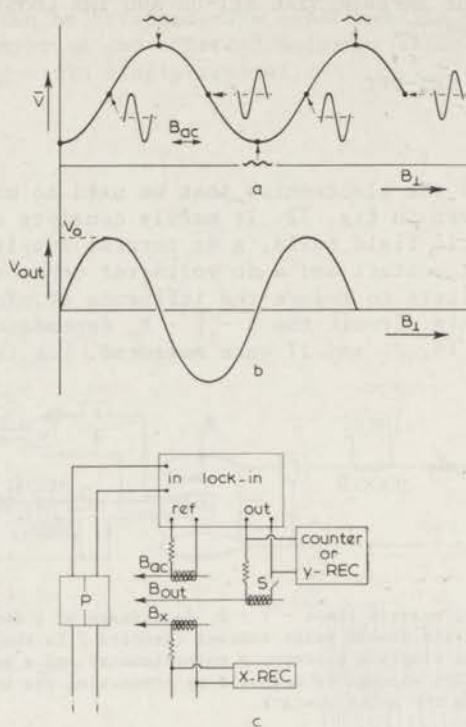


Fig. 33a) $\bar{V} - B_{\perp}$ dependence of a double point contact at constant applied current. For simplicity a sinusoidal form is assumed. In the inserts are given the $\bar{V} - t$ dependences, when a small ac magnetic field B_{ac} is applied on the contact. The amplitude and sign of the corresponding ac component of \bar{V} depend on the value of B_{\perp} .

b) Output V_{out} of a lock-in amplifier tuned at the frequency of the ac magnetic field. When the amplitude of B_{ac} is small, V_{out} is proportional to $d\bar{V}/dB_{\perp}$.

c) S closed: Double point contact operated in the feed-back mode. The output of the lock-in is approximately linear. Magnetic fields much smaller (1%) than one period can be detected.

S open : Magnetic fields much larger than one period can be measured by counting the number of pulses when the field is turned on.

point contact which is proportional to V_{out} (switch S of fig. 33c closed). Large magnetic fields (compared to ΔB_{\perp}) can be measured by counting the number of pulses when the unknown field is turned on (switch S of fig. 33c open). The equations determining the state of the system are

$$B_{out} = \alpha V_{out}$$

$$B_{\perp} = B_{out} + B_x$$

$$V_{out} = V_0 \sin 2\pi \frac{B_{\perp}}{\Delta B_{\perp}}$$

From these equations we obtain

$$\frac{B_{\text{out}}/\Delta B_{\perp}}{\alpha V_o/\Delta B_{\perp}} = \frac{B_{\text{out}}}{\alpha V_o} = \sin 2\pi \frac{B_{\text{out}} + B_x}{\Delta B_{\perp}}$$

If now $B_{\text{out}}/\Delta B_{\perp}$ is of the order of 1 and $\alpha V_o/\Delta B_{\perp} \gg 1$ (large feedback factor) then $B_{\text{out}}/(\alpha V_o) \ll 1$ and hence $(B_{\text{out}} + B_x)/\Delta B_{\perp} \approx n$ or

$$V_{\text{out}} = B_{\text{out}}/\alpha = -B_x/\alpha + n\Delta B_{\perp}/\alpha.$$

This is the required relationship between V_{out} and B_x . Although B_x can change over many periods, the total dc magnetic field ($B_{\text{out}} + B_x$) on the point contact is almost constant. The system is locked on a fixed point in the $\bar{V} - B_{\perp}$ curve. Furthermore it should be noted that the magnetometer sensitivity $dV_{\text{out}}/dB_x = -1/\alpha$. Hence it is in first approximation independent of the amplitude V_o of the \bar{V} oscillations.

The same procedure can be followed when the lock-in amplifier is tuned to twice the reference frequency. This has the advantage that pick-up from the leads to the ac magnetic field coils, can easily be eliminated.

Shielding.

In order to reduce the influence of external magnetic fields we took several precautions. The double point contacts were mounted on non-magnetic material such as "Delrin". They were 10 - 15 cm removed from slightly magnetized materials such as brass and stainless steel. We only used glass dewars. Shielding from external dc and ac magnetic fields (such as the earth magnetic field or 50 Hz and radio-frequency pick-up) was obtained by putting the sample in a superconducting (Nb) box and by surrounding the cryostat with two μ -metal cylinders (Allegheny Ludlum Moly Permalloy). These cylinders were hydrogen annealed in controlled atmosphere after forming. The length is 120 cm and the wall thickness 1.5 mm. The diameter of the inner cylinder is 12 cm and of the outer cylinder 20 cm. After properly "shaking" the cylinders by ac techniques, the external dc magnetic field (earth field) reduced to a value below 1 μ gauss at the site of the sample.

55.2 THE CONSTRUCTION OF DOUBLE POINT CONTACTS.

The simplest way to obtain a multiple point contact is to press a superconducting point on a superconducting sheet. One might think that this results in a single point contact but the irregularities on the surfaces of the two superconductors result in a contact region consisting of a combination of point contacts. Each pair of point contacts encloses a certain area. From fig. 17 it can be derived that a double point contact with a small area (small L) will have a larger amplitude in the i_c -oscil-

lations than double point contacts with a larger area. Hence the double point contact with the smallest area has the tendency to dominate the others. Therefore a superconducting point on a sheet behaves very often like a double point contact. The $\bar{I} - \bar{V} - B_{\perp}$ dependences described in the figures 13, 15, 16, 19, 21 and 25 were measured with this type of contacts.

The device in fig. 5 is a solder droplet junction first employed by Clarke²⁹⁾⁵²⁾. A droplet of tin-lead solder (which is superconducting at liquid-helium temperatures) is forced to encircle a niobium wire. An insulating oxide layer on the niobium wire provides that only point contacts are formed between the wire and the solder (due to the irregularities of the two surfaces). This type of junction has in common with the "point on a sheet" that in both cases the $\bar{I} - \bar{V} - B_{\perp}$ dependences are unpredictable.

The device of fig. 4 is developed by Omar et al.³¹⁾. The double junction is made by winding an uninsulated 50 μm niobium wire around a 100 μm niobium wire, from which the insulation on opposite faces has been partially removed. The weak contacts are anchored by means of a sealing wax droplet. The unremoved portion of the insulation, which is enclosed by the superconductors and the contacts, is the area giving rise to the period in the i_c and \bar{V} oscillations. However, also in this case a double point contact with a small enclosed area, accidentally formed between the two superconductors due to the roughness of the surfaces, can dominate the $\bar{I} - \bar{V} - B_{\perp}$ dependence.

The devices discussed so far all have the advantage of being small. The volume occupied is only a few mm^3 . The areas enclosed by the point contacts are also small and hence the amplitudes in the i_c and \bar{V} oscillations are large. Also the period ΔB_{\perp} is large. This makes them particularly useful to check theoretical results (fig. 16) but fairly in-attractive for the application as a sensitive magnetometer.

A more serious disadvantage is that the $\bar{I} - \bar{V} - B_{\perp}$ dependence of these devices does not reproduce. It may be changed completely when they are warmed up to room temperature and cooled back down again. Furthermore the enclosed area between the point contacts is unpredictable.

The device of fig. 6 is more sensitive to magnetic fields. Also the area between the point contacts has a well defined orientation with respect to the external magnetic field. The advantage of using tin is that one can easily work in the temperature region where the amplitude of the oscillations is a maximum. However, this device also lacks reproducibility. This is mainly due to the fact that the coefficients of thermal expansion of nylon, tin and niobium are different. The thermal stresses in the device change the adjustment of the screws. They have to be adjusted before cooling down to liquid-helium temperatures and one cannot be sure beforehand that oscillations will be observed at all.

An improved version of the device in fig. 6 is depicted in fig. 7⁷⁰⁾. It consists of two niobium blocks and two niobium screws, separated by a thin layer (150 μm) of Schott sealing glass 101. The niobium blocks and the glass were baked together in order to form a mechanically solid unit. The glass has the same coefficient of thermal expansion as niobium. Hence there are no thermal stresses in the device. This device does not require re-adjustment between two thermal cyclings and is sufficiently reliable to be used as a magnetometer. A summary of the data on these double point contacts is given in table I.

TABLE I

Summary of the data of double-point-contact devices with different enclosed area \bar{O} . They are all constructed according to fig. 7 with a normal metal cylinder in the hole. Sample number 2 was used for the experiment described in fig. 27. Sample number 17 is used to measure the London moment.

 Sample construction

| | | | | | |
|--|------|------|-----|------|-----|
| Sample number | 2 | 10 | 11 | 17 | 15 |
| Hole diameter (mm) | 1.8 | 3.1 | 5.2 | 10.1 | 15 |
| Cylinder length (mm) | 12 | 12 | 10 | 25 | 20 |
| % of the area \bar{O} , not shielded by the normal metal | 100 | 13 | 8 | 4 | 5 |
| Kind of normal metal | - | Pt | Pt | Pt | Pt |
| Total resistance at 300 K (Ω) | 1.25 | 1.65 | 1.8 | 2.2 | 1.3 |

Calculations

| | | | | | |
|---|------|------|------|------|------|
| Self-inductance of the cylinder (10^{-10} H) | - | 7.5 | 25 | 50 | 112 |
| Amplification factor due to the presence of the normal metal | - | 7.8 | 12.5 | 25 | 20 |
| Total flux noise/($h/2e$) in % | 6 | 10 | 19 | 27 | 47 |
| Reduction factor of the amplitude of the \bar{V} oscillations due to hf noise | 0.93 | 0.82 | 0.45 | 0.25 | 0.04 |
| Lf flux noise/($h/2e$) in % | 0.2 | 0.3 | 0.6 | 0.9 | 1.5 |
| Magn.field period ΔB_L (μ G) | 8.15 | 2.75 | 0.98 | 0.26 | 0.12 |

Observations

| | | | | | |
|--|-----|-----|-----|-----|------|
| i_c at 4.2 K (μ A) | 650 | 155 | 225 | 110 | 105 |
| Peak-to-peak amplitude of the \bar{V} oscillations ΔV (nV) | 250 | 600 | 330 | 200 | 140 |
| $\Delta V/\Delta B_L$ (mV/gauss) | 30 | 218 | 340 | 800 | 1200 |
| Lf. flux noise/($h/2e$) in % | 2 | 0.6 | 1.5 | 2 | 8 |
| Lf. magn. field noise (ngauss) | 160 | 16 | 15 | 5 | 10 |
| Number of thermal cyclings without readjustment | 28 | 21 | 8 | 21 | |

The first part of the paper is devoted to a general discussion of the problem. It is shown that the problem is equivalent to the problem of finding a function which is harmonic in the interior of a domain and which takes prescribed values on the boundary. This is a well-known problem in the theory of harmonic functions. The second part of the paper is devoted to the construction of a function which is harmonic in the interior of a domain and which takes prescribed values on the boundary. This is done by the method of conformal mapping. The third part of the paper is devoted to the construction of a function which is harmonic in the interior of a domain and which takes prescribed values on the boundary. This is done by the method of conformal mapping.

The fourth part of the paper is devoted to the construction of a function which is harmonic in the interior of a domain and which takes prescribed values on the boundary. This is done by the method of conformal mapping. The fifth part of the paper is devoted to the construction of a function which is harmonic in the interior of a domain and which takes prescribed values on the boundary. This is done by the method of conformal mapping. The sixth part of the paper is devoted to the construction of a function which is harmonic in the interior of a domain and which takes prescribed values on the boundary. This is done by the method of conformal mapping.

The seventh part of the paper is devoted to the construction of a function which is harmonic in the interior of a domain and which takes prescribed values on the boundary. This is done by the method of conformal mapping. The eighth part of the paper is devoted to the construction of a function which is harmonic in the interior of a domain and which takes prescribed values on the boundary. This is done by the method of conformal mapping. The ninth part of the paper is devoted to the construction of a function which is harmonic in the interior of a domain and which takes prescribed values on the boundary. This is done by the method of conformal mapping.

The tenth part of the paper is devoted to the construction of a function which is harmonic in the interior of a domain and which takes prescribed values on the boundary. This is done by the method of conformal mapping. The eleventh part of the paper is devoted to the construction of a function which is harmonic in the interior of a domain and which takes prescribed values on the boundary. This is done by the method of conformal mapping. The twelfth part of the paper is devoted to the construction of a function which is harmonic in the interior of a domain and which takes prescribed values on the boundary. This is done by the method of conformal mapping.

PART II

ELECTROSTATIC EFFECTS IN SUPERCONDUCTORS

DUE TO TEMPERATURE GRADIENTS*

CONTENTS

§6 INTRODUCTION. §6.1 Preliminary considerations. The analogy between superconductors and helium II. §6.2 Choice of the measuring method. The analysis of a simple circuit. §6.3 Apparatus design considerations. Conflicting requirements. §6.4 The temperature dependence of the work function. The entropy term in the temperature dependence of the work function is not the only term.

§7 ANALYSIS OF THE MEASURING METHOD; DISCUSSION OF THE EFFECTS CONTRIBUTING TO THE ELECTROSTATIC SIGNAL. §7.1 Analysis of the measuring method. §7.2 The temperature dependence of the work function. The contribution due to the thermal expansion of the metal. Continuous W-T dependence at T_c .

§8 DESCRIPTION OF THE APPARATUS; NOISE SOURCES AND ERRONEOUS SIGNALS. §8.1 Description of the apparatus. The construction of the sample. §8.2 Noise sources and erroneous signals. Thermal expansion in combination with a contact potential; thermocouples in the system; direct and rectified pick-up.

§9 EXPERIMENTAL RESULTS. Self-consistency tests. The measured W-T dependences of Nb, Pb and Cu. The influence of a helium layer on the W-T dependence.

§10 CONCLUSIONS OF PART II.

* Part of this research was done in cooperation with dr. P.B. Pipes during his stay at the Kamerlingh Onnes Laboratory from September 1969 to August 1970 (§6.2 - 6.4, §7, §8).

§6 INTRODUCTION

§6.1 PRELIMINARY CONSIDERATIONS

Since the publication of the books of London^{38,71)} the analogy between the behaviour of superconductors and helium II has been of continuing interest (Vinen⁷²⁾). A superconductor has got its name from the property that a dc electric current can flow through a superconducting wire without any voltage appearing across the terminals. Helium II (the liquid phase of ⁴He below 2.17 K at saturated vapour pressure) is called superfluid because it can flow through a narrow capillary without any pressure difference across the ends. The electrons in a superconductor and the helium atoms in helium II both behave as particles of a fluid that can flow without any friction. This similarity has a fundamental origin.

The helium atoms are bosons and therefore they obey Bose-Einstein statistics. Below 2.17 K a (Bose-Einstein) condensation takes place. This can be characterized by the conjecture that below 2.17 K the same single-particle quantum state is occupied by a macroscopic number (on the order of Avogadro's number) of helium atoms. The electrons in a metal are fermions and therefore obey Fermi-Dirac statistics. In a superconductor however, the interaction between the electrons via the lattice leads to the formation of the so-called Cooper-pairs⁴⁷⁾. These electron pairs have spin zero. Since these quasi particles are in a way bosons they can occupy the same single quasi-particle quantum state. The fact that in helium II and in a superconductor a single (quasi) particle quantum state is occupied by a macroscopic number of (quasi) particles is the basic reason that their behaviour is so similar. For both superfluids a complex order parameter can be introduced. This order parameter has an amplitude ψ_0 and a phase ϕ (eq. 1.1), as was discussed in Part I. The requirement that the wave function is single valued leads to the prediction that $\vec{p}_s \equiv 2m\vec{v}_s + 2e\vec{A} = 0$ for the electrons in a solid, isolated block of superconducting material and that $\vec{p}_s \equiv m\vec{v}_s = 0$ in a bulk volume of superfluid helium. H. London predicted in 1946 that this means for helium experimentally that it is impossible to make a singly-connected volume of superfluid helium rotate with respect to the fixed stars. For a rotating superconductor this means that a magnetic field is developed in a superconductor (the London moment) given by

$$\vec{B} = -\frac{2m}{e}\vec{\omega}$$

where ω is the angular velocity of the superconductor (see §4.7). This relation was derived by F. London³⁸⁾. It implies that a rotating superconducting rod will have a magnetic moment, the so-called London moment. It has been investigated first in 1964 by Hildebrandt⁷³⁾. The measured value of \vec{B} is in agreement with the calculated value.

When $\vec{\omega} = 0$ then $\vec{B} = 0$ even when an external magnetic field is applied on the superconductor. This fact is known as the Meissner effect (see part I, §1). The "Meissner effect in helium" is much more difficult to verify experimentally. In 1967 Hess and Fairbank⁷⁴⁾ succeeded in demonstrating that also the analogue of the Meissner effect exists in helium.

Under certain conditions it is thermodynamically unfavourable for a bulk volume of superfluid to maintain a complete Meissner effect. In that case the superfluid forms threads or rings of a non-superfluid core. The superfluid can then no longer be considered as a singly connected body. The requirement that the wave function is single valued then does not lead to $p_s = 0$ but to the quantization of the circulation integral of the generalized impulse:

$$\oint \vec{p}_s ds = nh.$$

Following Onsager and Feynmann this means that for helium the circulation of \vec{v}_s , $\oint \vec{v}_s ds$ is quantized in units of h/m (75). In a superconductor it gives fluxoid quantization in units $h/2e$ (see §1.1). In both types of superfluids a regular structure of vortex lines can build up. Also in multiple connected volumes the behaviour of superfluid helium is similar to the behaviour of superconductors. Due to the total absence of friction the circulation $\oint \vec{v}_s ds$ is conserved in time, as demonstrated by van Alphen et al. (76), while in a superconducting ring the magnetic flux is conserved.

The analogy between helium II and a superconductor can also be extended to the ac Josephson effect. Just as the ac Josephson effect in superconductivity is described by the relation $v = \frac{\Delta \mu}{h} = 2e\bar{v}_M/h$ (see part I), there exists an ac Josephson effect in liquid helium described by the relation $v = \Delta\mu/h = mgz/h$, in which z is the pressure head in cm helium (Anderson and Richards 77).

As a last example of the similarity between superfluid helium and a superconductor we discuss here the Bernoulli effects in the two superfluids. A gradient in the square of the velocity of the superfluid particles should give rise to a pressure gradient in helium II and an electrostatic voltage gradient in superconductors.

Landau (78) postulated in 1941 that in the two-fluid model for helium II the driving force for the superfluid component is equal to the gradient in the chemical potential. This leads to the equation of motion

$$\begin{aligned} m_4 \frac{D \vec{v}_s}{Dt} &\equiv m_4 \frac{\partial \vec{v}_s}{\partial t} - m_4 \vec{v}_s \times (\vec{\nabla} \times \vec{v}_s) + \vec{\nabla} \left(\frac{1}{2} m_4 v_s^2 \right) \\ &= -\vec{\nabla} \mu = -v_o \vec{\nabla} p + s \vec{\nabla} T + \frac{\rho_n}{\rho} \vec{\nabla} \left(\frac{1}{2} m_4 (v_n - v_s)^2 \right) - m \vec{\nabla} H \end{aligned} \quad (6.1)$$

where m_4 is the mass of a helium four atom, ρ is the density of the fluid, $v_o = m_4/\rho$ is the volume per particle, s is the entropy per particle, \vec{v}_n is the velocity of the normal fluid, \vec{v}_s is the velocity of the superfluid, and ρ_n is the density of the normal fluid.

When $\vec{\nabla} \times \vec{v}_s = 0$ everywhere in the fluid, this equation gives for a stationary flow ($\partial \vec{v}_s / \partial t = 0$) at constant temperature ($\vec{\nabla} T = 0$) and when the normal component is clamped by a superleak ($\vec{v}_n = 0$) that $\frac{1}{2} \rho_s v_s^2 + p/\rho$ is a constant everywhere in the fluid. Hence a difference in the superfluid velocity gives rise to a pressure difference. This so-called "Bernoulli pressure" cannot be measured in a Venturi tube (Meservey 79), van Alphen (80)). One has to use a membrane gauge (Hildebrandt 81)) or a Rayleigh disk (Pellam 82)).

The analogue of the Bernoulli pressure exists also in a superconductor. It can be generated by applying an external magnetic field on a superconducting cylinder (Bok and Klein ⁸³). The Meissner currents in the sample gives rise to a gradient in the velocity of the Cooper pairs. When the magnetic fields are sufficiently slowly varying (below the gap frequency) no currents of normal electrons are generated. Therefore the normal electrons are essentially clamped by the lattice just like the normal fluid in helium II is clamped by a superleak. The equation of motion for the Cooper pairs is ^{38,84,85,92}

$$\begin{aligned} 2m_e \frac{D \vec{v}_s}{Dt} &= 2m_e \frac{\partial \vec{v}_s}{\partial t} - 2m_e \vec{v}_s \times (\vec{\nabla} \times \vec{v}_s) + \vec{\nabla} \frac{1}{2} (2m_e v_s^2) \\ &= -\vec{\nabla} 2\mu + 2e (\vec{E} + \vec{v}_s \times \vec{B}) \end{aligned}$$

which together with the London equation $e\vec{B} = -m_e \vec{\nabla} \times \vec{v}_s$ (PART I, eq. (1.6)) gives

$$\begin{aligned} m_e \frac{\partial \vec{v}_s}{\partial t} &= -\vec{\nabla} (\mu + \frac{1}{2} m_e v_s^2) + e \vec{E} - m \vec{\nabla} H \\ &= -\vec{\nabla} (eV + \mu + \frac{1}{2} m_e v_s^2 + mH) \\ &= -\vec{\nabla} (\bar{\mu} + \frac{1}{2} m_e v_s^2 + mH). \end{aligned} \quad (6.2)$$

In this equation \vec{v}_s is the superfluid velocity, e the electron charge, m_e the electron mass and \vec{E} the electric field in the superconductor. Furthermore $\vec{\nabla} \mu$ is given by ⁸⁴⁻⁸⁶

$$\vec{\nabla} \mu = \vec{\nabla} \mu_0 - \frac{1}{2} \frac{\rho_n}{\rho} m \vec{\nabla} (\vec{v}_n - \vec{v}_s)^2$$

where μ is the chemical potential per electron when $\vec{\nabla} (\vec{v}_n - \vec{v}_s)^2 = 0$.

In eq. (6.2) is added a term $2e\vec{E} = -2e\vec{\nabla} V$ (compared with eq. (6.1)) because the Cooper pairs are charged quasi particles. In Part II the $\partial \vec{A} / \partial t$ term can always be neglected in \vec{E} (electrostatics). Hence $\vec{E} = -\vec{\nabla} V$ and $\bar{\mu} = \mu$.

A complete set of the two-fluid equations of motion in a superconductor, based on the analogy between a superconductor and helium II, is given by Putterman and de Bruyn Ouboter ⁸⁵) and by Putterman in his thesis.

In connection with the dissipative term $\vec{\nabla} H$ in eq. (6.2) exists a phenomenological relation

$$mH = -\zeta \vec{\nabla} \cdot \vec{J}_s.$$

For helium II the term $\vec{\nabla} H$ is introduced by Khalatnikov ¹¹⁴). In a superconductor it can be interpreted as a difference in the electrochemical potential of the normal and the superconducting electrons due to a non-equilibrium between the two fluids. The presence of this difference

can in certain situations lead to interesting consequences, which have recently obtained attention (115-118). In our discussion we will neglect possible contributions of the $\vec{\nabla}H$ term, because the influence of $\vec{\nabla}H$ is usually very small.

For a stationary flow ($\partial\vec{v}_s/\partial t = 0$) at constant temperature ($\vec{\nabla}\mu_0 = 0$), an electrostatic voltage difference exists between two points 1 and 2 in the superconducting metal equal to:

$$V_2 - V_1 = -\frac{m_e \rho_s}{e\rho} \frac{1}{2}(v_{s,2}^2 - v_{s,1}^2),$$

if the normal component is clamped ($\vec{\nabla}_n = 0$).

Since in a stationary situation $\vec{\mu}$ is constant, this electrostatic voltage difference cannot be measured by a voltmeter which is directly connected to the points 1 and 2 (see §1.1). It will be shown in §6.2 that the Bernoulli voltage can be measured if the coupling between the superconductor and the voltmeter is established via a capacitor and (phase sensitive) ac techniques are used. Bok and Klein⁸³⁾ and Morris and Brown⁸⁶⁾ measured the Bernoulli voltage in this way. Although the theory described above has been criticized by Adkins and Waldram⁸⁷⁾ on the basis of microscopic considerations, the experimental results are in agreement with this simple local two-fluid electron theory.

Eq. (6.1) is also the basic equation for the fountain pressure in helium II. The fountain effect arises when a temperature gradient is applied in helium II. The warm end will have a larger pressure than the cold end (from eq. (6.1) with $\vec{v}_n = \vec{v}_s = 0$ and $\partial\vec{v}_s/\partial t = 0$) according to

$$\Delta p = \frac{\rho_s}{m_4} \Delta T \quad (\text{H. London}).$$

When the liquid at the high pressure end can escape then the liquid will squirt like a fountain.

Apart from a paper of Ginzburg in 1944⁸⁸⁾, the superconducting analogue of the fountain effect in helium II has not been considered until recently. Since 1964 several papers showed that there should indeed be voltage differences in a superconductor that can be considered as the analogue of the fountain pressure in helium II (Luttinger⁸⁹⁾; Kresin and Litovchenko⁹⁰⁾, Stephen⁹¹⁾, Betbeder-Matibet and Nozieres⁹²⁾, Vinen⁹³⁾, Putterman and de Bruyn Ouboter⁸⁵⁾). A simple derivation of the fountain effect in a superconductor based on the analogy between a superconductor and helium II can be obtained from eq. (6.2). In a stationary situation $\vec{\mu}$ is constant. The contributions in $\vec{\mu}$ of the velocities of the superfluid and normal particles, analogous to the $\frac{1}{2}m_e v_s^2$ in eq. (6.2), are neglectable in this case. Hence we obtain for a superconductor that

$$\vec{\nabla}\vec{\mu} = \vec{\nabla}\mu + e\vec{\nabla}V = 0.$$

This relation implies that there is no Seebeck effect in a superconductor.

A temperature difference in a superconductor does not give rise to a difference in $\bar{\mu}$ and therefore not to a thermal emf. This property has been observed with great accuracy⁹⁴). It is perhaps the most convincing experimental proof for the validity of eq. (6.2).

When one uses for the chemical potential the naive relation

$$\mu = -\int_0^T s_e dT,$$

where s_e is the entropy of the electrons per electron, then a fountain voltage of the order of 1 μV per kelvin is expected for metals such as niobium or lead. Later on it will be shown that this naive expression (Vinen⁹³) for the change in μ due to a temperature gradient is very incomplete and misleading. It is clear from the beginning that the fountain effect in a superconductor will never be able to drive the electrons out of the metal. The binding forces between the electrons and the metal are much too strong. The fountain effect in a superconductor should be compared with the fountain effect in helium II in a closed vessel. Like the Bernoulli potential, the fountain potential cannot be measured with wires connected to the superconductor. Since the fountain voltage is part of the temperature dependence of the work function of the superconductor (§6.2), we used a capacitive method. Part II of this thesis describes the experiment in which we measured the temperature dependence of the work function of niobium and lead.

§6.2 CHOICE OF THE MEASURING METHOD.

An electrostatic voltage difference cannot always be measured by connecting a voltmeter directly to the two points of interest. Here we are interested in the voltage difference in a metal with a temperature difference between the ends. Since both terminals of the voltmeter have to be at the same temperature, this means that in a part of the circuit a temperature difference must exist that exactly cancels the temperature difference in the sample. Thus we have constructed a thermo couple. In order to demonstrate the principle of the measuring method, we consider a circuit that contains only elements of the same superconducting material. From eq. (6.2) it follows that $\bar{\mu}$ is constant in the stationary state ($\partial v_s / \partial t = 0$), even when there is a temperature gradient. Hence there is no thermal emf. The voltmeter will measure zero voltage when the wires are connected directly to the sample (fig. 34a). If, however, the contact between the voltmeter and the sample is established via a vacuum capacitor (fig. 34b), the voltmeter will measure the voltage difference in the sample if the temperature is cycled with a frequency f such that the resulting impedance $1/(2\pi f C_M)$ of the capacitance is much smaller than the impedance of the voltmeter ($C_M \gg C_V$, see eq. (7.9)). For these frequencies the voltage difference across the measuring capacitance C_M is practically zero. The chemical potential of the vacuum is taken to be zero. Hence the electrochemical potential is constant in the vacuum between the sample and the capacitor plate. Addition of eV and $\bar{\mu}$ in all parts of the circuit now shows that the electrochemical potential across the voltmeter terminals (C_V) is equal to $e\Delta V$ in the sample. Here it is

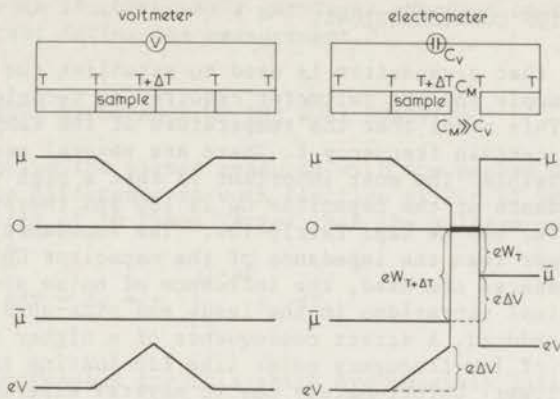


Fig. 34 Dependence of temperature (T), chemical potential (μ), electrostatic energy (eV) and electrochemical potential ($\bar{\mu}$) as a function of place in the sample and in the voltmeter connections. For simplicity *all* metals are supposed to be the same and *superconducting*.

a) The voltmeter is connected directly to the sample. The electrochemical potential is constant throughout the circuit. The voltmeter indicates zero voltage. Since the impedance of the circuit is low, the voltmeter can be an ordinary voltmeter with a fairly low input impedance.

b) An electrometer (high-input-impedance voltmeter) is connected capacitively to the sample. Since eV changes in the sample and V is constant across the capacitor C_M (with $C_V \ll C_M$, see eq. (7.9)) a voltage difference will appear across the terminals of the electrometer. Since μ is the same at both ends of the voltmeter, the change in $\bar{\mu}$ across the voltmeter is equal to the change in eV across the sample. The change in $\bar{\mu}$ across the voltmeter can be interpreted as due to a change in work function of the superconducting metal.

assumed that the surface dipole layer of the metal is constant as a function of temperature. When different materials are used in the circuit a dc voltage will be developed across the capacitor (§7.1). Only the time-dependent part in the electrochemical potential will be measured by the voltmeter (eq. (7.9)) and this is $e\Delta V$.

The argument for the measurement of the Bernoulli potential in superconductors is essentially the same as for the measurement of the fountain voltage. When the wires of the voltmeter are connected directly to the sample, contact voltages will be established that exactly cancel the Bernoulli voltage. Just as in the case of the fountain voltage a capacitive coupling gives rise to the desired signal in the voltmeter. The assumption here is that the surface dipole layer of a superconducting metal is independent of the velocity of the electrons at the surface. The agreement between theory and experiment shows that this assumption is justified. Later on we will see that the assumption that the surface dipole layer is temperature independent (a necessary condition for a correct measurement of the fountain voltage) is not correct (Herring and Nichols 95)).

§6.3 APPARATUS DESIGN CONSIDERATIONS.

The fact that a capacitor is used to establish the connection between the sample and the voltmeter requires ac techniques to measure the voltage. This means that the temperature of the sample should be varied with a certain frequency f . There are several reasons to make f as high as possible. The most important is that a high value of f means that the impedance of the capacitor C_M is low and therefore the impedance of the voltmeter can be kept fairly low. (The impedance of the voltmeter should be larger than the impedance of the capacitor C_M , eq. (7.9)). When low impedances are used, the influence of noise sources like thermal noise, mechanical vibrations in the leads and pick-up signals (50 Hz, rf stations) is reduced. A direct consequence of a higher frequency is that the influence of low-frequency noise like fluctuating thermal voltages in the leads is lower. Unfortunately due to several experimental circumstances the frequency f is in practice as low as 1.5 Hz. The basic reason for this low frequency is that one wants to warm the sample up and cool it back down to *well defined* temperatures. Warming the sample up quickly is no problem. With a good heater one can warm up the sample to the desired temperature in a short time. During the cool-down part of the period however one has to switch the heater off and wait till the sample comes back to its original temperature. The cool-down time constant is proportional to the length of the sample squared. Hence a short sample is necessary. Furthermore, the capacitive coupling between the sample and the voltmeter should be as large as possible (§7). This requires large cross dimensions. A short sample with large cross section implies that large amounts of heat are necessary to warm it up. The dimensions of the sample were mainly determined by the fact that the liquid helium in the dewar should not boil off too quickly. The niobium samples were typically 10 mm long and 5 mm in diameter.

The capacitive coupling between the sample and the voltmeter was 5 - 100 pF giving an impedance of 10^9 to $10^{11} \Omega$ at 1.5 Hz. The thermal noise of a $10^{10} \Omega$ resistance at room temperature is, for a time constant of 1 second, equal to 0.6 μV . Therefore powerful signal averaging techniques are necessary to get a good signal-to-noise ratio because there are important other noise sources (mainly due to mechanical vibrations) and the signal is expected to be of the order of 1 μV . We used a lock-in detector with a time constant of 100 seconds (fig. 40).

In order to avoid oxidation and contamination of the sample surfaces a vacuum of 10^{-10} to 10^{-12} torr is necessary. Furthermore the sample should be formed in this vacuum (by evaporation techniques) or it should be annealed and outgassed (for niobium at 1500 - 2000 K). In addition to these requirements it should be possible to mount a thermometer which can be used in the liquid-helium range, which is resistant against very high temperatures and that can measure the temperature within 0.1 K. Furthermore one wants to obtain a sensitivity of 1 μV . The usual sensitivity in work-function measurements is about 10 mV.

In this experiment one has to compromise between these requirements. We mounted the heater and thermometer on the sample in open atmosphere. The pressure in the inner vacuum can (see fig. 36) was 10^{-5} torr before the sample was cooled down to helium temperature. During the measurements the pressure was as small as the vapour pressure of nitrogen and oxygen

at 4.2 K. Hence if there was a gas layer adsorbed on the sample surface, it was constant during the measurement.

§6.4 THE TEMPERATURE DEPENDENCE OF THE WORK FUNCTION.

For niobium the signal measured with the method described in §6.2 and §6.3 (the difference in work function at $T + \Delta T$ and T) turns out to be of the order of 10 times larger than the voltage calculated with the naive formula

$$-e\Delta V = \Delta\mu = - \int_T^{T+\Delta T} s_e dT.$$

There are two reasons for this which are possibly intimately connected. First of all the assumption that the surface dipole layer of the metal is independent of temperature is probably not justified (Herring and Nichols). Secondly by writing $d\mu = -s_e dT$ we neglect terms in μ due to the thermal expansion of the metal. In fact $d\mu = -s_e dT + v_e dp$. Hence when p is temperature dependent (due to the expansion of the metal) an extra dependence of μ on T is introduced. This extra T dependence of μ can be calculated for a free-electron gas contained within the metal surface. The order of magnitude of the changes in μ due to this term turns out to be larger than the $s_e dT$ term; even at low temperatures where the thermal expansion of a metal is small.

Hence we calculate the change in the chemical potential $d\mu$ when we increase the temperature of an ideal Fermi gas⁹⁶) by dT and at the same time increase the volume of the system by $\alpha_M V dT$, where α_M is the experimental coefficient of the volume expansion of the metal:

$$\begin{aligned} d\mu &= -s_e dT + v_e dp \\ &= -s_e dT + v_e \left(\frac{dp}{dT}\right)_M dT \\ &= -s_e dT + v_e \left\{ \left(\frac{\partial p}{\partial T}\right)_V + \left(\frac{\partial p}{\partial V}\right)_T \left(\frac{dV}{dT}\right)_M \right\} dT \\ &= -s_e dT + \frac{v_e}{\chi_T} (\alpha_p - \alpha_M) dT. \end{aligned}$$

Since the Grüneisen constant

$$\gamma \equiv \frac{\alpha_p V}{\chi_T C_v} = \frac{\alpha_p v_e}{\chi_T s_e} = \frac{2}{3}$$

for an ideal fermi gas

$$d\mu = -s_e dT + \frac{2}{3} \frac{\alpha_p - \alpha_M}{\alpha_p} s_e dT. \quad (6.3)$$

In this expression $\alpha_p \equiv \frac{1}{V} \left(\frac{\partial V}{\partial T} \right)_p$ is the coefficient of volume expansion of an ideal Fermi gas at constant pressure and $\chi_T \equiv -\frac{1}{V} \left(\frac{\partial V}{\partial p} \right)_T$ is the isothermal compressibility of the ideal Fermi gas. The value of α_p is typically on the order of 10^{-10} T/K^2 . On the other hand α_M for niobium is of the order of $10^{-7}/\text{K}$ at liquid-helium temperatures. Therefore $\alpha_M \gg \alpha_p$ and eq. (6.3) can be approximated by

$$d\mu \approx -\frac{2}{3} \frac{\alpha_M}{\alpha_p} s_e dT. \quad (6.4)$$

This relation indicates that the change in μ is strongly dominated by the term due to the expansion of the metal. Although the electrons in niobium can certainly not be considered as being free, we can learn from this kind of observations, that the thermal expansion of the metal affects the interpretation of the fountain voltage in an important manner. An interpretation simply in terms of the entropy per particle (as in the case of helium II) is insufficient. This is basically due to the fact that electrons are charged fermions enclosed in a metal.

§7 ANALYSIS OF THE MEASURING METHOD; DISCUSSION OF THE EFFECTS CONTRIBUTING TO THE ELECTROSTATIC SIGNAL.

§7.1 ANALYSIS OF THE MEASURING METHOD.

In §6.2 we proved that the fountain voltage cannot be measured by connecting wires directly to the sample. A capacitance has to be used to provide the coupling between the sample and the voltmeter. We will give here a more general derivation of the signal that will appear across the voltmeter. Hence the material is not necessarily superconducting and different kinds of metal may be used for the sample and the leads to the voltmeter (fig. 35). The parts B and D of the circuit are the voltmeter leads and are of the same material. The electrometer is represented by its input impedance (parallel capacitance plus parallel resistance) and an ideal voltmeter V (voltmeter with infinite impedance).

From the entropy production and the Onsager relations for an isotropic metal without magnetic field, and with an electric current and a temperature gradient, one obtains (De Groot and Mazur ⁹⁷)

$$\vec{J}_{s, \text{tot}} = -\frac{\lambda}{T} \vec{\nabla} T - \eta \vec{I} \quad (7.1a)$$

$$\vec{\nabla} \left(\frac{\bar{\mu}}{e} \right) = -\eta \vec{\nabla} T + R \vec{I} \quad (7.1b)$$

where $\vec{J}_{s, \text{tot}}$ is the total entropy flux, λ the heat conductivity, η is the differential thermo-electric power and R is the resistivity of the metal. When $\vec{I} = 0$ (no current flow) we obtain from (7.1b) that

$$\Delta \bar{\mu} \equiv \bar{\mu}_2 - \bar{\mu}_1 = -e \int_1^2 \eta(T) dT$$

or

$$V_2 - V_1 = -\frac{1}{e} (\mu_2 - \mu_1) - \int_1^2 \eta(T) dT. \quad (7.2)$$

In parts of the circuit where $\vec{\nabla} T = 0$ and $\vec{I} = 0$ the value of $\bar{\mu}$ is constant. At the contact surface of two different metals for example the chemical potential μ is discontinuous but a dipole layer is formed in the contact region that gives rise to a discontinuity in V in such a way that $\Delta \bar{\mu} = \Delta \mu + e \Delta V = 0$. Hence

$$\mu_2 - \mu_1 = -e(V_2 - V_1) \quad (7.3)$$

at a contact surface between two metals.

In order to be able to calculate the signal appearing across the voltmeter in fig. 35 we need the definition of the true work function of a metal (Herring and Nichols ⁹⁵).

$$eW = \bar{\mu} - eV^V = e(V^M - V^V) + \mu ,$$

or

$$V^V - V^M = -W + \frac{\mu}{e} . \quad (7.4)$$

In eq. (7.4) V^V is the electrostatic voltage just outside the metal, V^M is the electrostatic voltage just inside the metal and W is the true work function.

With the Maxwell equation for the electrostatic case

$$\oint E_s ds = - \oint dV = 0 \quad (7.5)$$

we have the sufficient number of equations to calculate the voltage in the voltmeter. Following Domenicali⁹⁸⁾ we add all changes in the electrostatic potential in the metal (fig. 35):

$$V_1 - V_2 = -W^A(T) + \frac{1}{e} \mu^A(T) ,$$

$$V_2 - V_3 = -\frac{1}{e} \mu^A(T) + \frac{1}{e} \mu^A(T) = 0 ,$$

$$V_3 - V_4 = -\frac{1}{e} \mu^A(T) + \frac{1}{e} \mu^B(T) ,$$

$$V_4 - V_5 = -\frac{1}{e} \mu^B(T) + \frac{1}{e} \mu^B(T) = 0 ,$$

$$V_5 - V_6 = V , \quad (7.6)$$

$$V_6 - V_7 = -\frac{1}{e} \mu^D(T) + \frac{1}{e} \mu^D(T) = 0 ,$$

$$V_7 - V_8 = -\frac{1}{e} \mu^D(T) + \frac{1}{e} \mu^S(T) ,$$

$$V_8 - V_9 = -\frac{1}{e} \mu^S(T) + \frac{1}{e} \mu^S(T + \Delta T) - \int_{T+\Delta T}^T n_S(T) dT ,$$

$$V_9 - V_{10} = W^S(T + \Delta T) - \frac{1}{e} \mu^S(T + \Delta T) ,$$

$$V_{10} - V_1 = -V_{1,10} .$$

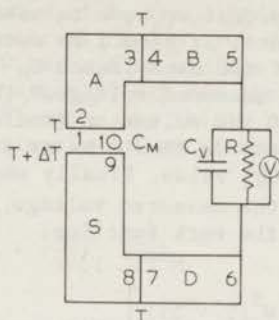


Fig. 35 Diagram of the measuring circuit. "S" represents the sample on which a temperature gradient is applied. "B" and "D" represent the electrometer leads. They are made of the same material. "A" represents the metal establishing the capacitive coupling C_M with the sample. The electrometer is represented by its equivalent circuit. The numbers in this figure distinguish the points in the circuit between which the electrostatic voltage difference is calculated in eq. (7.6).

Since B and D are the same material (the indices B and D simply distinguish the two voltmeter leads) $\mu^B(T) = \mu^D(T)$. Addition of all equations gives

$$V_{1,10} - V = -W^A(T) + \int_T^{T+\Delta T} \eta_S(T) dT + W^S(T + \Delta T). \quad (7.7)$$

In deriving this equation we assumed that currents flowing in the circuit are so small that they do not affect the validity of eqs. (7.2), (7.3) and (7.4). In practice the currents are of the order of 10^{-15} ampere (~ 6000 electrons per second).

The quantity on the right hand side of eq. (7.7) can be regarded as the emf acting on the circuit of the capacitance C_M and the voltmeter in series. Since dc voltages across the voltmeter leak away via the shunt resistance, $\bar{V} = 0$ and we get from eq. (7.7)

$$\overline{V}_{1,10} = \left[W^S(T + \Delta T) - W^A(T) + \int_T^{T+\Delta T} \eta_S(T) dT \right]_{dc}. \quad (7.8)$$

The index dc indicates that we have to take the dc component of the quantity between the brackets.

When $\Delta T = 0$ eq. (7.8) gives the volta potential of the two metals A and S. When the temperature is cycled with a frequency f such that $2\pi f C_V R \gg 1$ then the impedance of the voltmeter can be represented purely by its capacitance. Hence

$$V = - \frac{C_M}{C_V + C_M} \left[W^S(T + \Delta T) + \int_T^{T+\Delta T} \eta_S dT \right]_{ac}. \quad (7.9)$$

Here the index ac indicates that we have to take the ac component of the quantity between the brackets. It should be noted from eq. (7.9) that the nature of the other side of the capacitance C_M (metal A) has in first instance no influence on the measured voltage V (however see §8.2). Furthermore, the capacitance C_V of the voltmeter (including the leads) should be kept as small as possible and C_M should be as large as possible in order to give the best $C_M/(C_M + C_V)$ value. Finally when the metal S is a superconductor then $\eta_S = 0$ and the measured voltage is completely due to the temperature dependence of the work function:

$$V = - \frac{C_M}{C_V + C_M} \left[W^S(T + \Delta T) \right]_{ac} \quad (7.9a)$$

57.2 THE TEMPERATURE DERIVATIVE OF THE WORK FUNCTION.

In order to estimate the temperature derivative of the work function one would like to have an expression for the work function at arbitrary temperature. However, the elegant techniques for the calculation of the properties of the electrons in a metal (bulk properties) based on the periodicity of the lattice are invalid in the surface region of the metal. This complicates the calculation of the surface properties and therefore of the work function. The simplicity of the expression for the work function of a metal (eq. (7.4)) is misleading. The difference in the electric potential $V^M - V^V$ across the surface, and the chemical potential μ contain the many-body effects of the electrons interacting with the lattice. Even at absolute zero the work function is a complicated property of the bulk and surface structure of the metal. Crude models have to be introduced. Recently models are developed based on the formalism of Hohenberg, Kohn and Sham⁹⁹⁾ in which the electrons are treated as an inhomogeneous electron gas (at zero temperature) with density $n(\vec{r})$, moving in a self-consistent pseudopotential including the lattice potential, the electrostatic potential and the exchange and correlation energies. These potentials (except the lattice potential) are all functionals of $n(\vec{r})$. In first approximation the lattice is represented by a uniform positive background. The self-consistency problem described above is numerically solved by Lang and Kohn⁹⁹⁾. The calculated work function is in good agreement (10 - 20%) with the experimental values of elements in which the electrons can be reasonably approximated by a charged electron gas such as the alkali metals. From their numerical results it can be derived that

$$e(V^M - V^V) = (-40 + 6.5 r_s)/r_s^2 \quad (\text{eV}) \quad (7.9)$$

$$\mu = (60 - 24 r_s)/r_s^2 \quad (\text{eV}) \quad (7.10)$$

$$\text{and with eq. (7.4) } |e|W = (-20 + 17.5 r_s)/r_s^2 \quad (\text{eV}) \quad (7.11)$$

In these equations r_s is the radius (in atomic units) of a sphere which on the average contains one electron. (One atomic unit of length is equal

to $5.2 \times 10^{-11} \text{m}$). The value of r_s for different metals varies between 1.5 (high density of electrons) and 6 (low density of electrons). According to eq. (7.11) eW has a flat minimum of 3.94 eV at a r_s value of 2.23. The value of eW changes slowly for the r_s values of the elements of interest while $e(V^M - V^V)$ and μ are fairly strongly r_s dependent.

The temperature derivative of an electron gas contained in a metal can be estimated using

$$\left(\frac{dW}{dT}\right)_M = \left(\frac{\partial W}{\partial T}\right)_V + \left(\frac{\partial W}{\partial V}\right)_T \left(\frac{dV}{dT}\right)_M \quad (7.12)$$

The first term is the change in work function when the volume of the metal is kept constant. With eq. (7.4)

$$\begin{aligned} e\left(\frac{\partial W}{\partial T}\right)_V &= \left(\frac{\partial \mu}{\partial T}\right)_V + e\left(\frac{\partial(V^M - V^V)}{\partial T}\right)_V \\ &= \left(\frac{\partial \mu}{\partial T}\right)_p + \left(\frac{\partial \mu}{\partial p}\right)_T \left(\frac{\partial p}{\partial T}\right)_V + e\left(\frac{\partial(V^M - V^V)}{\partial T}\right)_V \\ e\left(\frac{\partial W}{\partial T}\right)_V &= -s_e + v_e \left(\frac{\partial p}{\partial T}\right)_V + e\left(\frac{\partial(V^M - V^V)}{\partial T}\right)_V. \end{aligned}$$

The value of $(\partial \mu / \partial T)_V$ can be estimated for a free electron gas⁹⁶ (see eq. (6.3)). It turns out to be small. The term $e\{\partial(V^M - V^V)/\partial T\}_V$ can contain all kinds of surface effects such as the possible evaporation of an absorbed gas layer during heating of the sample (§9). For a clean metal surface $(\partial \mu / \partial T)_V$ and $\{\partial(V^M - V^V)/\partial T\}_V$ are not independent. A change in μ affects also the distance over which the electrons tunnel into the vacuum region outside the metal. Hence it affects the double-layer moment. The sign is such that a change in μ is partly compensated by a change in the dipole layer term analogous to the observations of Heine and Höges discussed below. Therefore it is expected that $(\partial W / \partial T)_V$ in eq. (7.12) can be neglected.

The second term of eq. (7.12) gives the change in work function due to the thermal expansion of the metal. It can be written in terms of r_s by

$$\left(\frac{\partial W}{\partial V}\right)_T \left(\frac{dV}{dT}\right)_M = \left(\frac{\partial W}{\partial r_s}\right)_T \left(\frac{dr_s}{dT}\right)_M = \frac{\alpha_M r_s}{3} \left(\frac{\partial W}{\partial r_s}\right)_T.$$

We obtain the contribution in the temperature derivation of $e(V^M - V^V)$, μ and $|eW|$ due to the thermal expansion of the metal by using this relation and eqs. (7.9), (7.10) and (7.11),

$$\frac{3}{\alpha_M} \frac{d}{dT}(eV^M - eV^V) = (80 - 6.5r_s)/r_s^2 \quad \text{eV} \quad (7.13)$$

$$\frac{3}{\alpha_M} \frac{d\mu}{dT} = (-120 + 24r_s) / r_s^2 \quad \text{eV} \quad (7.14)$$

$$\frac{3}{\alpha_M} \frac{d}{dT} (|e|W) = (40 - 17.5r_s) / r_s^2 \quad \text{eV} \quad (7.15)$$

For high-density metals ($r_s < 2.2$) the work function increases with temperature, while for low density the work function decreases with approximately $0.7 \alpha_M$ V. For niobium ($r_s = 1.6$ when there are 5 free electrons per atom) the work function increases with $0.8 \alpha_M$ V. For lead ($r_s = 2.3$) the work function should be practically independent of temperature. For copper $r_s = 2.76$ and dW/dT is equal to $-0.3 \alpha_M$ V.

The agreement between the value of the work function calculated by Lang and Kohn⁹⁹) and the experimental value is a bit surprising. Contributions in the work function due to the fact that the lattice is not a homogeneously charged continuum but a lattice of positive ions seems to be only of second order, in agreement with the experiment; the work function of different metal (crystal) faces differs only by 10%. However, if one wants to answer the question of what the individual contributions of μ and $e(V^M - V^V)$ are in the temperature derivative of the work function, the model has to be handled with great care. Heine and Hodges¹⁰⁰) calculated the potential jump due to the surface dipole layer by substituting as many experimental parameters in the calculated μ as possible. The result is that the value of the electrostatic potential jump at the surface is much smaller than the value calculated by Lang and Kohn. Furthermore Heine and Hodges show that a difference in μ between two different metals is almost completely compensated by a change in $e(V^M - V^V)$, leading to a constant work function of 4.1 eV within an accuracy of 10%.

A discussion of the physical effects contributing in the temperature derivative of the work function is given by Herring and Nichols (ref. 95, table VIII). It should be noted that the effect of the atomic vibrations on the work function can possibly be neglected here because the temperature is low in this experiment. In a *pure* metal with a *clean* surface the main contribution to the temperature dependence of the work function should come from the *expansion effect*. Surface contamination can greatly affect the temperature dependence of the work function especially in a temperature region where the contamination is evaporated from the surface (§9.1).

As a conclusion of this paragraph we would like to remark that much work has to be done in order to calculate the temperature dependence of the work function. At the moment it seems likely that the *temperature derivative of the work function at low temperatures of clean metals is mainly due to the thermal expansion of the metal*

$$\left(\frac{dW}{dT}\right)_M \approx \left(\frac{\partial W}{\partial V}\right)_T \left(\frac{dV}{dT}\right)_M \approx \frac{\alpha_M r_s}{3} \left(\frac{\partial W}{\partial r_s}\right)_T .$$

In the special case of a superconductor a possible contribution in the temperature dependence of the work function could come from the influence of the presence of a gap in the density of states of a superconductor. The chemical potential of the electrons in a metal is defined by

$$N \equiv \int_0^{\infty} \{1 + \exp \frac{E - \mu}{kT}\}^{-1} (dN/dE)dE.$$

By using the fact that the number of states $\int_0^{\infty} (dN/dE)dE$ is conserved at the superconducting transition and that the difference $(dN/dE)_s - (dN/dE)_n$, which is the difference between the density of states of a superconducting and a normal metal, is symmetric with respect to the chemical potential of the superconductor, it can be derived that $\mu_s = \mu_n$. At the critical temperature one should expect this from thermodynamics. Hence we see no discontinuity of the W-T dependence at the superconducting transition temperature. From this point of view the result is quite different from other experiments associated with the work function of metals, such as the photoelectric observations of the energy gap of superconductors by Kunz¹⁰¹). In these electron yield experiments the highest occupied energy levels, in a region of large density of states, are involved. These are in a superconductor the levels just below the energy gap. The value of μ (measured in our experiment) is almost temperature independent, while the energy gap (involved in electron yield experiments) is strongly temperature dependent. Therefore the electron yield in a photoelectricity experiment will be more temperature dependent than one would expect from the temperature dependence of the work function.

58 DESCRIPTION OF THE APPARATUS; NOISE SOURCES AND ERRONEOUS SIGNALS.

58.1 DESCRIPTION OF THE APPARATUS.

Fig. 36 is a schematic drawing of the apparatus. It has three vacuum spaces which can be evacuated independently.

The inner vacuum can (sealed with an indium O-ring) contains the sample with the electrical connections to the electrometer (Analogue Devices 311 J). Attached to the sample are a heater H_s and a thermometer Th_s (see figs. 36, 37 and 38). The inner vacuum jacket can be evacuated by a diffusion pump (P_2) to a pressure of 10^{-5} torr at room temperature. On the outside of the inner vacuum can are attached a 100Ω heater (H) and a calibrated Ge thermometer (Th). Radiation shields in the pumping tube prevent warming up of the can. They also prevent that gas, originally absorbed and gradually released by the room temperature part of the apparatus, continuously flows in the inner vacuum can and thus changes the surface properties of the sample during a run.

The outer vacuum can contains the inner vacuum can. It can be pumped by a mechanical pump P_1 to a pressure of 0.1 torr in order to thermally isolate the inner vacuum can from the liquid-helium bath. Through the valve V_4 we can put helium gas in the outer can to provide good heat contact between the helium bath and the inner vacuum can. Hence the function of the outer vacuum can is to provide a heat switch between the helium bath and the inner vacuum can. The leads of the sample heater

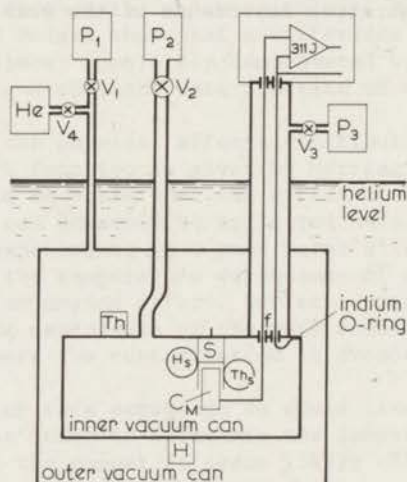


Fig. 36 Diagram of the apparatus. With the pump P_1 the outer vacuum can can be evacuated. Through the valve V_4 one can put helium gas in the outer vacuum can. P_2 is a diffusion pump. It can pump the inner vacuum can down to 10^{-5} torr at room temperature. In the inner vacuum can the sample S is mounted (fig. 37 and 38). On the outside of the inner vacuum can a heater H and a calibrated thermometer Th are attached. With P_3 the shielding tube (III) of the signal wires can be evacuated.

H_s and the sample thermometer Th_s are guided through the pumping tube of P_2 to room temperature. In the case of the niobium sample (fig. 37) the leads of the sample heater run via a feedthrough in the outer vacuum can and from there through the pumping line of P_1 to room temperature. The leads of the 100Ω calibration heater H and the calibrated Ge thermometer go via the pumping tube of P_1 to room temperature. The signal leads from the sample capacitor run via a feedthrough (f) in the third vacuum space (III) which is a stainless steel tube that can be evacuated with P_3 . Glass-to-metal feedthroughs are used to bring the wires outside the vacuum spaces at room temperature (not drawn in the figure).

The construction of the niobium sample and the support system of the measuring capacitance is given in fig. 37. The sample S is attached rigidly to the copper flange of the inner vacuum jacket with a locknut and an indium O-ring. This construction provides good heat contact between the sample and the wall of the vacuum jacket. The cool-down time constant is estimated to be of the order of 20 ms. The wires of the sample heater come from the outer vacuum can via a glass-to-metal feedthrough into the inner vacuum can. The sample heater is made from a $20 \mu\text{m}$ diameter non-inductively wound constantan wire with a total resistance of the order of $30 - 50 \Omega$. The thermal contact between the heater and the sample was provided with General Electric 7031 varnish. The heater was attached to the sample in a groove to provide good heat contact. This was important because a bad heat contact makes the time constant long and the heater can easily be burned out (currents as large as 0.1 A root mean square were passed through the $20 \mu\text{m}$ wire). A high-impedance system is very sensitive for pick-up. Therefore the heater was partly shielded from the measuring capacitance via a diaphragm in the support system.

The capacitive coupling of the electrometer with the high-temperature end of the sample, is realized via a cylinder (C) that is mounted in a hole drilled in the sample and a ring (R) around the sample. The total

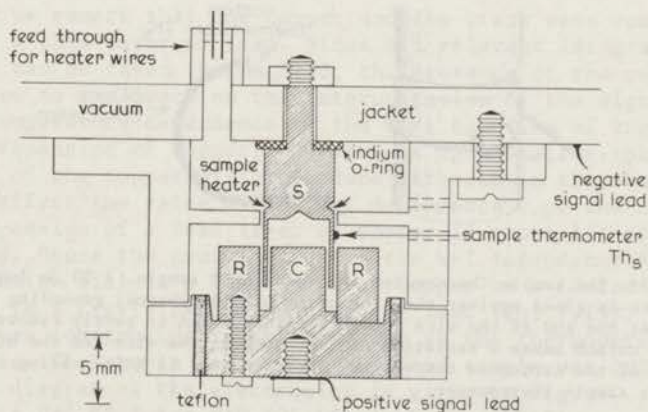


Fig. 37 The niobium sample and the sample capacitance. The sample is attached to the copper vacuum jacket through a hole and fixed by a lock nut. An indium O-ring provides vacuum sealing and good heat contact. The sample-heater wires run via a feed through into the outer vacuum can. The niobium parts are hatched.

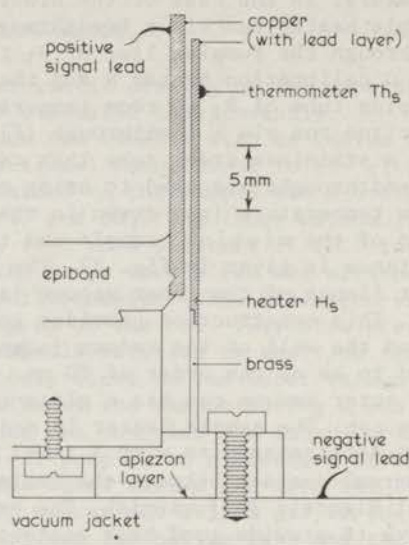


Fig. 38 The copper and lead sample, and the sample capacitance. The device is screwed against the vacuum jacket. The heat contact is provided via a thin layer of apiezon. In the copper sample the hatched parts are pure copper. In the *lead* sample the copper parts and the parts between the copper and the vacuum jacket are covered with a layer of lead. The value of the capacitance C_M was 100 pF for the lead sample, and 66 pF for the copper sample.

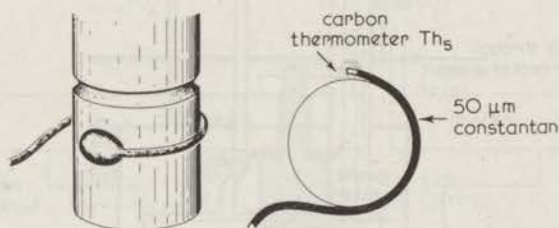


Fig. 39 The sample thermometer on the niobium sample. A 50 μm insulated constantan wire is glued against the niobium to provide thermal grounding and mechanical rigidity. At the end of the wire (where the insulation is partly removed) a small droplet of carbon makes a resistive contact between the wire and the niobium. The resistance of the carbon is temperature dependent and is (after being calibrated) used as the sample thermometer.

capacitance was on the order of 6 - 10 pF. The sample thermometer was attached on the outside of the sample between the diaphragm and the outer capacitance ring.

For the sample thermometer (fig. 39) we used a construction similar to the technique developed by Kunz¹⁰¹). First a 50 μm insulated constantan wire is glued with Ge 7031 varnish on the sample. Then a small droplet (0.5 mm) of Colloidal Graphite (Dag dispersion, Colloidal Graphite in Methylisobutylketon) is dipped on the sample and over the uninsulated end of the 50 μm constantan wire. When the droplet is dry the graphite makes electrical contact between the sample and the uninsulated end of the wire. The room-temperature resistance is of the order of a few hundred ohm. The value at 4.2 K is 2 - 3 times larger. The value of $\frac{1}{R} \frac{dR}{dT}$ at 4.2 K is typically 0.1 K^{-1} . We used this carbon resistance as our thermometer. The temperature can be measured very locally ($\approx 1 \text{ mm}^2$) and fast (time constant of the order of 10 ms). Since the calibration of the thermometer did not reproduce exactly between two thermal cyclings between liquid helium temperature and room temperature, it had to be calibrated at the beginning of every run. All components (heater, thermometer and sample) have a thermal time constant of the order of 10 ms. Hence when the temperature is cycled with 1.5 Hz the sample is continuously in quasi equilibrium. This means that there are no temperature gradients in the warm end of the sample and that the thermometer indicates the real temperature.

A cross section of the lead sample is given in fig. 38. The signal for lead turned out to be small (fig. 42b) and hence the capacitive coupling between the sample and the electrometer had to be large (eq. 7.9a). This implies a long sample and since the cool-down time constant of a rod is proportional to its length squared, the temperature distribution in the sample will not be equal to the quasi-equilibrium distribution. In order to insure that the temperature is at least homogeneous in the warm end of the sample, it is made of copper. A brass section between the heater and the vacuum jacket provides that not too much heat was necessary to warm the sample to the desired temperature. The thermal contact between the sample and the vacuum jacket was established by a thin layer of Apiezon.

Finally we remark that the copper and the brass were completely covered with a thin layer of lead. Since all relevant integration paths in eq. (7.6) can be taken in the lead, the presence of the copper and the brass have no influence on the interpretation of the signal as being due to the temperature dependence of the work function of the lead layer. The thermal expansion of copper, however, is much smaller than of lead. The presence of the copper will introduce stresses in the lead layer. These might affect the value of the W-T dependence *e.g.* the coefficient of volume expansion of a lead layer on copper is about 1/3 of the bulk value of lead. Hence the contribution in the W-T dependence due to the thermal expansion will in a lead layer on copper be a factor of 3 smaller than in a freely expanding piece of lead (eq. 7.15). The sample thermometer was constructed in the same way as the thermometer of the niobium sample. The sample heater for the lead sample was 200 Ω .

A block diagram of the electronics is given in fig. 40. The reference output of a PAR HR 8 (or PAR 124 Lf) lock-in amplifier, tuned at 1.5 Hz, is fed into a pulse generator (fig. 40b) that gives off pulses of ac current at 10 kHz with a repetition rate of 1.5 Hz. A filter F filters out all low-frequency currents. In this way pick-up at the reference frequency is avoided. The heater H_s warms the sample up with a frequency of 1.5 Hz. The signal is fed into an Analog Devices 311 J preamplifier

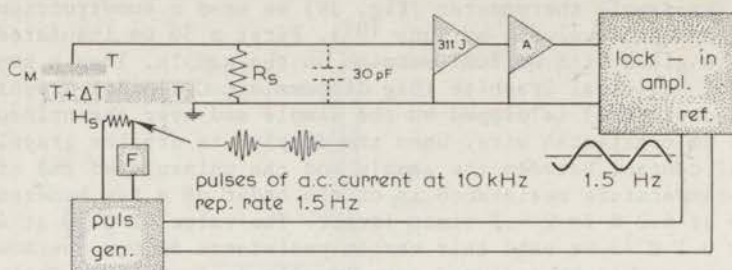


Fig. 40a Block diagram of the measuring circuit.

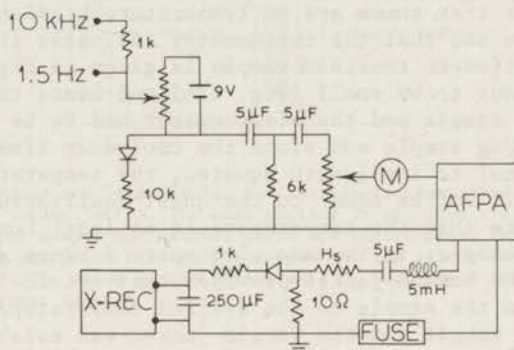


Fig. 40b Diagram of the pulse generator and the heater-current recording system. The reference output of the lock-in amplifier (fig. 40a) is connected to the 1.5 Hz terminal; the output of an audio-frequency oscillator to the 10 kHz terminal. With a motor (M) the input to the audio-frequency power amplifier (AFPA) can be varied slowly from a certain preset value, to zero. The current through the heater H_S is continuously recorded by connecting the rectified voltage across a 10 Ω resistance in series with H_S to the X-axis of an X-Y recorder. The output of the lock-in is connected to the Y-axis. In this way fig. 41 is obtained.

which amplifies the signal with a factor of two. Its main purpose is to match the impedance of the signal source (C_M) with the type A preamplifier of the lock-in amplifier. The leads from the sample to the 311 J preamplifier have a total capacitive coupling of 30 pF. A shunt resistance R_S of $10^9 - 10^{11} \Omega$ keeps the impedance between the leads as low as possible, thus reducing the influence of thermal noise, mechanical vibrations and pick-up as far as possible.

Of all noise sources, the noise due to mechanical vibrations turned out to be the largest. The origin of this kind of noise is that in the space between the signal wire (copper) and the shield (stainless steel) electric fields exist due to the contact potential of the two metals.

This field corresponds to a voltage difference of the order of 1 V. A change in the capacitive coupling C between the wire and the shield of ΔC gives rise to $\Delta C/C$ volt at the input terminal. Hence when $\Delta C/C$ is as small as 10^{-6} the noise voltage is 1 μ V. Because of this extreme sensitivity to mechanical vibrations the cryostat assembly was mounted against a rigid wall. Most of the measurements were performed during the night. The remaining noise was possibly due to fluctuations in the helium bath.

In a typical run we pumped during one or two days with P_1 , P_2 and P_3 . The pressure in the inner vacuum can was then 10^{-5} torr. Next we let the helium in the outer can through V_4 and precooled the apparatus to liquid-nitrogen temperature. Subsequently the valves V_2 and V_3 were closed and the cryostat was filled with liquid helium. Then the outer vacuum can was evacuated with P_1 so that the sample thermometer could be calibrated. In order to do this the inner vacuum can, including the sample and the sample thermometer, was heated with a heater H to several different temperatures between 4.2 and 11 K. A calibrated Ge thermometer was used to determine the temperature. When the calibration of the sample thermometer was completed, the outer can was again filled with helium gas to a pressure of about 1 atm. In the next step we determined the dependence of the temperature of the warm end of the sample $T + \Delta T$ on the peak-to-peak amplitude of the current through the heater H_g . Finally a plot is made of the root-mean-square value of the signal *versus* the peak-to-peak amplitude of the heater current (*e.g.* fig. 41). This last measurement was performed automatically, mostly during the night. The time constant of the lock-in amplifier was set at 100 s. It took 3 to 4 hours to get a complete curve. During this measurement the pumps P_1 , P_2 and P_3 were disconnected in order to reduce mechanical vibrations.

58.2 NOISE SOURCES AND ERRONEOUS SIGNALS

The most important random noise sources have been discussed in the previous chapters (§6, §7 and §8.1) of part II. Random noises like thermal noise, vibration noise and amplifier noise all have in common that they can be averaged out by using a phase-sensitive detector, tuned at the proper frequency and with a sufficiently long time constant τ . The root-mean-square value of the observed noise goes down with $1/\sqrt{\tau}$. If however the measuring technique introduces erroneous ac voltages that interfere with the signal at the reference frequency and with a well-determined phase, then a lock-in detector cannot distinguish between the signal and these (unwanted) ac voltages. Effects that give rise to such ac voltages are discussed below.

When the sample is heated, the warm end of the sample will expand and the distance d between the two capacitor sides of C_M will change by Δd . This means that the capacitance of the capacitor C_M is time dependent, with a frequency equal to the frequency of the temperature of the warm end of the sample. Hence we have a vibrating capacitor. If there is a contact potential V_c across C_M this change in the capacitance will give rise to a voltage according to

$$\frac{\Delta V}{V_c} = - \frac{\Delta C_M}{C_M} = + \frac{\Delta d}{d} = + \frac{\alpha r \Delta T}{d} .$$

When $V_C \approx 1$ volt and $d \approx 0.1$ mm then Δd must be smaller than 1 \AA to provide that $\Delta V < 1 \text{ \mu V}$. For the *lead* sample $r = 10$ mm, $d = 0.1$ mm and $\alpha \approx 2 \times 10^{-8}/\text{K}$ (the thermal expansion of copper in this region) and hence $\Delta V/\Delta T$ would be of the order of 1.6 \mu V/K when $V_C \approx 1$ volt. This might be possible when the two sides of C_M are made of different metals. Since we have lead on both sides V_C will be of the order of 10 mV and the interfering signal 16 nV. For the *niobium* sample $r = 2.5$ mm, $\alpha = 10^{-7}$, $d = 0.1$ mm giving a $\Delta V/\Delta T$ value of 2.5 \mu V/K when $V_C = 1$ volt. Also in this case we used the same metal (niobium) on both sides of the capacitor. Furthermore C_M was so designed that a ring on the outside of the sample compensates capacitance changes on the inside of the sample.

The presence of a contact potential can be simulated by applying a dc voltage on C_M . When the observed signal can be zeroed with a dc voltage in the mV region one can conclude that at least part of the signal might come from the presence of a contact potential.

Another voltage interfering with the signal arises when the low temperature part of the sample is not continuously at 4.2 K but oscillates in time with 1.5 Hz on a certain T level larger than 4.2 K. In that case a Nb-Cu or Pb-Cu thermocouple arises which might contribute to the signal. In the niobium case the temperature of the niobium-copper contact was within the measuring accuracy (0.1 K) equal to 4.2 K. In the lead case the thermal contact between the sample and the copper wall of the vacuum jacket (through a layer of apiezon) could not be considered as perfect. A thermometer on the base of the sample showed that the temperature there was larger than 4.2 but practically constant. Therefore an eventual thermocouple there will not contribute to the ac signal. Furthermore the (small) temperature oscillations of the base of the sample turned out to be out of phase with the temperature oscillations at the warm end of the sample.

Erroneous signals of a completely different nature arise from pick-up from the heater current by the measuring capacitance C_M . The preamplifier 311 J can be saturated by an audiofrequency voltage picked up from the heater current (depending on amplitude and frequency of the heater current). It then rectifies the pulses of this af voltage, leading to a 1.5 Hz output. This kind of pick-up was avoided by using a diaphragm (fig. 37) to shield the heater from the measuring capacitance or by establishing the capacitive coupling in the inside of the sample while the heater is attached on the outside (fig. 38). We used the fact that this erroneous signal is strongly dependent on the af frequency of the heater current to verify that the observed signal was not due to this kind of pick-up.

Pick-up from an eventual 1.5 Hz component in the heater current is avoided by putting a filter (tuned at 10 kHz) in series with the sample heater. Thus low-frequency currents were prevented to flow in the heater.

59 EXPERIMENTAL RESULTS.

The signal-to-noise ratio was of the order of 5 (fig. 41), and there are several sources of erroneous signals as discussed in § 8.2. Therefore several self-consistency tests were carried out. A signal that is due to

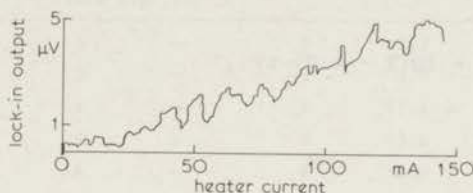


Fig. 41 Typical X-Y plot of the lock-in output versus rectified heater current of a niobium sample.

the temperature dependence of the work function of the sample must fulfil several requirements. Some of these are:

1. The signal must be in phase with the temperature of the sample or 180° out of phase, depending on the (so far unknown) sign of the signal.
2. The signal must be additive:

$$S(T + \Delta T) - S(T) = \{S(T + \Delta T) - S(T + \Delta T_1)\} + S(T + \Delta T_1) - S(T)$$

(the voltage measured when the sample is cycled between $T + \Delta T$ and T must be equal to the voltage measured when the sample is cycled between $T + \Delta T$ and $T + \Delta T_1$ plus the voltage when the temperature varies between $T + \Delta T_1$ and T).

3. The signal must be only dependent on $T + \Delta T$ and not *e.g.* on the value of the audio frequency of the heater current, used to obtain this temperature.
4. The signal must be proportional to C_M when $C_M \ll C_V$ (see eq. (7.9a)).
5. The signal should be different for different metals.
6. The signal should not be too strongly dependent on a dc voltage applied on C_M .

These requirements were investigated most extensively with the niobium samples. The observed signals are not due to one of the erroneous signals described in §8.2. We will now describe the results with niobium, lead and copper separately.

Niobium

The niobium sample is depicted in fig. 37. We obtained a plot of the rms value of the signal versus the amplitude of the heater current with the electronics described in fig. 40. A typical curve is given in

fig. 41. The noise is fairly large even at a time constant of 100 sec. of the lock-in amplifier. For this curve we can derive the signal-temperature dependence using the temperature-heater current calibration. The W-T dependence obtained this way was within the noise a straight line in the temperature range between 4.2 K and 11 K (fig. 42a). The slope was $10 \mu\text{V}/\text{K}$. Hence

$$W_T - W_{4.2} = 10(T - 4.2) \mu\text{V} . \quad (9.1)$$

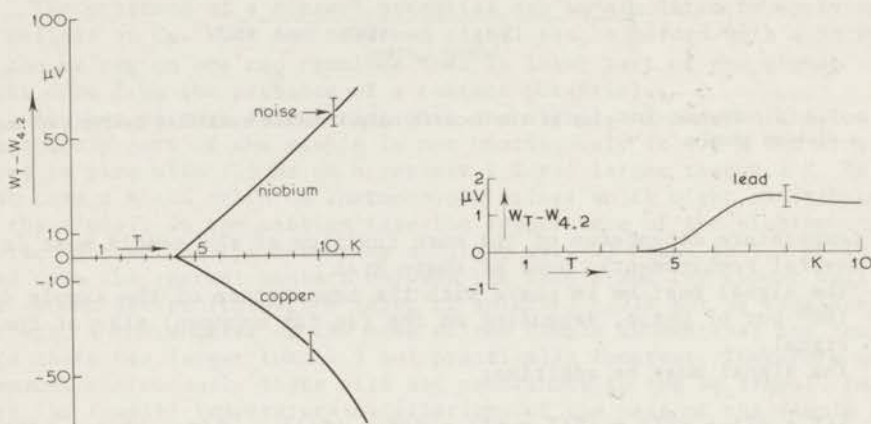


Fig. 42 Temperature dependence of the work function with respect to the value at 4.2 K of
 a) niobium and copper
 b) lead.
 The dW/dT value is for lead an order of magnitude smaller than of copper or niobium.

We observed no discontinuity of any kind at the T_c of the samples. The experimental result described with eq. (9.1) seems to be independent of the purity of the sample. We found the same W-T dependence for a sample with a broad critical temperature region (7.8 K to 8.2 K) as for a purer sample (99.8%) with a sharp T_c at 8.63 K. The W-T dependence was also independent of whether the sample was annealed during one hour at 1500 K, or whether the surface was etched or not. In order to check whether the observed signal could be due to a contact potential across C_M (as explained in §8) we applied a dc voltage on C_M . The signal could be zeroed with a dc voltage of the order of 5 to 10 V. This means that the observed signal cannot be due to a contact potential (which is of the order of 10 mV). A summary of the most important results with the niobium sample is given in Table II.

TABLE II
Summary of Niobium data

| Sample number (always Nb) | Material of Cylinder C ring R (see fig. 35) | C_M (pF) | $\frac{dW}{dT}$ in $\frac{\mu V}{K}$ | V_0 (V) | T_B |
|------------------------------|---|------------|--------------------------------------|-----------|-------|
| 1 | B — | 8 | 8.5 | — | 4.2 |
| 1 | B — | 8 | 9.5 | — | 2.5 |
| 1 | B — | 8 | 11.6 | — | 4.2 |
| 1 | B — | 8 | 13.6 | — | 2.3 |
| 1 | B — | 8 | 10.0 | — | 4.2 |
| 1* | B — | 8 | 11.5 | — | 4.2 |
| 1* | Nb — | 8 | 10.0 | 12 | 4.2 |
| 1** | Nb — | 8 | 10 | — | 4.2 |
| 2 | Nb Nb | 10 | 13 | — | 4.2 |
| 2 | Nb — | 5 | 13 | — | 4.2 |
| 2 | Nb Nb | 10 | 1600 ¹⁾ | — | 4.2 |
| 2 | Nb Nb | 10 | 10 | 20 | 4.2 |
| 2 | Nb — | 5 | 10 | 5 | 4.2 |
| 2 | Nb — | 8 | 8 | 8 | 4.2 |

1) leaking vacuum can.

Sample number one had a transition region between 7.8 K and 8.2 K. 1* is sample number one after etching the surface. 1** is sample number one after annealing it during 1 hour at 1500 K in a vacuum of 10^{-7} torr. Sample number two had a T_C at 8.63 K. B = brass, Nb = niobium, V_0 is the dc voltage that is necessary to zero the signal, T_B is the liquid-helium bath temperature.

Lead

The W-T dependence of lead measured with the sample depicted in fig. 38 is given in fig. 42b. The signal is of the order of 10 times smaller than the signal from niobium. The signal could be zeroed with a dc voltage of 0.1 V. Since contact potentials of different surfaces of the same metal are of the order of 10 mV it is possible that erroneous signals due to the thermal expansion effect as discussed in §8, form part of the measured W-T dependence given in fig. 42b.

Copper

The W-T dependence of copper is measured with the sample depicted in fig. 38, but where the copper was *not* covered with lead. The signal is then due to the work function of copper. The thermo-electric power of brass which might also give rise to a signal was in a separate

experiment shown to be small. The W-T plot is given in fig. 42a. The order of magnitude of dW/dT is the same as for niobium but the sign is different.

TABLE III

| Metal | r_s | $\frac{1}{3} \alpha$ at 10 K $\times 10^6$ K | $\frac{3}{\alpha} \frac{dW}{dT}$ from eq. (7.15) | $(dW/dT)_{10\text{ K}}$ (calculated) | $(dW/dT)_{10\text{ K}}$ (observed) |
|-------|-------|---|---|---|---------------------------------------|
| Nb | 1.6 | 0.3 | 2.4 (V) | $0.7 \frac{\mu\text{V}}{\text{K}}$ | $10 \frac{\mu\text{V}}{\text{K}}$ |
| Pb | 2.3 | 3.2 | -0.1 | -0.1 | ~ 0 |
| Cu | 2.76 | 0.04 | -1.1 | -0.04 | -15 |

Helium

A helium layer adsorbed on the sample surface at 4.2 K strongly affects the measured W-T dependence between 4 K and 10 K because in this temperature region the layer is evaporated from the surface. The W-T dependence of the copper sample, with a small amount of helium in the vacuum can is given in fig. 43. Our measurements show that when $T > 7$ K almost no helium is left on the surface. The W-T dependence is then the same as with no helium in the can. The difference of the work function at 8 K and at 4 K is in good approximation equal to the difference in work function of the sample due to an adsorbed helium layer at 4 K. By admitting helium in the can in discrete quantities, the work function difference saturates at a level of 6 mV

$$W_{\text{gas}} = W_{\text{clean}} - 6 \text{ mV.}$$

An order-of-magnitude calculation shows that this level is reached when an amount of helium is introduced in the can which is sufficient to cover the sample with a monolayer of helium atoms.

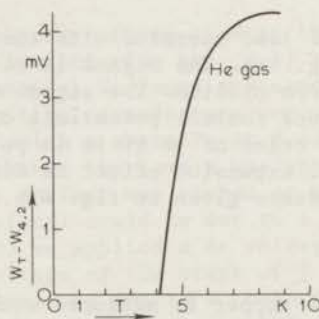


Fig. 43 Temperature dependence of the work function of the copper sample with respect to the 4.2 K value, when there is a small amount of helium in the inner vacuum can (compare the pure copper signal of fig. 42a).

§10 CONCLUSION OF PART II.

In conclusion we would like to remark that an electrostatic voltage difference in a superconductor due to a temperature difference has been observed, although the Thompson, Seebeck and Peltier coefficients are zero. This electrostatic voltage difference is due to the temperature dependence of the chemical potential of the electrons, which is a complicated function of temperature and the metal properties. It cannot be interpreted in the same simple terms as the pressure difference in the fountain effect in helium II. In simple metals the largest contribution in the temperature derivative of μ is probably due to the thermal expansion of the metal. It can be derived that the energy gap in a superconductor gives only a second order contribution on μ . Electrostatic voltage differences due to a difference in μ cannot be measured by connecting two wires to the sample. We used a capacitive coupling and hence measured the work function change of the superconductor. However, the work function is equal to μ plus a contribution due to the dipole layer at the metal surface. With our technique we were able to measure changes in the work function of our samples as small as 0.5 μ V. No discontinuity was detected at the critical temperature of the superconducting samples (niobium and lead). The signal was an order of magnitude larger than the value estimated from the thermal expansion effect. In order to obtain agreement between theory and experiment further investigations are necessary. From the experimental point of view one would like to get a pure sample with a pure surface in the way described at the end of §6.3. Furthermore the calculations should be extended to non-zero temperature and to more realistic cases where the electrons in a metal do not behave as an ideal fermi gas.

REFERENCES

1. P.W. Anderson, *Progress in Low Temp. Phys.* ed. by C.J. Gorter, (1967) (North-Holland Publ. Comp. Amsterdam) Vol. 5 Chap. 1; 1964 in: Lectures on the many-body problem, Ravello Spring School 1963, Vol. 2 ed. by E.R. Caianello (Academic Press) pag. 115; Rev. Mod. Phys. 38, 298 (1966). More recent reviews are published by J.E. Mercereau and B.D. Josephson, "Superconductivity", ed. R.D. Parks (1969; Marcel Dekker inc., New York) Vol. 1, Chaps. 8 and 9. See also ref. 51 and 107.
2. B.D. Josephson, Phys. Lett. 1, 251 (1962); Rev. Mod. Phys. 36, 216 (1964); Advan. Phys. 14, 419 (1965).
3. P.W. Anderson and J.M. Rowell, Phys. Rev. Lett. 10, 230 (1963).
4. J.M. Rowell, Phys. Rev. Lett. 11, 200 (1963).
5. R.C. Jaklevic, J. Lambe, J.E. Mercereau and A.H. Silver, Phys. Rev. 140, A1628 (1965); Phys. Rev. Lett. 12, 159 (1965); 12, 274 (1965); 14, 887 (1965).
6. S. Shapiro, Phys. Rev. Lett. 11, 80 (1963).
7. M.D. Fiske, Rev. Mod. Phys. 36, 221 (1964).
8. I.K. Yanson, V.M. Svistuno and I.M. Dmitrenko, Sov. Phys. JETP 48, 976 (1965) (21, 650).
9. R.E. Eck, D.J. Scalapino and B.N. Taylor, Phys. Rev. Lett. 13, 15 (1964).
10. D.N. Langenberg, W.H. Parker and B.N. Taylor, Phys. Rev. 150, 186 (1966), Phys. Rev. Lett. 18, 287 (1967); W.H. Parker, B.N. Taylor and D.N. Langenberg, Phys. Rev. Lett. 18, 287 (1967); Metrologia 3, 89 (1967); see also: J. Clarke, Phys. Rev. Lett. 21, 1566 (1968); T.F. Finnegan, A. Denenstein and D.N. Langenberg, Phys. Rev. B 4, 1487 (1971); Rev. Mod. Phys. 41, 375 (1969).
11. P.W. Anderson and A.H. Dayem, Phys. Rev. Lett. 13, 195 (1964); A.H. Dayem and J.J. Wiegand, Phys. Rev. 155, 419 (1967). See also ref. 103.
12. J.E. Zimmerman and A.H. Silver, Phys. Lett. 10, 47 (1964); Phys. Rev. 141, 367 (1966).
13. J.E. Zimmerman, J.A. Cowen and A.H. Silver, Appl. Phys. Lett. 9, 353 (1966).
14. A.H. Silver and J.E. Zimmerman, Phys. Rev. 158, 423 (1967).
15. J.E. Zimmerman and J.E. Mercereau, Phys. Rev. Lett. 13, 125 (1964).
16. J.E. Zimmerman and A.H. Silver, Solid State Comm. 4, 133 (1966).
17. J.E. Zimmerman and A.H. Silver, Phys. Rev. Lett. 19, 14 (1967).
18. A.H. Silver and J.E. Zimmerman, Appl. Phys. Lett. 10, 142 (1967).
19. A.H. Silver, J.E. Zimmerman, and R.A. Kamper, Appl. Phys. Lett. 11, 209 (1967).
20. J.E. Zimmerman and A.H. Silver, Phys. Rev. 167, 418 (1968).
21. J.E. Zimmerman and A.H. Silver, J. Appl. Phys. 39, 2679 (1968).
22. A.H. Silver and J.E. Zimmerman, Phys. Rev. Lett. 15, 888 (1965).
23. A.H. Silver and J.E. Zimmerman, Phys. Rev. 157, 317 (1967); J.E. Zimmerman, P. Thiene and J.T. Harding, J. Appl. Phys. 41, 119 (1970); J.E. Zimmerman, J. Appl. Phys. 42, 30 (1971).
24. A.H. Dayem and C.C. Grimes, Appl. Phys. Lett. 9, 47 (1966).
25. C.C. Grimes, P.L. Richards and S. Shapiro, J. Appl. Phys. 39, 3905 (1968); Phys. Rev. Lett. 17, 431 (1968); P.L. Richards, S. Shapiro and C.C. Grimes, Journ. of Physics 36, 690 (1968).
26. W.C. Stewart, Appl. Phys. Lett. 12, 277 (1968).
27. D.E. McCumber, J. Appl. Phys. 39, 297 (1968); 39, 2503 (1968); 39, 3113 (1968).
28. A. Baratoff, J.A. Blackburn and B.B. Schwartz, Phys. Rev. Lett. 25, 1096 (1970).
29. R. de Bruyn Ouboter, M.H. Omar, Miss A.J.P.T. Arnold, T. Guinau and K.W. Taconis, Physica 32, 1448 (1966).
30. M.H. Omar and R. de Bruyn Ouboter, Physica 32, 2044 (1966).
31. M.H. Omar, W.H. Kraan, A.Th.A.M. de Waele and R. de Bruyn Ouboter, Physica 34, 525 (1967).

32. R. de Bruyn Ouboter, W.H. Kraan, A.Th.A.M. de Waele and M.H. Omar, *Physica* 35, 335 (1967).
33. A.Th.A.M. de Waele, W.H. Kraan, R. de Bruyn Ouboter and K.W. Taconis, *Physica* 37, 114 (1967).
34. A.Th.A.M. de Waele and R. de Bruyn Ouboter, *Physica* 41, 225 (1969).
35. A.Th.A.M. de Waele, W.H. Kraan and R. de Bruyn Ouboter, *Physica* 40, 302 (1968).
36. A.Th.A.M. de Waele and R. de Bruyn Ouboter, *Physica* 42, 626 (1969).
37. T.A. Fulton and R.C. Dynes, *J. Appl. Phys.* 42, 45 (1971).
38. F. London, *Superfluids* (1950, John Wiley and Sons Inc) Vol. I; *Phys. Rev.* 74, 562 (1948).
39. V.L. Ginzburg and L.D. Landau, *Zh. Eksperim.i Teor. Fiz.* 12, 1064 (1950). English Transl.: *Men of Physics*, L.D. Landau, ed. by D. ter Haar (Pergamon Press, London, 1965) Vol. 1, p. 138.
40. B.S. Deaver and W.M. Fairbank, *Phys. Rev. Lett.* 7, 43 (1961).
41. M. Doll and M. Näbauer, *Phys. Rev. Lett.* 7, 51 (1961); *Zeitschrift für Physik* 169, 526 (1962).
42. N. Byers and C.N. Yang, *Phys. Rev. Lett.* 7, 49 (1961); C.N. Yang, *Rev. Mod. Phys.* 34, 694 (1962).
43. Y. Aharonov and D. Bohm, *Phys. Rev.* 115, 485 (1959).
44. F. Bloch, *Phys. Rev.* 137, A787 (1965); *Phys. Rev. Lett.* 21, 1241 (1968).
45. B.B. Schwartz and L.N. Cooper, *Phys. Rev.* 137, A829 (1965).
46. R.P. Feynman, R.B. Leighton and M. Sands, *The Feynman Lectures on Physics* (1965, Addison-Wesley Publ. Comp. New York) Vol. III, Chap. 21, sec. 21-9.
47. L.N. Cooper, *Phys. Rev.* 104, 1189 (1956); J. Bardeen, L.N. Cooper and J.R. Schrieffer, *Phys. Rev.* 108, 1175 (1957).
48. C.J. Gorter and H.B.G. Casimir, *Physica* 1, 306 (1934); *Phys. Z.* 35, 963; *Z. techn. Phys.* 15, 539.
49. P.W. Anderson, *Progress in Low Temp. Physics*. Vol. 5, Chap. 1, pag. 32 (1967).
50. S.R. de Groot and P. Mazur, *Non-Equilibrium Thermodynamics* (1969 North-Holland Publ. Cy., Amsterdam-London) Chap. XIII, §4 - §6.
51. W. Schroen, *Journ. Appl. Phys.* 39, 2671 (1968); J.E. Zimmerman, *Appl. Supercond. Conf.*, May 1-3 (1972) Annapolis, Maryland.
52. J. Clarke, *Phil. Mag.* 13, 115 (1966); *New Sci. Mar.* 1966, p. 611; *Phys. Rev. Lett.* 21, 1566 (1968); S. Shapiro, *Phys. Lett.* 25A, 537 (1967).
53. H.J. Levinstein and J.E. Kunzler, *Phys. Lett.* 20, 581 (1966).
54. T.D. Clarke, *Phys. Lett.* 27A, 585 (1968).
55. B.N. Taylor, *J. Appl. Phys.* 39, 2490 (1968).
56. J.W. McWane, J.E. Neighbor and R.S. Newbower, *Rev. Sci. Instr.* 37 1602 (1966).
57. R.L. Forgas and A. Warnick, *Rev. Sci. Instr.* 38, 214 (1967); *IEEE Trans. on Instr. and Measurement* IM-15, 113 (1966).
58. B.T. Ulrich, *Phys. Rev. Lett.* 20, 381 (1968).
59. A. Contaldo, *Rev. Sci. Instr.* 38, 1543 (1967).
60. L.G. Aslamazov and A.I. Larkin, *Sov. Phys. JETP* 9, 87 (1969).
61. J. Warman and J.A. Blackburn, *Appl. Phys. Lett.* 19, 60 (1971).
62. N.R. Werthamer, *Phys. Rev.* 147, 225 (1966).
63. P.G. de Gennes, *Superconductivity of metals and alloys*, (1966, W.A. Benjamin Inc. New York-Amsterdam).
64. F.B. Silsbee, *J. Wash. Acad. Sci.* 6, 597 (1916).
65. I.M. Dmitrenko and S.I. Bondarenko, *Sov. Phys. JETP Lett.* 7, 241 (1968).
66. B.S. Deaver and W.S. Goree, *Rev. Sci. Instr.* 38, 311 (1966).
67. P. Meservey, *J. Appl. Phys.* 39, 2598 (1968).
68. J.E. Lukens and J.M. Goodkind, *Phys. Rev. Lett.* 20, 1363 (1968).
69. L.L. Vant-Hull, *Phys. Rev.* 173, 1412 (1968).
70. A.Th.A.M. de Waele, C.P.M. Vergouwen, A.A.J. Matsinger and R. de Bruyn Ouboter, *Physica* 59, 155 (1972).

71. F. London, *Superfluids* (Wiley, New York) Vol. I and II.
72. W.F. Vinen, "Superconductivity", ed. R.D. Parks (1969; Marcel Dekker Inc., New York) Vol. II, Chap. 20.
73. A.F. Hildebrandt, *Phys. Rev. Lett.* 12, 160 (1964); see also A.F. Hildebrandt and M.M. Saffren; C.A. King Jr., J.B. Hendricks and H.E. Rorschach Jr.; M. Bol and W.M. Fairbank in *Proc. of the Ninth Intern. Conf. on LT Physics*, 1964, Eds. J.G. Daunt et al. (Plenum Press, New York, 1966).
74. G.B. Hess and W.M. Fairbank, *Proc. of the Tenth Intern. Conf. on LT Physics*, Moscow, 1966, Vol. I (M.P. Malkov, ed. in chief), Viniti, Moscow, 1967, p. 423.
75. L. Onsager, *Nuov. Cim.* 6, Supp. 2, 249 (1949).
R.P. Feynman, *Progress in LT Physics*, ed. C.J. Gorter (1955, North-Holland Publ. Co., Amsterdam) Vol. 1, Chap. 2.
76. R. de Bruyn Ouboter, K.W. Taconis and W.M. van Alphen, *Progress in Low Temperature Physics*, ed. C.J. Gorter (1967, North-Holland Publ. Co.) Vol. 5, Chap. 2.
77. P.W. Anderson and A.H. Dayem, *Phys. Rev. Lett.* 13, 195 (1964).
78. L.D. Landau, *J. Phys. USSR* 5, 71 (1941), see also ref. 76.
79. R. Meservey, *Phys. Fluids* 8, 1209 (1965).
80. W.M. van Alphen, Thesis, see also 76.
81. H.E. Corke and A.F. Hildebrandt, *Phys. Fluids* 11, 465 (1968).
82. J.R. Pellam, *Progress in LT Physics*, ed. C.J. Gorter (1955, North-Holland Publ. Co.) Vol. 1, Chap. 3.
83. J. Bok and J. Klein, *Phys. Rev. Lett.* 20, 660 (1968).
84. A.G. van Vijfeijken and F.A. Staas, *Phys. Lett.* 12, 175 (1964).
85. S. Putterman and R. de Bruyn Ouboter, *Phys. Rev. Lett.* 24, 50 (1970).
86. J.B. Brown and T.D. Morris, *Proc. 11th Int. Conf. on LT Phys.*, St. Andrews, 1968, p. 768;
T.D. Morris and J.P. Brown, *Physica* 55, 760 (1971).
87. C.J. Adkins and J.R. Waldram, *Phys. Rev. Lett.* 21, 76 (1968).
88. J. Ginsburg, *Zh. Eksp. teor. Fiz.* 14, 177 (1944).
89. J.M. Luttinger, *Phys. Rev.* A136, 1481 (1964).
90. V.Z. Kresin and V.A. Litovchenko, *Sov. Phys. JETP* 26, 1216 (1968).
91. M.J. Stephen, *Phys. Rev.* A139, 197 (1965).
92. O. Betbeder-Matibet and P. Nozieres, *Ann. of Phys.* 51, 392 (1969).
93. W.F. Vinen, see ref. 72, p. 1226.
94. K. von Steiner and P. Grassmann, *Phys. Z.* 36, 527 (1935).
95. C. Herring and M.H. Nichols, *Rev. Mod. Phys.* 21, 185 (1949).
96. R.C. Tolman, *The principles of Stat. Mech.* (Oxford Univ. Press, 1962) p. 388.
L.D. Landau and E.M. Lifschitz, *Stat. Physics* (Pergamon Press, London-Paris, 1959) §55.
97. S.R. de Groot and P. Mazur, *Non-Equilibrium Thermodynamics* (North-Holland Publ. Co., Amsterdam-London, 1969) Chap. XIII.
98. C.A. Domenicali, *Rev. Mod. Phys.* 26, 237 (1954).
99. P. Hohenberg and W. Kohn, *Phys. Rev.* B136, 864 (1964).
W. Kohn and L.J. Sham, *Phys. Rev.* A140, 1133 (1965).
N.D. Lang and W. Kohn, *Phys. Rev.* B1, 4555 (1970).
100. V. Heine and C.H. Hodges, *J. Phys. C., Solid St. Phys.* 5, 225 (1972).
101. L.W. Kunz, *Phys. Rev. Lett.* 26, 1311 (1971).
102. J. Bardeen and J.L. Johnson, *Phys. Rev.* B5, 72 (1972).
103. P.E. Gregers-Hansen, M.T. Levinsen and G. Fog Pedersen, *Journ. of Low Temp. Physics* 7, 99 (1972).
104. N.F. Brickman, *Phys. Rev.* 184, 460 (1969).
105. J.B. Hendricks, C.A. King and H.E. Rorschach, *Journ. of Low Temp. Physics* 4, 209 (1971).
106. J.E. Zimmerman and J.E. Mercereau, *Phys. Rev. Lett.* 14, 887 (1965).
107. R.P. Giffard, R.A. Webb and J.C. Wheatley, *Journ. of Low Temp. Physics* 6, 533 (1972).

108. K. Nordvedt Jr., Phys. Rev. B1, 81 (1970).
109. D.N. Langenberg and J.R. Schrieffer, Phys. Rev. B3, 1776 (1971).
110. J.B. Hartle, D.J. Scalapino and R.L. Sugar, Phys. Rev. B3, 1778 (1971).
111. M.J. Stephen, Phys. Rev. Lett. 21, 1629 (1968).
112. M.O. Scully and P.A. Lee, Phys. Rev. 23, 1228 (1969).
113. D.B. Sullivan and J.E. Zimmerman, Am. J. of Physics 39, 1504 (1971).
114. I.M. Khalatnikov, *Intr. to the theory of Superfluidity* (W.A. Benjamin, inc. New York, 1965) Ch. 9.
115. T.J. Rieger, D.J. Scalapino and J.E. Mercereau, Phys. Rev. Lett. 27, 1787 (1971).
116. M.L. Yu and J.E. Mercereau, Phys. Rev. Lett. 28, 1117 (1972).
117. J. Clarke, Phys. Rev. Lett. 28, 1363 (1972).
118. M. Tinkham and J. Clarke, Phys. Rev. Lett. 28, 1366 (1972).

SAMENVATTING

DEEL I

In deel I van dit proefschrift worden eigenschappen beschreven van een systeem dat bestaat uit twee supergeleiders, die zwak met elkaar zijn verbonden. Speciale aandacht wordt besteed aan het geval waarin het zwakke contact tot stand komt, doordat een supergeleider van een punt wordt voorzien en daarmee zacht tegen een andere supergeleider wordt gedrukt. Contacten tussen twee supergeleiders die op deze manier zijn gemaakt heten puntcontacten. Evenals bij andere soorten zwakke contacten worden hierbij macroscopische quantumverschijnselen waargenomen die sterk verwant zijn aan de in 1962 door Josephson voorspelde effecten voor een systeem waarbij de twee supergeleiders zijn gescheiden door een isolatielaagje met een dikte van ongeveer 10 \AA .

In hoofdstuk I wordt het Josephson effect ingeleid. Verder worden er een aantal verschijnselen uit de supergeleiding besproken die nauw verwant zijn aan het Josephson effect. Dit heeft ten doel om het Josephson effect een plaats te geven tussen andere bekende verschijnselen uit de supergeleiding zoals fluxquantisatie en het Meissner effect.

In hoofdstuk II wordt de stroom-spannings karakteristiek besproken voor het geval dat de twee supergeleiders door slechts één puntcontact zijn verbonden. Een model wordt ingevoerd waarin het puntcontact vervangen wordt door een parallelschakeling van een ideaal Josephson contact en een normale weerstand. Indien de stroom door het contact constant wordt gehouden bevat de spanning over het contact een component die in de tijd varieert met een frequentie die gegeven wordt door de ac Josephson relatie. Volgens deze relatie is de frequentie evenredig met de gelijkspanning over het contact. Zo komt bijvoorbeeld $1 \text{ } \mu\text{V}$ overeen met $0,5 \text{ GHz}$. Uit het beschouwen van enkele geïdealiseerde gevallen blijkt dat wisselstroomimpedanties, die gekoppeld zijn aan het puntcontact, grote invloed hebben op de waargenomen tijdgemiddelde i - V afhankelijkheid. Ook de invloed van een wisselspanning op het puntcontact wordt besproken.

Enkele toepassingen worden genoemd. De belangrijkste zijn: het gebruik bij het vastleggen van een spanningsstandaard en bij het nauwkeurig meten van de fundamentele grootheid h/e .

In een „dubbelpuntcontact“ zijn twee supergeleiders verbonden door twee puntcontacten. In hoofdstuk III wordt de afhankelijkheid afgeleid tussen een uitwendig aangelegd magneetveld en de maximale gelijkstroom die men door een dubbelpuntcontact kan sturen zonder dat er een gelijkspanning tussen de twee supergeleiders ontstaat. Het blijkt dat deze zogenaamde „kritische stroom“ oscilleert als functie van het aangelegde magneetveld (gelijkstroom interferentie). De periode in het magneetveld is omgekeerd evenredig met het oppervlak dat door de twee puntcontacten en de supergeleiders wordt omsloten. Als dat oppervlak bijvoorbeeld 1 cm^2 is dan is de periode $0,2 \text{ } \mu\text{gauss}$.

Volledige overeenstemming tussen theorie and experiment kan worden verkregen als men de door Josephson afgeleide sinusvormige stroom-fase relatie aanneemt en de invloed van de zelfinductie van het omsloten oppervlak in rekening brengt. Dit is een sterke aanwijzing dat de sinusvormige stroom-fase relatie juist is voor een puntcontact. Het hier bedoelde experiment over gelijkstroom interferentie was het eerste in zijn soort dat kwantitatief in overeenstemming kon worden gebracht met de dc Josephson relatie.

In hoofdstuk IV komt een dubbelpuntcontact ter sprake in de situatie waarbij de gelijkspanning tussen twee supergeleiders ongelijk nul is. Wanneer de stroom door het systeem constant wordt gehouden oscilleert de gelijkspanning over het contact als functie van het magneetveld met dezelfde periode als de kritische stroom: dit zijn de zogenaamde gelijkspanningsoscillaties. Zowel de spanning over het contact als de magnetische flux in het omsloten oppervlak oscilleren beide in de tijd met een frequentie die wordt gegeven door de ac Josephson relatie. Van dit effect wordt gebruik gemaakt om de amplitude van de gelijkspanningsoscillaties te vergroten door een buisje van een normaal metaal in de holte te stoppen.

Eveneens in hoofdstuk IV wordt een experiment beschreven waarbij een dubbelpuntcontact in een trilholte is geplaatst. Ook de gelijkrichtwerking van een asymmetrisch dubbelpuntcontact wordt besproken. Tenslotte wordt in dit hoofdstuk een kort overzicht gegeven van een aantal toepassingsmogelijkheden van dubbelpuntcontacten, voornamelijk als gevoelig element in magneetveldmeters (en dus ook in stroom en spanningsmeters). Het blijkt dat magneetvelden van 1 nanogauss nog kunnen worden gemeten. Als concreet voorbeeld wordt de mogelijkheid van een nauwkeurige meting van het London moment besproken.

In hoofdstuk V wordt de experimentele opstelling behandeld evenals de methode waarop men betrouwbare, reproduceerbare dubbelpuntcontacten kan maken. Essentieel voor de betrouwbaarheid van de constructie is dat de twee supergeleiders blokken zijn van niobium die met een glaslaagje aan elkaar worden gesmolten dat dezelfde uitzettingscoëfficiënt heeft als niobium.

DEEL II

In deel II van dit proefschrift worden electrostatische effecten besproken die optreden in supergeleiders als er een temperatuurgradient in wordt aangelegd. Een temperatuurgradient heeft een gradient in the chemische potentiaal ten gevolge. Aangezien echter de electrochemische potentiaal constant is moet er een electricch veld in de supergeleider bestaan dat de verandering in de chemische potentiaal compenseert; dit ondanks het feit dat de gebruikelijke thermoelectrische effecten nul zijn in een supergeleider.

In hoofdstuk VI worden enkele analogieën in de eigenschappen van supergeleiders en van superfluïde helium besproken. Op grond van een twee fluida model wordt aangetoond dat een temperatuurverschil over een supergeleider aanleiding geeft tot een electrostatisch spanningsverschil. Dit spanningsverschil vertoont een zekere analogie met de fonteindruk in helium II. Het kan niet worden gemeten door middel van een voltmeter die met draden aan het preparaat is verbonden. Daar deze spanningsverschillen een belangrijke bijdrage leveren tot de temperatuurafhankelijkheid van de uittreepotentiaal van de supergeleider kan een capacitatieve koppeling tussen voltmeter en preparaat echter wel informatie geven over het electricch veld in het metaal. Men moet dan gebruik maken van wisselstroom technieken.

In hoofdstuk VII wordt de capacitatieve meetmethode geanalyseerd. Enkele termen die bijdragen tot de temperatuurafhankelijkheid van de uittreepotentiaal van eenvoudige metalen worden besproken.

In de hoofdstukken VIII en IX wordt nader ingegaan op de experimentele aspecten van het probleem. Er wordt beschreven hoe de thermometer,

het verwarmingselement en het preparaat werden gemaakt. De temperatuur van het preparaat kon worden gevarieerd tussen 4 en 12 Kelvin met een frequentie van 1,5 Hz. De thermometer was voldoende snel om deze variaties te kunnen volgen. Verder wordt aangegeven hoe eventuele storende signalen kunnen worden geïdentificeerd en vermeden.

De meting aan niobium toont aan dat de kromme die het verband aangeeft tussen de uittreepotentiaal en de temperatuur in goede benadering een rechte lijn is met een helling van $10 \mu\text{V/K}$. Voor lood is deze kromme niet recht. De hellingen zijn van de orde van $0,5 \mu\text{V/K}$. Voor koper heeft deze kromme een helling van $-5 \mu\text{V/K}$ bij 4,2 K en van $-15 \mu\text{V/K}$ bij 10 K.

In hoofdstuk X wordt erop gewezen dat er op dit moment nog geen goede overeenstemming bestaat tussen theorie en experiment. In tegenstelling tot het fonteineffect in superfluide helium, waar de waargenomen drukverschillen kunnen worden beschreven in termen van de entropie per deeltje, kunnen de waargenomen spanningsverschillen in een supergeleider niet eenvoudig worden berekend uit de entropie per geleidingselectron. Effecten, zoals bijvoorbeeld de verandering in de chemische potentiaal van de elektronen ten gevolge van de uitzetting van het metaal, spelen een belangrijke rol.

CURRICULUM VITAE

van A.Th.A.M. de Waele, geboren op 11 januari 1944 te Koewacht (thans gemeente Axel).

In juni 1961 behaalde ik het diploma HBS-B aan het Jansenius Lyceum te Hulst. Aansluitend daarop ben ik begonnen met mijn studie in Leiden. Het kandidaatsexamen in de studierichting d' (hoofdvakken natuur- en wiskunde met bijvak scheikunde) legde ik af in februari 1965. In augustus 1966 ving mijn werkzaamheden aan op het Kamerlingh Onnes Laboratorium en wel in de groep ter bestudering van puntcontacten tussen twee supergeleiders. Deze groep staat onder leiding van prof. dr. K.W. Taconis en dr. R de Bruyn Ouboter.

Ter voorbereiding van mijn doctoraalexamen in de experimentele en theoretische natuurkunde (gemengde richting) heb ik tentamens afgelegd bij de hoogleraren dr. P. Mazur, dr. P.W. Kasteleyn en dr. J.A.M. Cox in respectievelijk statistische mechanica, electromagnetisme en quantum mechanica en klassieke mechanica. Eveneens bij prof. dr. J.A.M. Cox legde ik een uitgebreid tentamen quantum mechanica af. Mede naar aanleiding daarvan heb ik in de zomer van 1967 2½ maand in CERN, Genève, doorgebracht als vakantiestudent. Tenslotte legde ik bij dr. R. de Bruyn Ouboter een tentamen experimentele natuurkunde af over het onderwerp supergeleiding. Mijn doctoraal-examen deed ik in mei 1968.

Sinds september 1967 ben ik assistent bij het college „Het Electromagnetische Veld" van dr. R. de Bruyn Ouboter.

In 1972 werd ik door de Koninklijke/Shell in de gelegenheid gesteld om gedurende de maanden augustus en september een studiereis te maken door de Verenigde Staten van Amerika.

Vele personen hebben actief meegewerkt aan het tot stand komen van dit proefschrift. Een aantal van hen wil ik met name noemen. Aldus hoop ik iets van de dank over te brengen die ik hen verschuldigd ben.

Dit onderzoek heeft plaats gehad in de researchgroep van prof. dr. K.W. Taconis waarin het verschijnsel superfluiditeit in helium en supergeleiding wordt bestudeerd.

Aan de dagelijkse uitvoering van de experimenten hebben medegewerkt dr. M.H. Omar, drs. W.H. Kraan, drs. C.P.M. Vergouwen, drs. P.A.J. Tindemans en de heren A.A.J. Matsinger en D.J. Schaap. Een gedeelte van het onderzoek dat in DEEL II is beschreven, is verricht in samenwerking met dr. P.B. Pipes. De computerberekeningen van § 4 zijn uitgevoerd door drs. C.C.P. den Ouden. De heren L.S. Prins en J. Post waren betrokken bij het ontwerpen en maken van de instrumenten. De heer P.J.M. Vreeburg heeft een belangrijk aandeel gehad bij de ontwikkeling van stabiele dubbelpuntcontacten. De levering van andere metalen dan niobium werd verzorgd door de heer C.E. Snel. Het typewerk werd verricht door mej. S.M.J. Ginjaar en mevr. E. de Haas-Walraven. De heren B. Kret, A.J.J. Kuyt en G. Vis zorgden voor de cryostatens en de andere cryogene voorzieningen. De heer W.F. Tegelaar verzorgde de tekeningen.

De leden van de groep waarin ik werkzaam was hebben door hun belangstelling en discussies een stimulerende invloed gehad op het onderzoek. Dit geldt in het bijzonder voor prof. dr. K.W. Taconis en dr. H. van Beelen.

Faint, illegible text covering the page, possibly bleed-through from the reverse side.



